EVALUATION OF MICRO-SCALED TiO_2 ON DEGRADATION AND RECOVERY OF $mTiO_2$ FROM TREATED DRINKING WATER

Submitted in fulfilment of the requirements of the degree of Master of Engineering: Chemical Engineering in the Faculty of Engineering and the Built Environment at the Durban University of Technology

CHAZEKILE PRECIOUS DLAMINI

April 2016

Supervisor: Prof. Paul Musonge

DECLARATION

I hereby declare that the content in this dissertation is a record of my original research work towards achieving the Master of Engineering in Chemical Engineering at the Durban University of Technology (DUT). The content of this research document has not been previously published or written by another person for the award of any other degree at DUT or in any other educational institution. Furthermore, I declare that the content of this dissertation does not violate any copyright as every work of others has been indicated and recognized by means of in text referencing and comprehensive list of references.

The document is the property of Durban University of Technology.

Chazekile P. Dlamini

Signature:……..Date:……..

Supervisor:
Prof. P. Musonge

Signature:……..Date:……..

DEDICATIONS

To GOD ALMIGHTY and the people in my life who have always believed in me and prayed for me, seen me at my best and worst, and always stood by me.

ABSTRACT

River water is a life supporting watercourse to most communities in rural areas. It is used for both human and animal consumption, and is well becoming a collection channel for defecation and urination due to shortage or lack of access to running water and sanitation facilities. This has resulted to the contamination of water sources, which poses a great risk to human health. This has motivated researchers to study simple but yet robust systems to produce safe drinking water. Photocatalysis is one of such emerging disinfection technologies.

Titanium dioxide (TiO_2) which is one of the basic materials used for paint manufacturing has emerged as an excellent photocatalyst material for water purification. TiO_2 was selected in this study because it is locally available with a potential to open a new market in water purification for the manufacturers. The setback in previous studies is the recovery of nano-scaled TiO_2 ($nTiO_2$) after purification when used as a suspension in treated water. Thus this study evaluates the performance of four grades of micro-scaled TiO_2 ($mTiO_2$) on the degradation of organic matters, Escherichia coli (*E. coli*) and total coliform in river water and to investigate the percentage recovery of the $mTiO_2$ using a locally manufactured Polyester Woven Fabric Microfiltration (PWFMF) membrane. The PWFMF though uncharacterized has been used in a number of studies for treating domestic and industrial waste waters. The best-performing grade was used to optimize the degradation efficiency of *E. coli* in river water using the Design of Experiments (DOE) methodology.

Grade 2 of the $mTiO_2$, which is hydrated titanium dioxide with additions ($ahTiO_2$) of particle size range of 0.2 – 53 µm at a concentration of 2.5 g/l displayed an advantageous photocatalytic activity. The results show that 80 % of the organics were removed in 3 hours and increased to 93% after 6 hours. Two particle size ranges of 0.2 – 53 µm and 54 – 75 µm at a concentration of 5 g/l degraded organic matters to 90 % and 77 % in 3 hours respectively. The particle size range of 0.2 – 53 µm at a concentration of 5 g/l was then filtered using a PWFMF and turbidities went below 1 NTU after 20 minutes from feed turbidity of 470 NTU for all three trials. The average percentage recovery in 2 hours was 98.91 %.

The four grades of $mTiO_2$ were analyzed for *E. coli* and total coliform for 4 hours at concentrations of 2, 5 and 7 g/l. Grade 2 achieved the *E. coli* specification of 0 count/ 100 mL at 5 g/l in 2 hours and at 7 g/l in 0.5 hours. Grade 4 *E. coli* specification was achieved with 7g/l in 4 hours. Grades 2 and 4 performed better since they both achieved the *E. coli* and total coliform specifications. Grade 2 was the best performing grade and was considered for statistical studies.

Grade 2 was then used on a comparative study between the Central Composite Design (CCD) and Box-Behnken Design (BBD), which are two of the major Response Surface Methodologies (RSM). The CCD compared to BBD provides high quality predictions over the entire design space. The CCD obtained optimum results for concentration of $mTiO_2$ (X_1), temperature (X_2), initial pH (X_3) and aeration (X_4) which were 6.94 g/l, 28.75 ^{O}C, pH = 6.04, and 13.35 L/min for the maximum degradation efficiency of 99.85 % which showed comparable optimum results to the BBD that were 6.45 g/l, 28.28 ^{O}C, pH = 6.02 and 12.21 L/min for the maximum degradation efficiency of 99.80%. These theoretical model results were validated by practical experiments that produced the maximum degradation efficiency for CCD and BBD of 99.67 and 99.26 % respectively.

Grade 2 of the $mTiO_2$ can be used as a photocatalyst for river water purification due to its strong ability for the removal of *E. coli*. The additions used in grades 2 and 4 during production improved the photocatalytic activity. The PWFMF membrane showed a great performance of above 98 % particle recovery of $mTiO_2$ from treated water, although there was an indication that the smallest particles were passing through the membrane. The RSM results gave approximately the same optimum results that were well within the limits, which were experimentally validated and showed that the models were sustainable. It is recommended that the effect of additions be studied on the structures or the charge stability of the two grades.

PUBLICATIONS

Journal Publication

Submitted for publication

1. Dlamini, C.P., Musonge, P., 2015. Photocatalytic disinfection of river water using four grades of micro-scaled TiO_2 ($mTiO_2$). South African Journal of Chemical Engineering.

ACKNOWLEDGEMENTS

This research was supported and funded by the Research and Postgraduate Support, Water Research Institute of Durban University of Technology and most importantly, Huntsman Tioxide SA.

The research was completed due to a sincere and great guidance by my supervisor, Prof. Paul Musonge. His great knowledge that he freely shares with open heart is greatly appreciated. I thank him for encouraging and supporting me during the course to this study.

I acknowledge my colleagues; the academic and technical staff for their great support and encouragement in lecturing and laboratory during and after hours. I appreciate the relationship, encouragement and help of my fellow postgraduates in the Department of Chemical Engineering and the Faculty of Engineering and The Built Environment. I greatly appreciate the assistance of Zwane Xolani, Zulu Fanele, Soobramoney Nadine and James Janien towards the project.

TABLE OF CONTENTS

CONTENT **PAGE**

DECLARATION ii
DEDICATIONS iii
ABSTRACT iv
PUBLICATIONS vi
ACKNOWLEDGEMENTS vii
TABLE OF CONTENTS viii
LIST OF FIGURES xii
LIST OF ABBREVIATIONS xxii
LIST OF UNITS xxiii
CHAPTER 1 1
INTRODUCTION 1
1.1. Background 1
1.2 Problem Statement 3
1.3 Objectives 4
1.4 Scope 5
1.5 Dissertation Outline 6
CHAPTER 2 8
LITERATURE REVIEW 8
2.1 General Introduction 8
2.2 Earth's Water Distribution 8
2.3 Water Scarcity 10
2.4 Ground and Surface Water Sources 11
2.5 Water Quality and Pollution 13
2.5.1 Health Effect of Microorganisms Present in Freshwater 14
2.6 Drinking Water Quality Standards 16
2.6.1 Disinfection of river water 18

2.6.1.1 Turbidity of the water and $mTiO_2$ concentration 19
2.6.1.2 Chemical Oxygen Demand (COD) 19
2.6.1.3 *E. coli* concentration 19
2.7 Water Treatment Systems 20
2.7.1 Conventional Technology 20
2.7.2 Membrane Technology Overview 22
2.7.2.1 Classification of Membrane Processes 23
2.7.2.2 Modes of Operation of Membrane 26
2.7.2.3 Immersed Membrane Microfiltration (IMM) 28
2.7.3 Strategies to reduce fouling 30
2.8 Titanium Dioxide or Titania 32
2.8.1 Production of Titanium Dioxide. 33
2.8.1.1 The chloride process route 35
2.8.1.2 The sulphate process route 35
2.8.2 Mechanism of TiO_2 Photocatalytic Chemistry 37
2.8.3 Factors Affecting Photocatalytic degradation 39
2.8.3.1 Light Source (UV light intensity and wavelength) 39
2.8.3.2 Temperature 40
2.8.3.3 Initial pH 41
2.8.3.4 Photocatalyst loading 42
2.8.3.5 Dissolved Oxygen 43
2.9 Design of Experiments (DOE) 43
2.9.1 One Factor At- a Time (OFAT) Design 46
2.9.2 Factorial Design 47
2.9.3 Response Surface Methodology Design 50
2.9.3.1 The Central Composite Design (CCD) 52
2.9.3.2 The Box-Behnken Design (BBD) 52
2.9.4 Analysis of Design Model 53
2.9.4.1 Model Adequacy Checking for first-order regression 53
2.9.4.2 Polynomial Regression Models in Two or More Variables 57
2.10 Summary 60
CHAPTER 3 61
RESEARCH DESIGN AND METHODOLOGY 61
3.1 General Introduction 61

3.2 Materials and Methods 61
3.2.1 Materials and Chemicals 61
3.2.1.1 Sampling of the grades of $mTiO_2$ for the Research Project. 62
3.3 Experimental Set-up 64
3.3.1 Photocatalytic activity of the $mTiO_2$ pigment using the Batch process. 64
3.3.2 Photocatalytic activity using the Continuous Tubular Reactor. 65
3.3.3 Evaluation of the PWFMF on recovery of the photocatalyst ($mTiO_2$). 66
3.3.4 Optimization of the system by DOE. 68
3.4 Selected methods of analysis. 70
3.4.1 Turbidity 70
3.4.2 E. coli or total coliform 72
3.4.3 COD 73
3.5 Design of Experiments (DOE) Experimental Matrix. 75
CHAPTER 4 79
RESULTS AND DUSCUSSION 79
4.1 General Introduction 79
4.2 Photocatalytic Activity of $mTiO_2$ pigment 79
4.2.1 The effect of reaction time on degradation efficiency of organics 79
4.2.2 The effect of particle size and catalyst loading of $ahTiO_2$ on degradation efficiency of organics 80
4.2.3 Photocatalytic activity using the Continuous Tubular Reactor. 82
4.2.4 Recovery of TiO_2 from treated water. 83
4.3 Performance of the four Grades of $mTiO_2$ 86
CHAPTER 5 89
OPTIMISATION OF THE PHOTOCATALYTIC REACTOR USING RSM 89
5.1 General Introduction 89
5.2 Optimization of the $mTiO_2$ photocatalytic reactor system using DOE 89
5.3 Analysis using the central composite design 94
5.4 Analysis using the box behnken design 98
5.5 Verification of the design models 102

CHAPTER 6 103
CONCLUSSIONS AND RECOMMENDATIONS 103
REFERENCES 105
APPENDICES 116
APPENDIX A: 117
APPENDIX B: 122
APPENDIX C: 124
APPENDIX D: 132
APPENDIX E: 141
APPENDIX F: 148

LIST OF FIGURES

Figure 1.1: (a) The Water Distribution of the Planet, (b) Water available to be used by humans (Mulder, 1998). 1

Figure 1.2: Layout of the Dissertation 7

Figure 2.1: The Planet's water distribution (supply) (Phillips, 2010, Wikipedia, 2014b). 8

Figure 2.2: (a) Global physical and economical water scarcity, (b) Water scarcity in Africa (World Resources Institute, 2009, Pravettoni, 2011). 10

Figure 2.3 (a) & (b): The predicted effect of climate change on water scarcity in 2095 without a curb of carbon emissions (Phys Org, August 2014). 11

Figure 2.4: A flowchart for the sources of Freshwater (About Civil.org, 2014) 12

Figure 2.5: Hyrologic Cycle (Phillips, 2010). 12

Figure 2.6: A string of Microorganisms (LennTech, 1998-2014b) 15

Figure 2.7: Flow diagram of a conventional potable water treatment plant (Leckie et al., 2004) 20

Figure 2.8: Coagulation, flocculation and sedimentation in a conventional treatment process. 21

Figure 2.9 (a) & (b): The use of a Membrane as an inter-phase between two phases (Feed and Permeate) 23

Figure 2.10: Process Flow for Micro-filtration: (a) Dead –end flow, (b) Cross-flow (Ní Mhurchú, 2008). 26

Figure 2.11: Schematic representation of (a) flux and cake thickness for constant pressure dead-end filtration (b) TMP and cake thickness for constant flux dead-end filtration (Winston Ho and Sirkar, 2001, Achisa, 2013) 27

Figure 2.12: Schematic representation of the flux and cake thickness for cross-flow filtration (Winston Ho and Sirkar, 2001, Ní Mhurchú, 2008, Achisa, 2013). 28

Figure 2.13: Schematic representation of Immersed Membrane (a) A gentle suction of permeate by pump, (b) Filtration by gravity head. 28

Figure 2.14: Fluid flow in Cross-flow and Immersed Membranes (Pillay and Jacobs, 2005). 29

Figure 2.15: (a) Constant Pressure Operation, (b) Constant Flux Operation (Pillay and Jacobs, 2005) 30

Figure 2.16: Effect of backflushing (Pillay and Jacobs, 2005). 31

Figure 2.17: The crystal structure of (a) Rutile, (b) Brookite, (c) Anatase (Smyth and Bish, 1988) and (d) Unit cell 3D-balls of the same crystal structure (Moellmann et al., 2012). 32

Figure 2.18: The Chloride and Sulphate Process TiO_2 Production Routes (McNulty, 2007). 34

Figure 2.19: Energy band diagram and fate of electrons and holes in a semiconductor particle in the presence of water containing a pollutant (Malato et al., 2009). 38

Figure 2.20: The band gap of the Anatase and Rutile (Yu et al., 2002, Di Paola et al., 2013) 40

Figure 2.21: Effect of initial pH on the photocatalytic degradation efficiency of organic pollutants in the sewage water (Shivaraju, 2011) 41

Figure 2.22: Effect of photocatalyst loading on the photocatalytic degradation efficiency of organic pollutants in the sewage water (Shivaraju, 2011) 42

Figure 2.23: A general model of system variables (Montgomery, 2009) 44

Figure 2.24: Adaptive OFAT as Applied to a System With Three Two-Level Factors (A, B, and C) (Frey and Wang, 2006) 47

Figure 2.25: A two-factor factorial experiment (a) with the response (y) shown at the corners (b) without interaction (Montgomery, 2009). 49

Figure 2.26: A two-factor factorial experiment (a) with the response (y) shown at the corners (b) with interaction (Montgomery, 2009). 49

Figure 2.27: Response along the path of steepest ascent (Montgomery, 2009) 51

Figure 2.28: Central Composite Design (a) Generation of a CCD, (b) Illustrative representation of where the star points are placed for the 3 types of CCD..... 52

Figure 2.29: Box-Behnken Design for three factors. 53

Figure 2.30: Normal probability plots: (*a*) ideal; (*b*) light-tailed distribution; (*c*) heavy-tailed distribution; (*d*) positive skew; (*e*) negative skew (Montgomery et al., 2012). 54

Figure 2.31: Normal probability plot of the externally studentized residuals for the delivery time data (Montgomery et al., 2012)..... 55

Figure 2.32: Patterns for residual plots: (*a*) satisfactory; (*b*) funnel; (*c*) double bow; (*d*) nonlinear (Montgomery et al., 2012). 56

Figure 2.33: Prototype residual plots against time displaying autocorrelation in the errors: (*a*) positive autocorrelation; (*b*) negative autocorrelation (Montgomery et al., 2012) 57

Figure 2.34: (a) Normal probability plot of the studentized residuals, (b) Studentized versus predicted conversion, (c) Studentized residuals run order (Montgomery et al., 2012). 59

Figure 2.35: (a) Response Surface of predicted conversion, (b) Contour plot of predicted conversion (Montgomery et al., 2012). 59

Figure 3.1: Tioxide Sulphate Process with sampling of the grades of mTiO_2..... 63

Figure 3.2: Schematic image for the investigation of Photocatalytic activity of the mTiO_2 pigment..... 65

Figure 3.3 (a): The image of the Ultra Zap UV sterilizer with the UV light fitted inside. 65

Figure 3.3 (b): The schematic diagram of the Continuous tubular reactor. 66

Figure 3.4: The experimental schematics for evaluation of PWFMF on Recovery of the $mTiO_2$ particle. 67

Figure 3.5: Polyester Woven Fabric Micro-Filtration membrane design, (a) Woven Fabric, (b) Flat sheet design, and (c) Final PWFMF membrane (Pillay and Jacobs, 2005, Pikwa et al., 2009) 68

Figure 3.6: The experimental Apparatus for the degradation of bacteria and Separation of the catalyst from treated water. 69

Figure 3.7: The set-up to optimize the system of the degradation of bacteria. 70

Figure 3.8: The schematic image of the turbidity meters (grey and blue, grey and black), and pH meter (black). 70

Figure 3.9: Quanti-trays after incubation (initial and treated water samples) 72

Figure 4.1: Effect of Irradiation Time on degradation of organics 80

Figure 4.2: Effect of particle size and catalyst loading on degradation of organics. 81

Figure 4.3: The Calibration Curve for the $mTiO_2$ concentration 83

Figure 4.4: Evaluation of PWFMF on Recovery of particle size range of 0.2 – 53 µm 84

Figure 4.5: Differential pressures and Permeate flowrate changes with time. 85

Figure 4.6 (a): Effect of Anatase grades of mTiO2 on degradation efficiency of *E. coli* and total coliform in river water. 87

Figure 4.6 (b): Effect of the Rutile grades of $mTiO_2$ on degradation efficiency of *E. coli* and total coliform in river water 88

Figure 5.1: Response Surface of predicted degradation efficiency of *E. coli* in river water ... 96

Figure 5.2: Contour plot of predicted degradation efficiency of *E. coli* in river water 97

Figure 5.3: Overlay plot of predicted degradation efficiency of *E. coli* in river water 97

Figure 5.4: Response Surface of predicted degradation efficiency of *E. coli* in river water .100

Figure 5.5: Contour plot of predicted degradation efficiency of *E. coli* in river water 100

Figure 5.6: Overlay plot of predicted degradation efficiency of *E. coli* in river water 101

Figure 7.1: Schematic diagram of the Tioxide Sulphate Process for the sampling of the grades of $mTiO_2$. 116

Figure D -7.1: Normal Probability plot of the Studentized Residuals of the $mTiO_2$ water treatment.....136

Figure D -7.2: Residuals vs the Fitted values the $mTiO_2$ water treatment. 136

Figure D -7.3: Residuals vs Run Order of the $mTiO_2$ water treatment.....137

Figure D -7.4: Plot of Predicted values vs Actual values. 137

Figure D -7.5: Box-Cox Plot Power Transforms. 138

Figure D -7.6: Plot of Leverage vs Run Order.....138

Figure E -7.1: Normal Probability plot of the Studentized Residuals of the $mTiO_2$ water treatment.....145

Figure E -7.2: Residuals vs the Fitted values the $mTiO_2$ water treatment. 145

Figure E -7.3: Residuals vs Run Order of the $mTiO_2$ water treatment. 146

Figure E -7.4: Plot of Predicted values vs Actual values. 146

Figure E -7.5: Box-Cox Plot Power Transforms. 147

Figure E -7.6: Plot of Leverage vs Run Order. 147

LIST OF TABLES

Table 2.1: Estimate of global water distribution (Mulder, 1998, http://mptbc.nic.in, 2013).....9

Table 2.2: Various health effects and their causes (LennTech, 1998-2014b). 15

Table 2.3: Drinking water quality guidelines on physical, aesthetic, chemical and microbiological determinands (World Health Organisation, 2011) (South African National Standard, 2011) 17

Table 2.4: Settling Time for Particles of Various Diameters (Peterson, 2001). 21

Table 2.5: Membrane Processes Classification (Winston Ho and Sirkar, 2001, Baker, 2002, Mulder, 1996).....24

Table 2.6: Application range of various membrane processes (Pearce, 2007).....25

Table 2.7: Main feedstocks used for production of TiO_2 (McNulty, 2007) 33

Table 2.8: Band-gap energy for some common semiconductor materials at 0K (Thiruvekatachari et al., 2008).....37

Table 2.9: Description of experimental objectives (Nist/SEMATECH, 2012, Filliben and Heckert, 2012).....45

Table 2.10: Design Selection Guideline (Nist/SEMATECH, 2012, Filliben and Heckert, 2012). 45

Table 2.11: In general, the various types of OFAT DOE approaches (Milani et al., 2008). ...46

Table 2.12: Number of Runs for a Two Level (n^k) and Three Level Full Factorial 48

Table 2.13: Analysis of Variance for the Chemical Process Example 57

Table 2.14: Observed Values, Predicted Values, Residuals, and Other Diagnostics for the Chemical Process Example (Montgomery et al., 2012).....58

Table 3.1: The description of the grades of $mTiO_2$ used in this project. 63

Table 3.2: The turbidity meter's specification (James, 2015). 71

Table 3.3: COD Vial types and ranges 74

Table 3.4 (a): Experimental Range and Levels of the four Variables or Factors for the CCD 76

Table 3.4 (b): Experimental Range and Levels of the four Variables or Factors for the BBD 76

Table 3.5: The Central Composite Design Matrix for Four Factors. 77

Table 3.6: The Box-Behnken Design Matrix for Four Factors..... 78

Table 4.1: Effect of concentration on degradation efficiency of organics in Isipingo river water 82

Table 4.2: The effect of 2 g/l of $mTiO_2$ on degradation of bacteria in river water..... 86

Table 4.3: The effect of 5 g/l of $mTiO_2$ on degradation of bacteria in river water..... 86

Table 4.4: The effect of 7 g/l of $mTiO_2$ on degradation of bacteria in river water..... 86

Table 5.1: Manipulated variables and output for this study..... 90

Table 5.2 (a): The CCD experimental matrix results..... 91

Table 5.2 (b): The BBD experimental matrix results 92

Table 5.3: Minimum and maximum limits for the solutions of optimum conditions..... 93

Table 5.4: ANOVA for Response Surface Quadratic model on the CCD..... 94

Table 5.5: The R-Squared Results. 95

Table 5.6: ANOVA for Response Surface Quadratic model on the BBD..... 98

Table 5.7: The R-Squared. 99

Table 5.8: The results of optimum Values..... 101

Table 5.9: Verification of the design models. 102

Table A-7.1: Calibration data curve for the TiO_2 Concentration 117

Table A-7.2: Effect of Irradiation time on Organic degradation 117

Table A-7.3: Effect $mTiO_2$ concentration on organic degradation using particle size range of 0.2-53 µm. 118

Table A-7.4: Effect $mTiO_2$ concentration on organic degradation using particle size range of 53-75 µm 118

Table A-7.5: Trial 1 on Percentage Recovery of TiO_2 using a new PWFMF. 119

Table A-7.6: Trial 2 Percentage Recovery of TiO_2 using PWFMF (cleaned after trial 1) 120

Table A-7.7: Trial 3 Percentage Recovery of TiO_2 using PWFMF (cleaned after trial 2) 121

Table B-7.1: Effect of Grades of mTiO2 on *E. coli* and Total coliform bacteria for 2g/L 122

Table B-7.2: Effect of Grades of mTiO2 on *E. coli* and Total coliform bacteria for 5g/L 122

Table B-7.3: Effect of Grades of mTiO2 on *E. coli* and Total coliform bacteria for 7g/L 123

Table C-7.1: The raw data for run 16 CCD and run 13 BBD 124

Table C-7.2: The raw data for run 19 CCD and run 6 BBD 124

Table C-7.3: The raw data for run 27 CCD and run 25 BBD 124

Table C-7.4: The raw data for run 11 CCD and run 21 BBD 125

Table C-7.5: The raw data for run 23 CCD and run 23 BBD 125

Table C-7.6: The raw data for run 8 CCD and run 4 BBD 125

Table C-7.7: The raw data for run 2 CCD and run 18 BBD 125

Table C-7.8: The raw data for run 30 CCD and run 29 BBD 126

Table C-7.9: The raw data for run 1 CCD and run 14 BBD 126

Table C-7.10: The raw data for run 10 CCD and run 22 BBD 126

Table C-7.11: The raw data for run 4 CCD and run 7 BBD 126

Table C-7.12: The raw data for run 21 CCD and run 12 BBD 127

Table C-7.13: The raw data for run 5 CCD and run 19 BBD 127

Table C-7.14: The raw data for run 25 CCD and run 28 BBD 127

Table C-7.15: The raw data for run 6 CCD and run 20 BBD 127

Table C-7.16: The raw data for run 20 CCD and run 2 BBD 128

Table C-7.17: The raw data for run 17 CCD and run 11 BBD 128

Table C-7.18: The raw data for run 7 CCD and run 9 BBD 128

Table C-7.19: The raw data for run 29 CCD and run 26 BBD 128

Table C-7.20: The raw data for run 12 CCD and run 16 BBD 129

Table C-7.21: The raw data for run 18 CCD and run 1 BBD 129

Table C-7.22: The raw data for run 14 CCD and run 5 BBD 129

Table C-7.23: The raw data for run 15 CCD and run 17 BBD 129

Table C-7.24: The raw data for run 28 CCD and run 27 BBD 130

Table C-7.25: The raw data for run 9 CCD and run 3 BBD 130

Table C-7.26: The raw data for run 24 CCD and run 8 BBD 130

Table C-7.27: The raw data for run 3 CCD and run 15 BBD 130

Table C-7.28: The raw data for run 22 CCD and run 10 BBD 131

Table C-7.29: The raw data for run 13 CCD and run 24 BBD 131

Table C-7.30: The raw data for run 26 CCD and run 30 BBD 131

Table D-7.1: Sequential Model Sum of Squares [Type I] on the Box-Behnken Design 132

Table D-7.2: Lack-of-fit Test on the Box-Behnken Design 132

Table D-7.3: Model Summary Statistic on the Box-Behnken Design 132

Table D-7.4: ANOVA for Response Surface Quadratic model on the Box-Behnken Design 133

Table D-7.5: Diagnostics Case Statistics on the Box-Behnken Design 135

Table D-7.6: Optimization Report of Constrains and Solutions on the Box-Behnken Design 139

Table E-7.1: Sequential Model Sum of Squares [Type I] on the Central Composite Design. 141

Table E-7.2: Lack-of-fit Test on the Central Composite Design. 141

Table E-7.3: Model Summary Statistic on the Central Composite Design. 141

Table E-7.4: ANOVA for Response Surface Quadratic model on the Central Composite Design 142

Table E-7.5: Diagnostics Case Statistics on the Central Composite Design 144

LIST OF ABBREVIATIONS

AOP	-	advanced oxidation process
ahTiO_2	-	Hydrated Titanium dioxide with additions (anatase Calciner feed)
anTiO_2	-	Anhydrous Titanium dioxide (Rutile Calciner discharge)
BBD	-	Box-Behnken Design
CCC	-	Central Compose Circumscribed
CCD	-	Central Compose Design
CFMF	-	Crossflow Microfiltration
COD	-	Chemical Oxygen Demand
DOE	-	Design of Experiments
DUT	-	Durban University of Technology
hTiO_2	-	Hydrated Titanium dioxide (Predominantly Anatase)
IMM	-	Immersed Membrane Microfiltration
MF	-	Micro-Filtration
mTiO_2	-	micro-scaled or micro-sized particles of TiO_2
NF	-	Nano-Filtration
NOM	-	natural organic matter
nTiO_2	-	nano-scaled or nano-sized particles of TiO_2
NTU	-	Nephelometric turbidity units
OFAT	-	One Factor at a Time
POU	-	Point-of-use system
pTiO_2	-	Pigment Titanium dioxide coated with additions
PWFMF	-	Polyester Woven Fabric Microfiltration
RO	-	Reverse Osmosis
RSA	-	Republic of South Africa
TiO_2	-	Titanium Dioxide
TMP	-	Trans Membrane Pressure
ΔP	-	Pressure differential

LIST OF UNITS

^{O}C	-	Degree Celsius
g	-	Gram
h	-	Hour(s)
L	-	Litre
mg	-	Milligram
mL	-	Millilitre
µm	-	Micrometre

CHAPTER 1

INTRODUCTION

1.1. BACKGROUND

Quality drinking water is the most basic human need, and every human has a right to clean water (Third World Academy of Sciences, 2002). There is still a setback in the accessibility of safe drinking water and it is highly noticeable in developing economies and rural areas, and South Africa is no exception. The natural sources of water are considered not safe for drinking due to contamination or pollution. River water is one of the natural water sources used as drinking water in many rural communities in South Africa.

From a global perspective, the supply of clean drinking water is diminishing, while demand is increasing. An increase in water demand is proportional to an increase in population and industrialization. Most industries are using clean drinkable water for processing of products due to an increasing product demand. In addition, clean drinking water supply is decreasing because of pollution while natural sources of water are decreasing due to global warming.

Global water distribution shows evidence of decreasing water supply whereby the freshwater that is readily available is geographically at a very low percentage of abundant planet water as displayed in Figure 1.1.

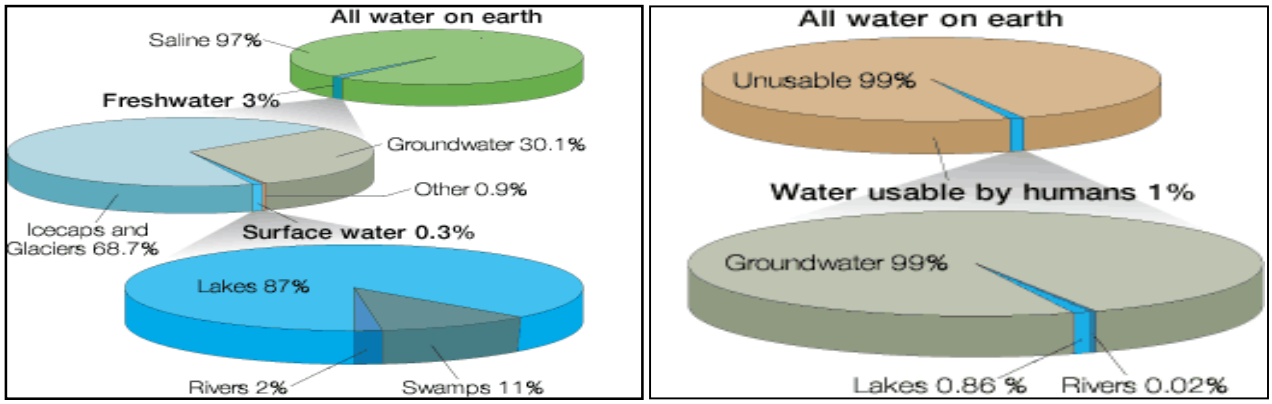

Figure 1.1: (a) The Water Distribution of the Planet, (b) Water available to be used by humans (Mulder, 1998).

The freshwater that is readily available as surface water comes from rainfall, man-made reservoirs, lakes and rivers. The small fractions of natural water sources as shown in Figure 1.1 are contaminated with bacteria and viruses from human and animal excretion due to poor sanitation. Industries contribute to pollution of natural freshwater sources by discharging and emitting their waste that is out of specification into the ground, surface water and air. Fertilizers washed off from farmlands could increase the amount of natural substances already available in water causing pollution. The pollution of natural freshwater sources causes diseases that leads to fatalities and that is why the natural freshwater sources require treatment to break the cycle of diseases (Rand Water, 2014).

The conventional treatment systems in rural areas are considered to be expensive and require time with good infrastructure to install and commission. This is because many of these conventional treatment systems are a combination of coagulation, sedimentation, filtration and disinfection. Even the use of disinfection to purify water for drinking purposes is challenged by effective execution of dosing of chemicals. On the other hand, the population distribution in most rural communities is over a very wide area (Pikwa et al., 2009) which will require long distance piping systems and pumping power. Other challenges to clean water provision is lack of skills for operation and maintenance of water treatment plants, difficult logistics, difficult topographies and most importantly lack of finances (Pikwa et al., 2009).

Small scale treatment systems are the main focus for recent studies in developing systems that are robust, easy to operate and maintain and cost effective. These are decentralized systems that treat potable water just for drinking and cooking for a single household (point-of-use systems) or a community (small-scale systems) (Peter-Varbanets et al., 2009, Pritchard et al., 2009). DeZuane (1997) and Peter-Varbanets et al. (2009) declared the minimum requirement for drinking water, which is about 2 L per person per day and the maximum for drinking and cooking of 8 L per day. Decentralized systems also refer to the point-of entry (POE) systems and small-scale systems (SSS). POE systems deal with all water that is supplied to a household, where the treatment capacity is much higher than that of a POU system (Craun and Goodrich, 1999, Peter-Varbanets et al., 2009). The capacity for the POE is approximately 100 -150 L per person per day. The treatment systems that can be used by several families or a small village usually referred to as SSS. SSS is larger than

the POU and POE but smaller than centralized systems, and the capacity varies between 1000 and 10 000 L per day (Peter-Varbanets et al., 2009).

Photocatalytic oxidation is an alternative potable water solution, which is receiving a lot of attention as a decentralized treatment system. Photocatalytic oxidation is the generation of an electron-hole pair upon irradiation of a catalyst with UV light to mineralize a wide range of organic compounds, viruses and bacteria, and to reduce heavy toxic metals to non-toxic metals. Nano-scaled particles of Titanium dioxide ($nTiO_2$) used in photocatalytic water treatment are well-known as advanced oxidation process (AOP). The TiO_2 is known to be environmentally friendly and it mineralizes organic compounds and bacteria into harmless end-products such as carbon dioxide, water and inorganic salts. The limitation on the practical application of the nano-sized particles of TiO_2 ($nTiO_2$) as a photocatalytic water treatment, is the recovery of the $nTiO_2$.

Thus, the overall aim of the study is to evaluate the photocatalytic activity of the locally produced TiO_2 which is a micro-sized particles (mTiO2) on the degradation of bacteria and organics in river water to produce potable water, and hence optimize the TiO_2 water treatment process.

1.2 PROBLEM STATEMENT

The outbreak of diseases due to direct consumption of contaminated river water and lack of access to running water has propelled interest in the development of small treatment systems. These small treatment systems must provide safe potable water at the lowest possible cost for the rural communities with poor infrastructure. Therefore, this study focused on photodegradation of organics and bacteria in river water using a photocatalyst that is locally produced, cheap and environmentally friendly. This TiO_2 is produced as a micro-scale product. Therefore, the percentage recovery of the particles from treated water was evaluated using the locally manufactured woven fabric membrane. Numerous studies have used a commercial TiO_2 (P-25) which is a final product and little attention has been given to the evaluation of the performance of intermediate forms of TiO_2 within the Sulphate process. This study sampled TiO_2 at different points in the Sulphate process in order to evaluate the photocatalytic activity of these grades of TiO_2 on the degradation of bacteria in river

water. The grades of TiO_2 sampled at the early stages of the process are cheaper to produce than the final product meant for paint manufacturing.

1.3 OBJECTIVES

The main aim of the research was to evaluate the photocatalytic activity of locally produced micro-sized particles of TiO_2 ($mTiO_2$) on the degradation of bacteria and organics in river water for potable water purposes and hence optimize the process variables. The specific objectives were as follows:

- To evaluate the photocatalytic activity of the locally produced $mTiO_2$ on degradation of organic compounds in river water to produce clean potable water.
- To investigate the extent of removal of $mTiO_2$ in treated water using a Polyester Woven Fabric Microfiltration (PWFMF) membrane.
- To investigate the best performing grade of the four grades of $mTiO_2$ on the degradation of E.coli and total coliform bacteria present in river water.
- To investigate the effect of parameters such as temperature, initial pH of the solution, aeration and $mTiO_2$ loading on the degradation of bacteria in river water for portable water purposes by optimizing the process using the Response Surface Methodology (RSM).

This local product is a micro-sized TiO_2 with a particle size range of 0.2 - 0.4 µm produced at Huntsman Tioxide primarily as pigment for paint. This commercial $mTiO_2$ pigment, which is the Rutile form of TiO_2 coated with additions is produced through a Sulphate process. This coated Rutile is widely used as white pigment in products such as paints, coatings, plastics, paper, inks, fibers, food and cosmetics because of its brightness and high refractive index of more than 2.4 (Kuznesof and Rao, 2006). The coated Rutile form of TiO_2 produced at Huntsman Tioxide has not been tested for its photocatalytic activity or ability.

The $nTiO_2$ are well researched and known to be effective photocatalysts. The particle size of TiO_2 used in this study is of a micro-scaled size to overcome the limitation of recovering the $nTiO_2$. Recovered $mTiO_2$ can be reused. However, an increase in particle size from $nTiO_2$ to $mTiO_2$ is likely

to have a reduced photocatalytic activity due to reduced surface area. The $mTiO_2$ has a reduced surface area, which makes it difficult for the adsorption of water and oxygen to form radicals responsible for secondary degradation reactions. Therefore, the loading of the $mTiO_2$ to degrade organics and bacteria will have to be increased in order to obtain acceptable degradation efficiency for drinking water quality. The advantages of using the $mTiO_2$ are that it is locally available and will be easily recovered from treated water when using appropriate membrane size.

1.4 SCOPE

The study focuses on the treatment of river water using $mTiO_2$, which is a locally produced pigment for paint (Rutile type of TiO_2). The $mTiO_2$ is basically used in the study to degrade and mineralize the organics and bacteria in river water. The $mTiO_2$ is then recovered from treated water using PWFMF. The study is divided as follows:

- An overview of water scarcity, pollution and water treatment technologies.
- General idea on Titanium dioxide, production, and its reactions and uses.
- Evaluation of photocatalytic activity of the $mTiO_2$ on degradation of organics since it is locally produced for paint.
- Evaluating the performance of the four (4) grades (samples of TiO_2 taken in the Sulphate process of producing Coated Rutile) of $mTiO_2$ on degradation of bacteria and thereafter select the best performing grade to be used for optimization.
- General discussion on the experimental design methods for the response variables.
- Presentation of the final results and its discussion
- The conclusion and recommendations.

The experimentation for preliminary research particularly, the photocatalytic activity and the performance of the four grades of $mTiO_2$ were carried out in the department of Chemical Engineering DUT on a laboratory bench scale. Thereafter, the best performing grade of $mTiO_2$ was carried out in a pilot scale to optimize the four variables in the photocatalytic degradation of organics and bacteria.

The ranges for the variables used in the experimental design were taken from the literature and preliminary investigations.

1.5 DISSERTATION OUTLINE

The findings of the research study conducted are presented in the following five chapters of the dissertation

Chapter two: The literature review considers general information on the importance of freshwater readily available for use and pollution of these watercourses. The general information on potable water treatment technologies, Titanium dioxide production processes, mechanism of TiO_2 photocatalytic chemistry, factors affecting photodegradation and the design of experiment methods used for optimization and prediction model.

Chapter three: This chapter describes the materials and methods used in the study.

Chapter four: The results and discussion of the final results from the laboratory tests are presented in this chapter.

Chapter five: The optimization of the photodegradation using Design of Experiments is covered in detail in this chapter.

Chapter six: The conclusions and recommendations drawn on the main findings are summarized in this chapter.

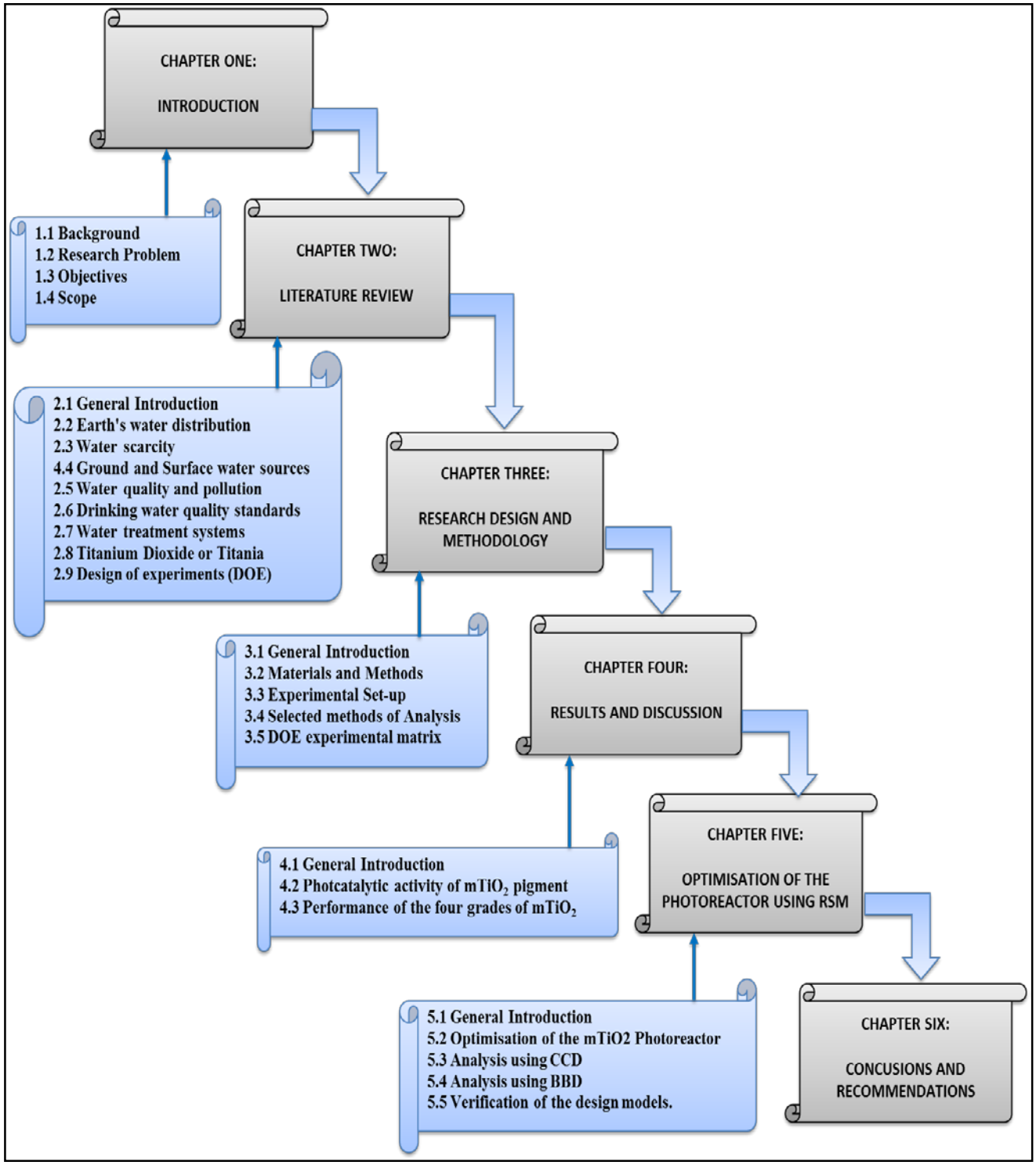

Figure 1.2: Layout of the Dissertation

CHAPTER 2

LITERATURE REVIEW

2.1 GENERAL INTRODUCTION

The background of the research is outlined in this section. The first topics to be discussed are Earth's water distribution, water scarcity and sources followed by the water quality and pollution, drinking water quality standards and water treatment systems. The production of titanium dioxide and its photocatalytic chemistry, and Design of Experiments are also discussed in detail herein.

2.2 EARTH'S WATER DISTRIBUTION

Water in the form of freshwater is fundamental to all living organisms e.g. plants, animals and human beings due to the fact that a certain percentage of our bodies is made up of water. Scientifically, freshwater available to living organisms is just a small fraction of the planet's abundant water. The oceans and other saline water makes up approximately 97.5 % by volume of planet's water. The remaining 2.5 % is freshwater, which is also divided into three parts i.e. 70 % glaciers and ice caps, 29 % groundwater and 1 % surface water (lakes, rivers and streams). Figure 2.1 shows a graphical distribution of the locations of water on Earth (Wikipedia, May 2014) and table 2.1 gives a detail explanation of where Earths water are distributed (Mulder, 1998).

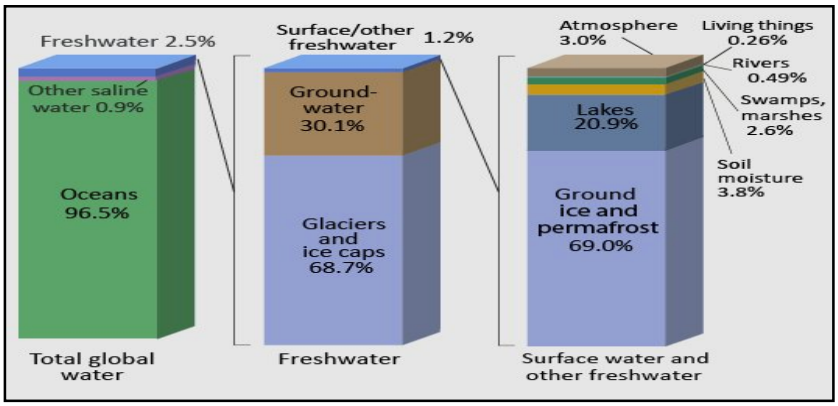

Figure 2.1: The Planet's water distribution (supply) (Phillips, 2010, Wikipedia, 2014b).

The freshwater that is readily available is used for drinking, cooking, industrial production, agriculture and development. The vast increase in population, industrialization and development is proportional to freshwater requirements resulting in increasing demand on this limited supply of planets freshwater. The above users of freshwater also contaminate these natural sources through pollution.

Table 2.1: Estimate of global water distribution (Mulder, 1998, Unit-3, 2013)

Total Area Water source	Volume in miles^3	Volume in kilometers^3	% of Freshwater	% of Total Water
Oceans, Seas, & Bays	321,000,000	1,338,000,000	–	96.5
Ice caps, Glaciers, & Permanent Snow	5,773,000	24,064,000	68.7	1.74
Groundwater	5,614,000	23,400,000	–	1.7
Fresh	2,526,000	10,530,000	30.1	0.76
Saline	3,088,000	12,870,000	–	0.94
Soil Moisture	3,959	16,500	0.05	0.001
Ground Ice and Permafrost	71,970	300,000	0.86	0.022
Lakes	42,320	176,400	–	0.013
Fresh	21,830	91,000	0.26	0.007
Saline	20,490	85,400	–	0.006
Atmosphere	3,095	12,900	0.04	0.001
Swamp Water	2,752	11,470	0.03	0.0008
Rivers	509	2,120	0.006	0.0002
Biological Water	269	1,120	0.003	0.0001
Total	**332,500,000**	**1,386,000,000**	**–**	**100**

Table 2.1 shows that the world's total water supply is about 1,386 million cubic kilometers. It is estimated that over 96 percent is saline. Out of the estimated total freshwater, over 68 percent is locked up in ice and glaciers, and another 30 percent of freshwater is in the ground. Thus, surface-

water sources (such as rivers) only constitute about 93,100 cubic kilometers, which is about 1/700th of one percent of total water, yet rivers are the source of most of the water people use (Mulder, 1998).

2.3 WATER SCARCITY

Out of the small fraction of surface water that is readily available, Africa is still facing water scarcity. Figure 2.2 (a) & (b) show the global water scarcity where most African countries suffer from economic water scarcity with few encountering physical water scarcity. The fact is that Africa is facing or will be facing water scarcity.

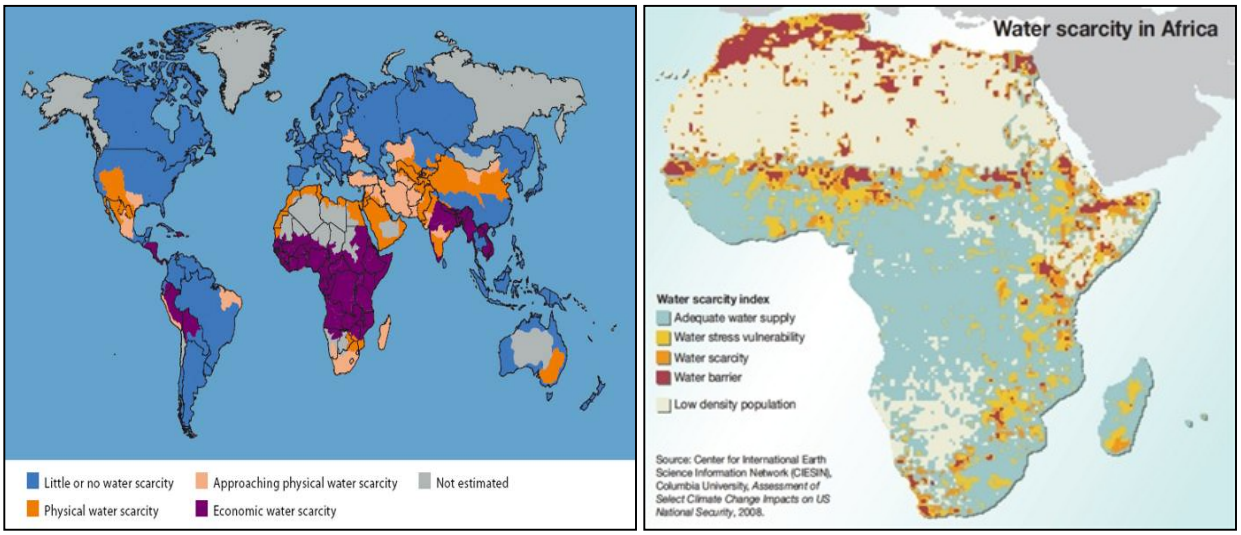

(a). **(b)**

Figure 2.2: (a) Global physical and economical water scarcity, (b) Water scarcity in Africa (World Resources Institute, 2009, Pravettoni, 2011).

Economic water scarcity in most African countries is due to the lack of infrastructure where there is little or no investment in developing water infrastructures. Water resources in the case of economic water scarcity is abundantly available to meet the demand of the communities. Countries that are 'Approaching physical scarcity' are having river water withdrawal of 60% and will soon be facing physical water scarcity in the near future. It is quantified that more than 75% of the river water is withdrawn for agriculture, industries and domestic use in the countries facing physical water scarcity. The water demand is higher than river water availability. Figure 2.2 (a) & (b) show the continent's

water scarcity and water scarcity in Africa. Figure 2.3 (a) shows the higher demanders i.e. industries and agriculture of the freshwater.

Apart from physical water scarcity due to water demand and economic water scarcity due to the lack of investments, there is climate change that is exacerbating water scarcity (Phys Org, August 2014). A study done at the Joint Global Change Research Institute (2009) shows a devastating effect of climate change on water scarcity by 2095 as demonstrated in figure 2.3 (b), if greenhouse gas emissions are not mitigated.

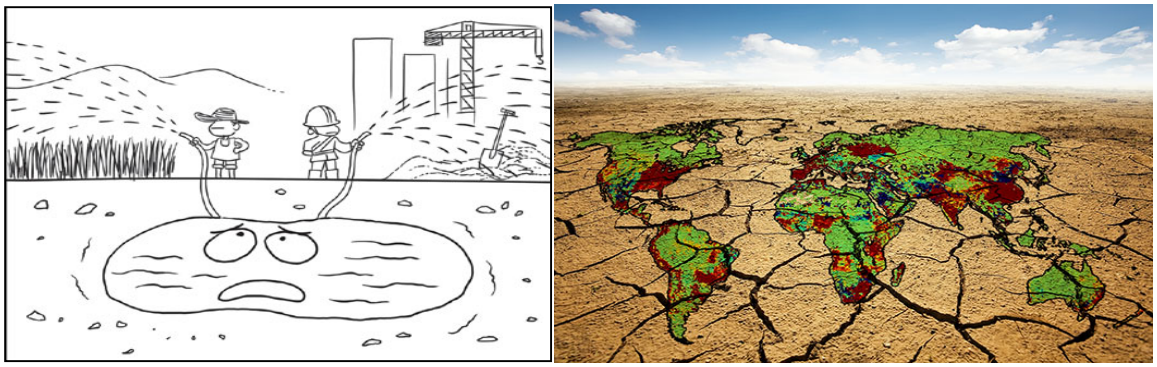

(a). **(b)**

Figure 2.3 (a) & (b): The predicted effect of climate change on water scarcity in 2095 without a curb of carbon emissions (Phys Org, August 2014).

Greenhouse emissions and climate adaptation may also exacerbate water scarcity because growing bioenergy crops (an important component of many technology strategies that reduce greenhouse gas emission) to replace fossil fuel sources require plentiful water (Phys Org, August 2014).

2.4 GROUND AND SURFACE WATER SOURCES

Ground and Surface water are the two main natural water supplies of freshwater. Surface water occurs as rivers, streams, ponds, lakes, and wetlands as shown in figure 2.4 (Haney, 1997). Ground water occurs in the pore spaces within rocks, in-fractures, and in solution openings or conduits in areas underlain by soluble carbonate rocks (Haney, 1997). Although ground water and surface water are referred to as two different things, ground water is the sustaining supply for surface water, and,

surface water often enters or returns to the ground-water system through sinkholes and cave openings (Haney, 1997). Figure 2.4 shows a flowchart of the sources of clean drinking water.

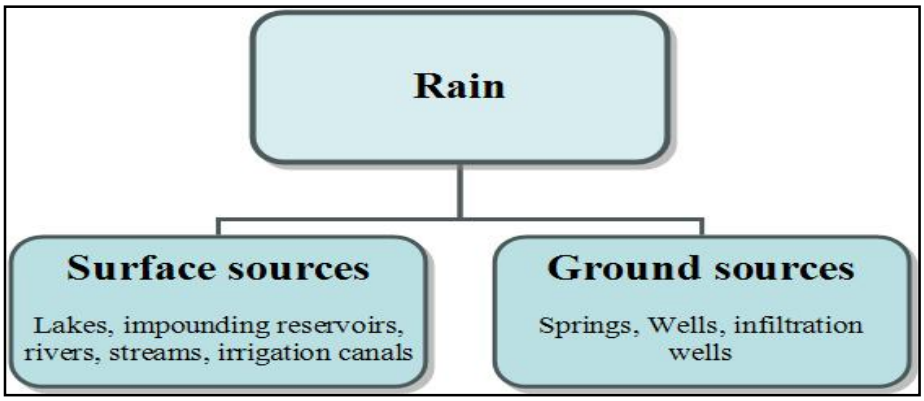

Figure 2.4: A flowchart for the sources of Freshwater (About Civil.org, 2014)

Sophocleous (2002) comprehensively outlined the mechanisms of interaction between groundwater and surface water (GW-SW) as they affect recharge-discharge processes and emphasized on the ecological significance and the human impacts on the interactions. The link between GW-SW is best indicative in hydrologic Cycle in figure 2.5.

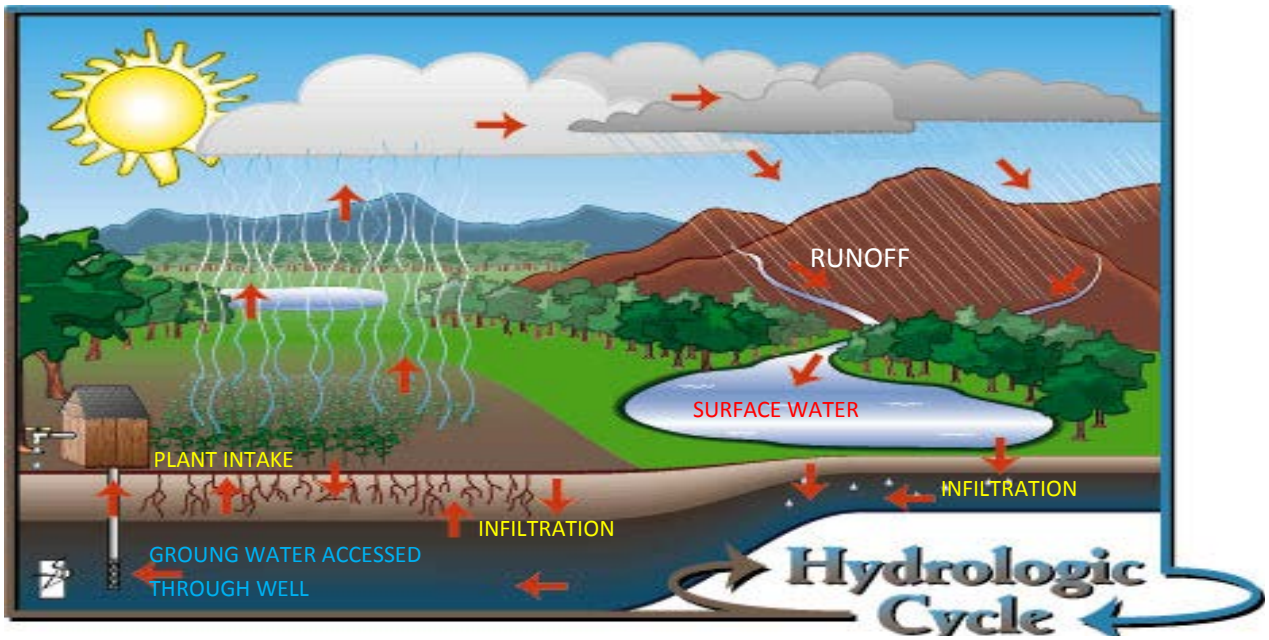

Figure 2.5: Hyrologic Cycle (Phillips, 2010)

Formerly, ground water and surface water were regarded as clean sources of freshwater and were adequately safe for drinking and cooking purposes. These water sources are now contaminated and are becoming scarce due to climate change and demand with less return flow to the sources. Previously, there was no need for treatment systems or cleaning water regimes because natural water sources had fresh clean water more especially in rural areas.

Currently, these freshwater sources are highly contaminated or polluted and need to be treated before utilization for human consumption. Contamination is due to the rainwater (acid rain water) from roofs, lands and roads that runoff into the rivers. This runoff water picks-up toxic chemicals, dirt and disease carrying organisms along the way. It can be well said that everything that happens in a catchment area is reflected in the quality of the water that flows through it, because the results of human activity and lifestyle ultimately end up in rivers, through runoff (Rand Water, 2014).

2.5 WATER QUALITY AND POLLUTION

Water that is safe, drinkable and appealing to all life on earth is characterized as quality water (Rand Water, 2014). Therefore, water quality is used to describe the condition of the water, including its chemical, physical and biological characteristics, usually with respect to its suitability for a particular purpose (i.e., drinking, swimming or fishing) (Diersing, 2009).

Water pollution can then be described as contamination of water bodies (e.g. lakes, rivers, oceans, aquifers and groundwater) and it occurs when pollutants are directly or indirectly discharged into water bodies without adequate treatment to remove harmful compounds (Wikipedia, 2014a). Water flowing on and through the heart of the surface has an ability to react with the minerals that occur in the soil and rocks and, to dissolve a wide range of materials and ends up with its natural state not being pure (LennTech, 1998-2014).

It is well documented that water always contains a variety of soluble inorganics, soluble organics and organic compounds and in addition, water can carry large amounts of insoluble materials that are held in suspension (LennTech, 1998-2014). The quantities and type of impurities in natural water

depends on the place, seasons of the year and other factors which include geology, climate, topography, biological processes and land use (LennTech, 1998-2014, Ritter *et all*, 2002, Sophocleous, 2002).

Rivers can also be polluted by fertilizers washed from farmlands although it is made of chemicals that do occur naturally in the environment, but only in small amounts. Chemical components of fertilizers are used by Algae to grow and multiply, rapidly turning the water green and that leads to pollution (Ritter *et all*, 2002). When the algae die they are broken down by the action of the bacteria which quickly multiply, using up all the oxygen in the water which leads to the death of many animals (LennTech, 1998-2014a).

Human sewage or cattle excrement has the same pollution effect as fertilizers, although human sewage also contains germs that cause diseases such as hepatitis and cholera (Rand Water, 2014). Soaps and washing detergents contain both natural and manmade (artificial) chemicals and the natural chemicals can cause a pollution problem similar to that caused by fertilizers (Rand Water, 2014).

2.5.1 Health Effect of Microorganisms Present in Freshwater

Rand Water (2014) documented that most diseases in the world are related to water and sanitation, and this cycle of disease can be broken by improving the quality of water that people use. Rand Water (2014) also documented the fact that most rural communities in South Africa do not have access to running water, toilets or latrines and they use watercourses for defecation and urination. The faecal pollution due to defecation and urination into natural water sources increases the risk of infection of various diseases to those using that water as their life supporting water source. Amongst the many water-related diseases, South Africa's most common are Bilharzia which is mostly found in the Northern Province, the Lowveld and KwaZulu-Natal, Malaria which is found in the Northern Province, Mpumalanga, Northern KwaZulu-Natal and parts of the northern Cape, and Cholera which can be found in most places where there is poor sanitation (Rand Water, 2014).

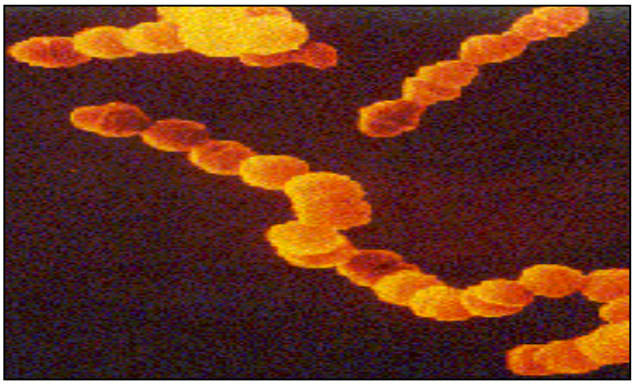

Figure 2.6: A string of Microorganisms (LennTech, 1998-2014b)

Microorganisms as shown in figure 2.6 are well known as the perpetrators of many health effects instigated through contaminated drinking water. For example, the bacteria Legionella can cause legionellosis, a lung disease and the cryptosporidium parasite is the cause of gastrointestinal diseases (LennTech, 1998-2014a). Table 2.2 summarizes various health effects and types of organisms causing diseases.

Table 2.2: Various health effects and their causes (LennTech, 1998-2014b).

Type of organism	*Disease*	Effects
Bacteria	*Typhoid fever*	Diarrhea, severe vomiting, enlarged spleen, inflamed intestines; often fatal if untreated
	Cholera	Diarrhea, severe vomiting, dehydration; often fatal if untreated
	Bacterial dysentery	Diarrhea; rarely fatal except in infants without proper treatment
	Enteritis	Severe stomach pain, nausea, vomiting; rarely fatal
Viruses	*Infectious Hepatitis*	Fever, severe headache, loss of appetite, abdominal pain, jaundice, enlarged liver; rarely fatal but may cause permanent liver damage
Parasitic protozoa	*Amoebic dysentery*	Severe diarrhea, headache, abdominal pain, chills, fever; if not treated can cause liver abscess, bowel perforation and death
	Giardiasis	Diarrhea, abdominal cramps, flatulence, belching, fatigue
Parasitic worms	*Schistosomiasis*	Abdominal pain, skin rash, anaemia, chronic fatigue, chronic general ill health

The well-known indicator of water quality is oxygen. The aquatic organisms use dissolved oxygen for their survival. Oxygen also affects other water indicators such as biochemical and aesthetic, which are odor, clarity and taste of water (LennTech, 1998-2014a).

2.6 DRINKING WATER QUALITY STANDARDS

The suitability of drinking water quality is managed and accepted based on national standards and international drinking water guidelines. The guidelines and standards are used to provide safe and acceptable water quality defined in terms of microbiological, chemical, aesthetic and physical aspects at the point of delivery. The drinking water shall comply with the physical, aesthetic, chemical and microbiological numerical limits for lifetime consumption specified in Table 2.3 (South African National Standard, 2011) (World Health Organisation, 2011).

Table 2.3: Drinking water quality guidelines on physical, aesthetic, chemical and microbiological determinands (World Health Organisation, 2011) (South African National Standard, 2011).

Determinand	Unit	Standard limits	
		SANS 214-1 Standards	WHO Guidelines
Physical and aesthetic quality determinands			
Colour	mg/L Pt-Co	≤ 15	≤ 15
Odour or taste	-	Inoffensive	
pH at 25 ^{0}C	pH units	≥ 5 to ≤ 9.7	≥ 6. to ≤ 8
Total dissolved solids	mg/L	≤ 1 200	≤ 1000
Turbidity	NTU	≤ 1	≤ 1
Chemical quality determinands - macro-determinands			
Ammonia as N	mg/L	≤ 1.5	≤ 1.5
Chloride as Cl^-	mg/L	≤ 300	≤ 250
Fluoride as F^-	mg/L	≤ 1.5	≤ 1.5
Nitrate as N	mg/L	≤ 11	≤ 50
Nitrite as N	mg/L	≤ 0.9	≤ 0.2
Sodium as Na	mg/L	≤ 200	≤ 200
Sulfate as SO_4^{2-}	mg/L	≤ 500	≤ 250
Titanium Dioxide as TiO_2	mg/L	Not specified	Not specified
Zinc as Zn	mg/L	≤ 5	≤ 5
Chemical quality determinands - micro-determinands			
Aluminium as Al	µg/L	≤ 300	≤ 200
Antimony as Sb	µg/L	≤ 20	≤ 20
Arsenic as As	µg/L	≤ 10	≤ 10
Cadmium as Cd	µg/L	≤ 3	≤ 3
Copper as Cu	µg/L	≤ 2 000	≤ 200
Cyanide (recoverable) as CN^-	µg/L	≤ 70	≤ 70
Iron as Fe	µg/L	≤ 2 000	≤ 2 000
Lead as Pb	µg/L	≤ 10	≤ 10
Manganese as Mn	µg/L	≤ 500	≤ 400
Mercury as Hg	µg/L	≤ 6	≤ 6
Nickel as Ni	µg/L	≤ 70	≤ 70
Selenium as Se	µg/L	≤ 10	≤ 10
Titanium Dioxide as TiO_2	µg/L	Not specified	Not specified
Total chromium as Cr	µg/L	≤ 50	≤ 50
Uranium as U	µg/L	≤ 15	≤ 15
Microbiological quality determinands			
Cytopathogenic viruses	Count/10 L	0	0
E. coli	Count/100 mL	0	0
Faecal Coliforms	Count/100 mL	0	0
protozoan parasites	Count/10 L	0	0
total coliforms	Count/100 mL	≤ 10	0

This study on the photocatalytic degradation of organic materials and bacteria focused on the treatment of river water, which is used by many rural communities in South Africa as their life supporting water source. The most important contaminant to be determined or managed and treated in rural water sources is faecal matter due to the lack of toilets or latrines and the use of watercourses for defecation and urination (Rand Water, 2014).

This study focused on degradation of organic compounds and mineralization of bacterial because the photocatalyst, which is TiO_2, has an ability to purify water and air, reduce toxic metals to safe metals, to degrade organic materials and mineralizing bacteria and viruses. Although, it is expected that the chemical contamination might be relatively low in rural areas due to low industrial activities, the study also focused on determining the degradation of organic materials.

2.6.1 Disinfection of river water

Since most watercourses through our rural communities contain microbiological contaminants, disinfection of these watercourses before use is the most important aspect of drinking water quality. Membrane technology specifically MF and UF has been used as water disinfectant. This is done by using a membrane with a pore size less than the size of the microorganisms. The attachment of smaller viruses to larger or other particles makes the membrane technology a possible disinfectant. Achisa (2013) noted and mentioned a major drawback on MF membranes where some bacteria tends to break-through the membrane after a period of time. According to Achisa (2013) the drawback on MF membrane can be prevented by cleaning the membrane regularly (Achisa, 2013).

Escherichia coli (*E. coli*), Chemical Oxygen Demand (COD) and turbidity are the parameters of interest in this study and are limited as follows.

2.6.1.1 Turbidity of the water and $mTiO_2$ concentration

Turbidity is used to indicate physical contaminants like suspended matter in treated water (World Health Organisation, 2011, LennTech, 1998-2014). It is also used as an indication for concentrations of $mTiO_2$ in treated water after being filtered through PWFMF, e.g. high turbidities indicate higher concentrations of $mTiO_2$ and low turbidities is an indication of low concentration of $mTiO_2$. Turbidity of less than 1 NTU is a desired target and it indicates low $mTiO_2$ concentrations in treated water, which makes treated water by photocatalytic $mTiO_2$ acceptable for drinking.

2.6.1.2 Chemical Oxygen Demand (COD)

The main reason for the treatment of river water is to have clean drinking water that is acceptable for human consumption defined in terms of chemical determinants (World Health Organisation, 2011, South African National Standard, 2011). Sources of chemical contaminants in river water include industrial effluent and run off from farms that are using fertilizer (LennTech, 1998-2014, Ritter *et all*, 2002). These chemicals use up oxygen in water to react and forming complex chemical structures (World Health Organisation, 2011). The demand in which oxygen is required by other species other than the water habitat is indicated by measuring the COD.

2.6.1.3 *E. coli* concentration

Escherichia coli indicate recent faecal pollution of which the normal habitat of *E. coli* is the large intestine of humans and animals (South African National Standard, 2011). This *E. coli* enters the watercourses when human and animals use watercourses for defecation and urination. These *E. coli* organisms are referred to as indicator organism and they show the presence of pathogens (Schutte and Focke, 2006, Achisa, 2013). Potable water should be free of *E. coli* as indicated in table 2.3 of standards.

2.7 WATER TREATMENT SYSTEMS

2.7.1 Conventional Technology

Many water treatment plants employ a combination of coagulation, sedimentation, filtration and disinfection for the provision of clean, safe drinking water to the public (Safe Drinking Water Foundation, 2014). A flow diagram of the conventional water treatment is shown in figure 2.7. It shows the combination of the first three steps used primarily to remove colloids (including some microorganisms) and natural organic matter (NOM). The following step which is 4 (rapid sand filtration) is a polishing step that removes much of the colloidal material remaining after step 3 (sedimentation) (Leckie et al., 2004).

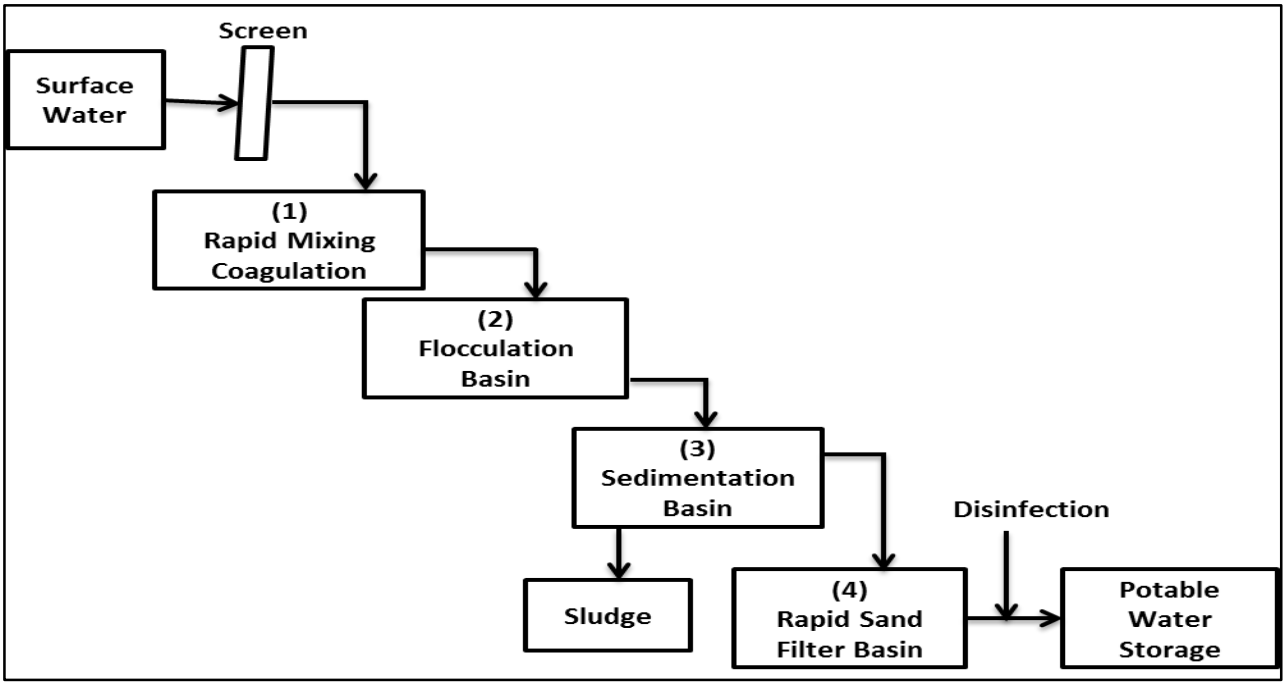

Figure 2.7: Flow diagram of a conventional potable water treatment plant (Leckie et al., 2004).

Leckie et al. (2004) reported that systems outlined in Figure 2.7 can provide good quality, potable water and the design is well understood. It is also well known that there is sludge discharge associated with the system that must be carefully handled to prevent pollution, which may result in surface water pollution and may cause air pollution.

A summary of a conventional treatment process is that in coagulation, a coagulant (usually an iron or aluminum salt) is added in water in order to combine small particles to form big particles as illustrated in figure 2.8.

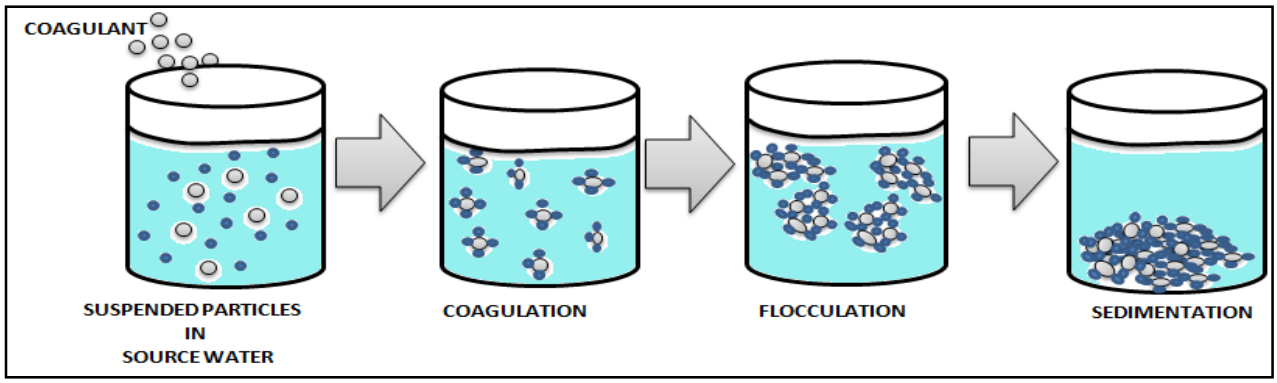

Figure 2.8: Coagulation, flocculation and sedimentation in a conventional treatment process.

Since small particles take a longer time to settle, coagulant is used to form bigger particles that settle faster as the approximate settling time of various particle size diameters in water is shown in table 2.4.

Table 2.4: Settling Time for Particles of Various Diameters (Peterson, 2001).

Diameter of Particle	Type of Particle	Settling time through 1 m. of water
10mm	Gravel	1 seconds
1mm	Sand	10 seconds
0.1mm	Fine Sand	2 minutes
10 micron	Protozoa, Algae, Clay	2 hours
1 micron	Bacteria, Algae	8 days
0.1 micron	Viruses, Colloids	2 years
10 nm	Viruses, Colloids	20 years
1 nm	Viruses, Colloids	200 years

The formation of big particles is termed flocculation. The flocculants then settle to the bottom to form sludge in a process called sedimentation. Suspended particles that do not settle during sedimentation are removed in a subsequent step of filtration.

The commonly used filters in the conventional treatment process are dual-media filter comprising of anthracite and sand, mono-media (sand), multi-media (garnet, anthracite, and sand), and other media configurations which include the use of granular activated carbon (United States Environmental Protection Egency, 2014). The conventional filtration process improves turbidity and colour, while coagulation and flocculation also treat Guardia and Cryptosporidium, bacteria, and viruses by trapping them to settle with the flocculants (Peterson, 2001, United States Environmental Protection Egency, 2014).

Coagulation and most disinfection processes require chemical addition, which needs to be carefully administered to obtain quality water suitable for human consumption (Pillay and Jacobs, 2005, Pillay and Commission, 2009). The conventional treatment process is long, and expensive to design and install more especially for rural communities (Pillay and Commission, 2009).

2.7.2 Membrane Technology Overview

Membrane technology is a separation technology that has gained its popularity in water treatment and water reuse because membranes treat water without the addition of chemicals (Thuy, 2010, Schwinge et al., 2004). In most of the separation processes, membranes have been used to clean groundwater, surface water and wastewater (Pillay et al., 2007, Pearce, 2007). A membrane acts as an inter-phase separating two phases and selectively controlling the transport of materials between the phases as in figure 2.9 (a) & (b). A membrane is therefore used as a selective barrier that allow certain entities (i.e. water) to pass through it while retaining other entities such as suspended solids and other impurities (Persahd, 2003). In figure 2.9 (a), phase 1 is the feed water with contaminants (suspended and dissolved) and phase 2 is permeate or filtrate (water and small particles). The driving force for the separation to take place can be created by the difference in pressure, concentration, temperature or electrical potential as presented in table 2.5 that illustrates membrane classifications (Pillay and Jacobs, 2005).

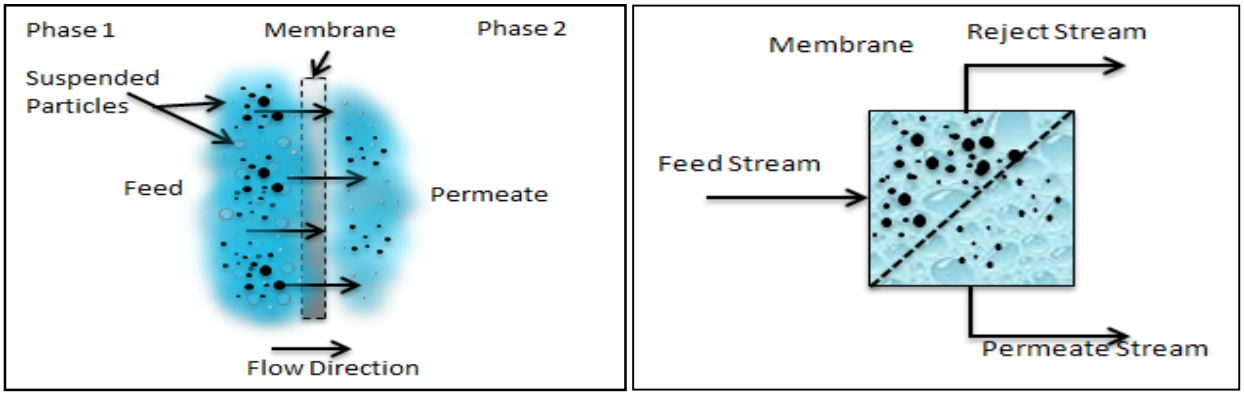

(a). **(b)**

Figure 2.9 (a) & (b): The use of a Membrane as an inter-phase between two phases (Feed and Permeate)

The membrane technology is now believed to be very competitive to the conventional techniques with a relatively low energy use with an easy and well-arranged process operation (Winston Ho and Sirkar, 2001). Membrane filtration provides the possibility of producing a very high quality of treated water, and membrane systems are in a modular form which enables easy adaptation of process scale (Thuy, 2010, Peter-Varbanets et al., 2009). Membrane Filtration is divided into four processes (from small to large pore size), which are Reverse Osmosis, Nano-filtration, Ultra-filtration and Micro-filtration. Each membrane filtration process has a pore size that removes certain size range contaminants (Ní Mhurchú, 2008).

2.7.2.1 Classification of Membrane Processes

The membrane processes are classified according to size range of materials they are to separate, driving force used in the separation, solubility, charge, etc., depending on the type of membrane process used (Baker, 2002, Winston Ho and Sirkar, 2001). They may be applicable for the purification (removal of unwanted contaminants), concentration and fractionation (separating a mixture into two or more components), see Table 2.5. Membranes used for the pressure driven separation processes are Reverse Osmosis (RO), Nano-Filtration (NF), Ultra-Filtration (UF) and Micro-Filtration (MF), and are most often made from Polymers. The advanced Polymers have improved chemical stability and resistance to microbial degradation (Pearce, 2007). Table 2.6 summarizes the application of various membrane processes.

Table 2.5: Membrane Processes Classification (Winston Ho and Sirkar, 2001, Baker, 2002, Mulder, 1996)

Membrane Process	Separation Potential	Pore Size	Driving Force (bar)
Reverse Osmosis	Aqueous low mass solutions and organic solutions	<1 nm	10-80
Nano-Filtration	Low to medium molar mass solutions	2-1 nm	3.0-20
Ultra-Filtration	Macromolecular solutions, emulsions	100-2 nm	1.0-10
Micro-Filtration	Suspensions	>0.1 µm	1.0-2.0
Pervaporation	Organic mixtures, organic aqueous mixtures	-	Difference on partial pressure and saturation pressure on permeate side
Liquid Membranes	Aqueous low mass solutions and organic solutions	-	Concentration difference
Electro-dialysis	aqueous solutions	-	Electrical Potential gradient
Osmosis	aqueous solutions	-	Concentration difference
Dialysis	aqueous solutions	-	Concentration gradient

RO is used in the removal of very fine particulates including bacteria, viruses and protozoan producing effluent with turbidities less than 0.3 NTU (Thuy, 2010). RO has become much more attractive in the treatment of seawater or brackish water, which is approximately 96 -97 % of planet's water as illustrated in figure 2.1 and table 2.1.The treatment units based on RO that are used to treat seawater requires influents with turbidities less than 1 NTU, therefore, pre-treatment is essential (Thuy, 2010).

Table 2.6: Application range of various membrane processes (Pearce, 2007)

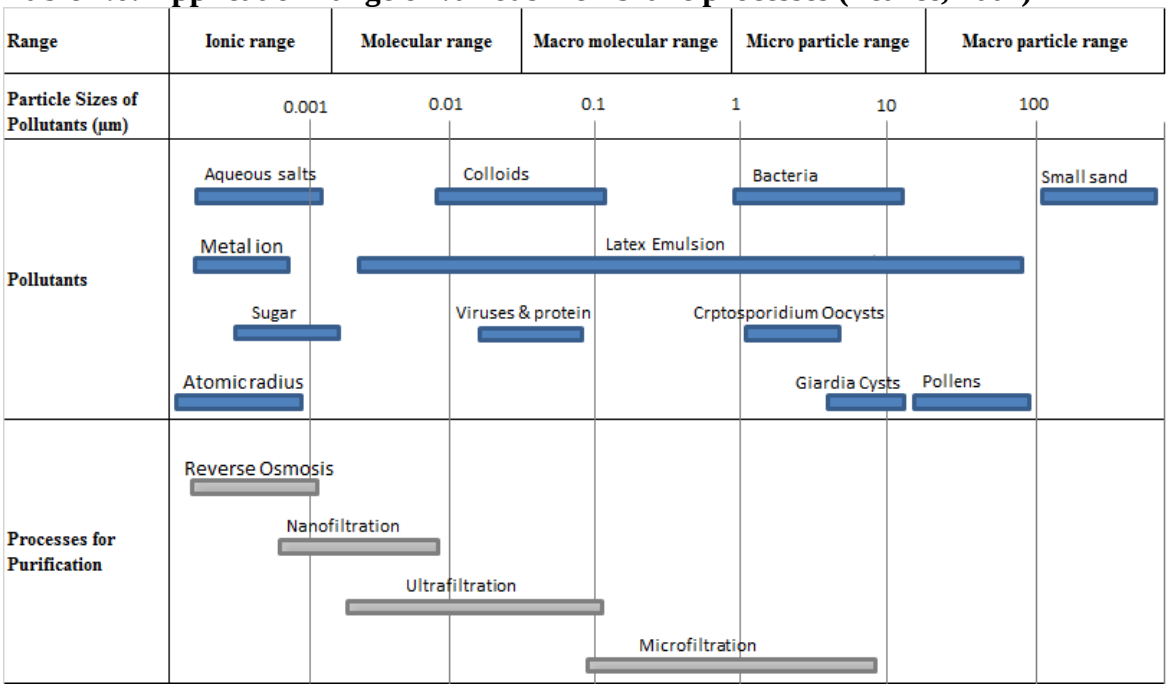

The RO unit require high pressure to drive permeate through the membrane, which means high-energy requirement. NF can be regarded as a "loose" RO process, where mono-valent charges can travel through the membrane however, the multivalent ions are rejected (Pearce, 2007). The essential difference between RO and NF relates to the size of the rejected entities as shown in table 2.6, where RO rejects mono-valent ions. The pressure requirement of the NF to drive permeate through the membrane is less than that of the RO unit (Mulder, 1996).

UF membranes have the ability to completely retain pathogens (Mulder, 1996). On the other hand, the pressure requirements of UF membrane are less than the RO membrane because the osmotic pressure counteracting water pressure through RO membrane is higher than that of UF membrane (Thuy, 2010). MF and UF deal with a physical separation in a way that the dissolved solids, turbidity and microorganisms removed are determined by the size of the pores in the membrane (Thuy, 2010, Mulder, 1996). Particles larger than the pores of the membrane are fully removed, while smaller particles are partially removed. They are pressure dependent processes, which remove substances from water to a lesser extent than NF and RO.

2.7.2.2 Modes of Operation of Membrane

There are two modes of membrane filtration operation, which are dead end and cross-flow as illustrated in figure 2.10 (a) & (b).

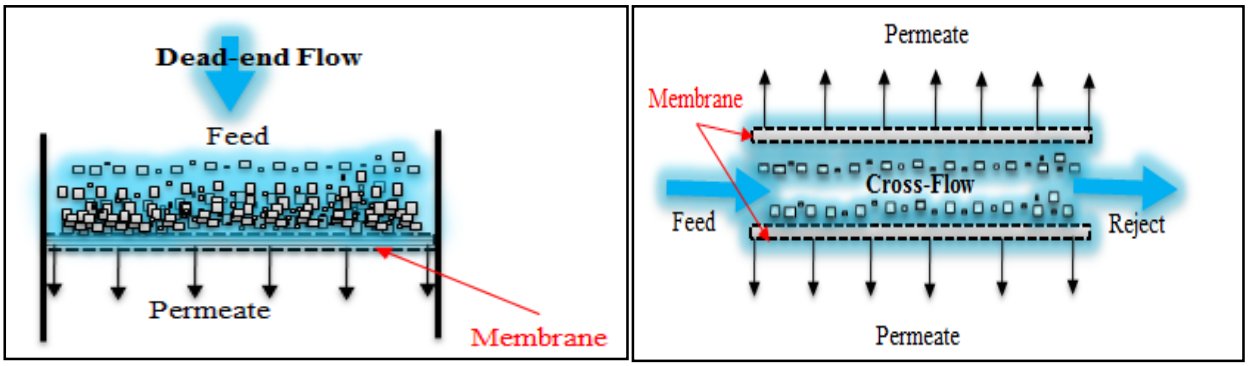

(a). **(b)**

Figure 2.10: Process Flow for Micro-filtration: (a) Dead –end flow, (b) Cross-flow (Ní Mhurchú, 2008).

The two modes of operation are mostly used in microfiltration membranes. In dead-end microfiltration, the feed suspension flows perpendicularly to the membrane as shown in figure 2.10 (a) (Ní Mhurchú, 2008). Solids in the feed that are larger than the pore size of the membrane deposit on the membrane surface forming a cake of solids. The liquid that passes through the membrane is called the filtrate or permeate (Ní Mhurchú, 2008). Most dead-end filtration processes are carried out in a batch mode, therefore the mass of the filter cake grows until all the particles are deposited or until the capacity of the filter has been reached, in which case further filtration is not possible (Ní Mhurchú, 2008).

Dead-end has a high collection rate (almost 100%), low cost, and backwashing and chemical cleaning is not required (Pillay et al., 2007). There is a continuous increase in resistance due to increase in cake thickness and flux decreases with time. The flux can be regained by removing the cake layer and cleaning the membrane as illustrated by figure 2.11 (a) (Pillay and Jacobs, 2005).

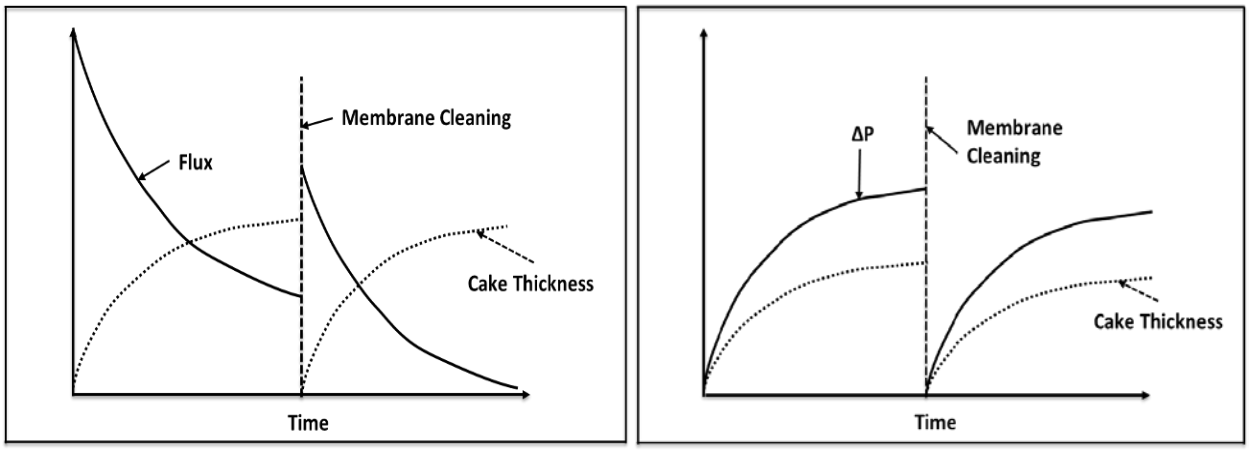

(a). **(b)**

Figure 2.11: Schematic representation of (a) flux and cake thickness for constant pressure dead-end filtration (b) TMP and cake thickness for constant flux dead-end filtration (Winston Ho and Sirkar, 2001, Achisa, 2013)

The pressure differential (ΔP) across the dead-end membrane filtration for constant flux needs to be increased due to an increase in cake thickness as shown in figure 2.11 (b). ΔP decreases after cake removal and membrane cleaning (Pillay and Jacobs, 2005). Dead-end operation requires substantially low capital and operating energy, however, the permeate fluxes are usually lower. Dead-end is generally only applicable when the feed stream has a low concentration of contaminants (Pillay and Jacobs, 2005).

In crossflow microfiltration, (CFMF), the feed suspension flows tangentially to the membrane surface (Ní Mhurchú, 2008). CFMF is operated with two effluent streams: a permeate stream (or filtrate stream) and a retentate stream (Ní Mhurchú, 2008). Only a part of the feed suspension passes through the medium as recovered product (permeate), and the other part flows tangentially along the membrane surface (retentate) as shown in figure 2.10 (b) (Ní Mhurchú, 2008). The advantages of the CFMF is that it has a low filter maintenance frequency, it can be used even if the large amounts of insoluble materials are included and can be used for viscous liquids, and it can be reused with backwashing and chemical cleaning (Pillay and Jacobs, 2005). It has a low collection rate with relatively high cost. The cake layer does not build up indefinitely because the high shear applied by the feed flowing tangentially to the membrane surface removes the deposited particles on the way to exiting the membrane so that the cake remains thin as shown in figure 2.12 (David et al., 1992).

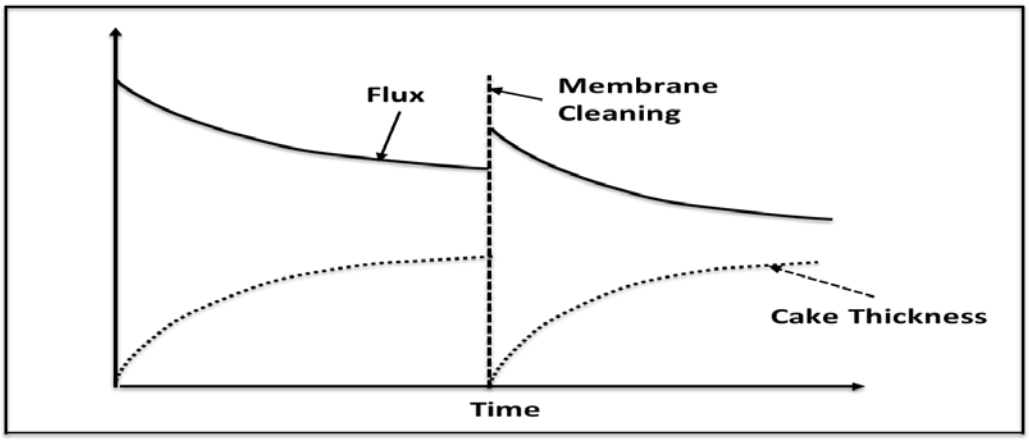

Figure 2.12: Schematic representation of the flux and cake thickness for cross-flow filtration (Winston Ho and Sirkar, 2001, Ní Mhurchú, 2008, Achisa, 2013).

Cross-flow operation usually produces high fluxes, however, there is greater capital costs and energy requirements. It is usually essential if the feed water has a very high level of contaminants or high turbidity (Pillay and Jacobs, 2005).

2.7.2.3 Immersed Membrane Microfiltration (IMM)

The membranes are submerged in the feed suspension as shown in figure 2.13 (a) & (b). In IMM, permeate is sucked through the membrane walls either by a pump or gravity head leaving the contaminants in the feed suspension.

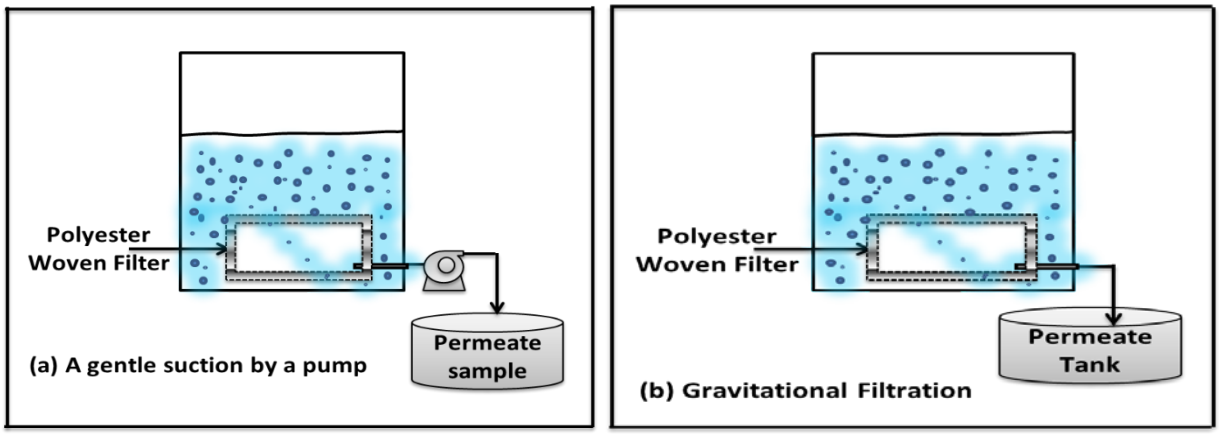

(a) . (b)

Figure 2.13: Schematic representation of Immersed Membrane (a) A gentle suction of permeate by pump, (b) Filtration by gravity head.

Hence, permeate flow occurs from the outside of the membrane into the membrane, in contrast to conventional membranes where permeate flow occurs from the inside to the outside as shown in Figure 2.14 (Pillay and Jacobs, 2005).

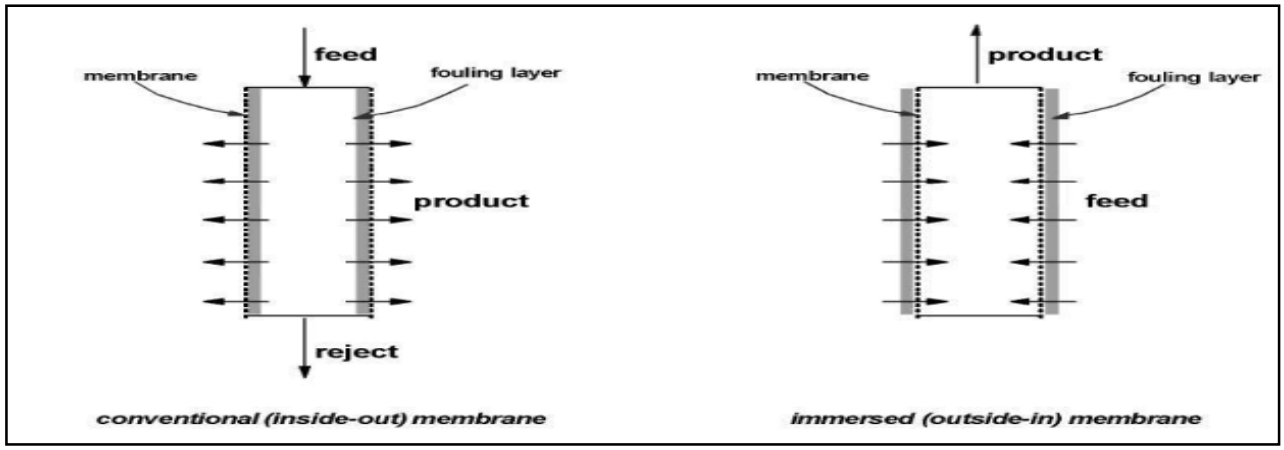

Figure 2.14: Fluid flow in Cross-flow and Immersed Membranes (Pillay and Jacobs, 2005).

In immersed membrane systems, permeate flows through the walls of the membrane from the outside to the inside (Pillay and Jacobs, 2005). This permeate flow causes contaminants to accumulate at the outer wall of the membrane, forming a fouling layer which increases the hydrodynamic resistance to permeate flow. This increased resistance manifests either as an increase in the differential pressure across the membrane (TMP), or as a decrease in the permeate flux (Pillay and Jacobs, 2005, Pillay et al., 2007).

Constant pressure and constant flux operations are the two extreme operating modes for IMM (Pillay and Jacobs, 2005). The differential pressure across the membrane is maintained at a steady value in constant pressure operation. Therefore, the permeate flux turns to decrease as the resistance of the fouling layer increases with time. The permeate flux decreases until an unacceptable low value is reached, then the membrane has to be cleaned to remove the fouling layer and that restores the permeate flux as illustrated in figure 2.15 (a) (Pillay and Jacobs, 2005).

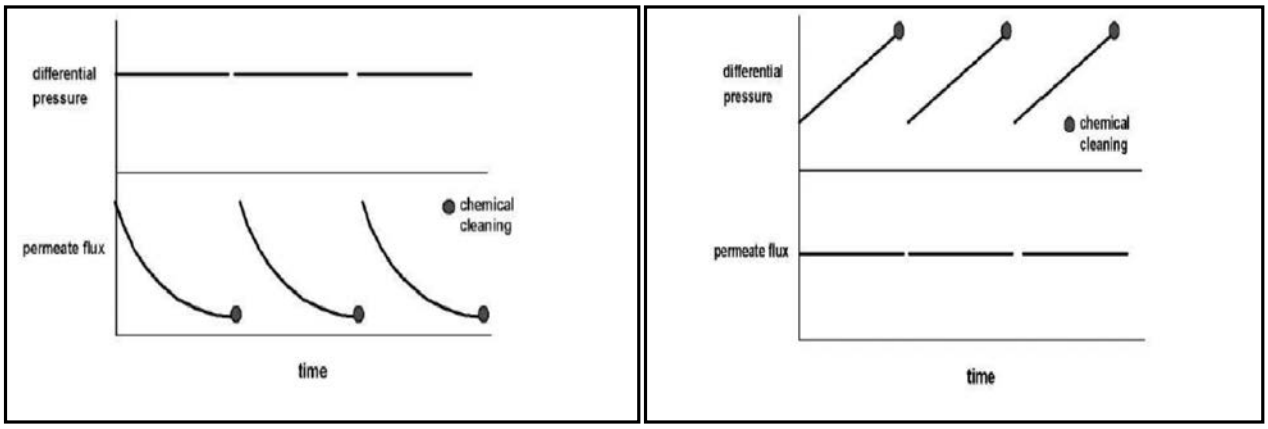

(a). **(b)**

Figure 2.15: (a) Constant Pressure Operation, (b) Constant Flux Operation (Pillay and Jacobs, 2005)

The permeate flux is maintained at a steady value in the constant flux mode while the TMP across the membrane increases with time as the resistance of the fouling layer increases in figure 2.15 (b). The membrane has to be cleaned when the TMP reaches a high value. The cleaning is carried-out to remove the fouling layer and that restores a lower TMP. One physical limitation to the TMP is the vapour pressure of the feed liquid, because when the TMP approaches the vapour pressure, the liquid will boil (Pillay and Jacobs, 2005).

2.7.3 Strategies to reduce fouling

If fouling could be controlled or reduced, the operating time before cleaning could be extended. According to Pillay and Jacobs (2005) a common method of reducing the rate of fouling is to use air bubbles to scour the outer wall of the membrane and this approach is employed by two of the current market leaders in IMM systems, namely Zenon and Kubota. Air diffusers are usually placed strategically below the immersed membrane(s) for coarse air bubbles forming at the diffusers to rise through the membrane scouring the surface of the membrane (Li et al., 2002, Liu et al., 2012). This reduces the fouling layer. The efficiency of air scouring is a function of the bubble size, bubble rise velocity, interaction with the membrane surface etc., all of which are very strictly dependant on scale (Liu et al., 2012, Pillay and Jacobs, 2005). Hence, in practice, any air scouring strategy cannot be

determined on a laboratory scale and extrapolated to larger scales. Development of the strategy must occur on a "slice" of a full-scale reactor (Pillay and Jacobs, 2005).

According to Pillay and Jacobs (2005) backflushing is commonly used in inside-out capillary and hollow fibre membrane systems, and applies equally well to outside-in (immersed) membrane systems. When doing backflushing the direction of permeate flow is periodically reversed (Staff, 2011, Mallevialle et al., 1996). Which causes foulants to detach from the fouling layer and be swept out into the reject stream or bulk fluid. In general, backflushing cannot remove all foulants. Over time there will be a build-up of residual fouling which will eventually necessitate chemical cleaning (Mallevialle et al., 1996). Therefore, it can be concluded that backflushing serves to increase the time between chemical cleans (constant pressure and constant flux operation), and can also increase the permeate production (constant pressure operation only) as illustrated in figure 2.16 (Pillay and Jacobs, 2005). Both air scouring and backflushing can be combined and used to reduce fouling.

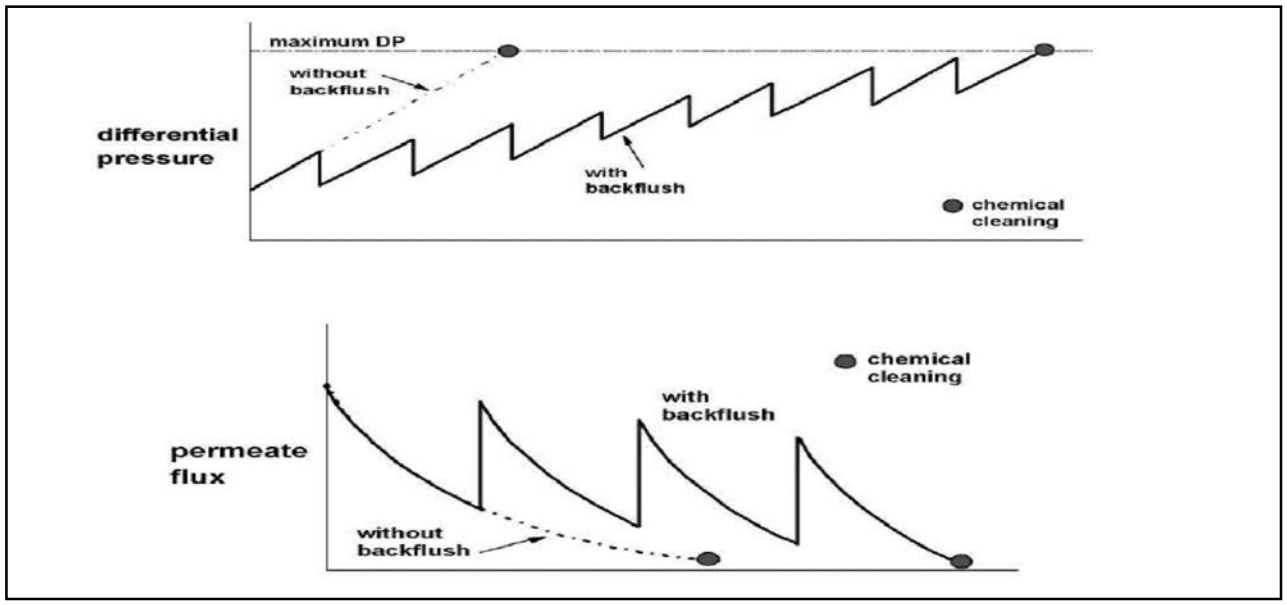

Figure 2.16: Effect of backflushing (Pillay and Jacobs, 2005).

This project study is using aeration to evaluate the effect of aeration on Photocatalytic degradation, which also works as air scouring to the immersed membrane. Since gravitational filtration is used, the membrane is washed with a brush and reused.

2.8 TITANIUM DIOXIDE OR TITANIA

Titania is a very well-known and well-researched material due to the stability of its chemical structure, biocompatibility, physical, optical, and electrical properties (Beydoun et al., 1999, Macwan et al., 2011, Hanaor and Sorrell, 2011). It exist in three different crystal forms, which are anatase, rutile and Brookite (figure 2.17 (a), (b), (c) & (d)) (Macwan et al., 2011). It is produced either in anatase or rutile crystal form. The anatase form is produced as a white powder while various grades of rutile are off-white and can even exhibit a slight colour which affects light reflectance (Kuznesof and Rao, 2006). Titanium dioxide may be coated with small amount alumina and silica to improve technological properties (Kuznesof and Rao, 2006). Anatase type TiO_2 has a crystalline structure that corresponds to the tetragonal system with di-pyramidal habit as shown in figure 2.17 (b) (Smyth and Bish, 1988).

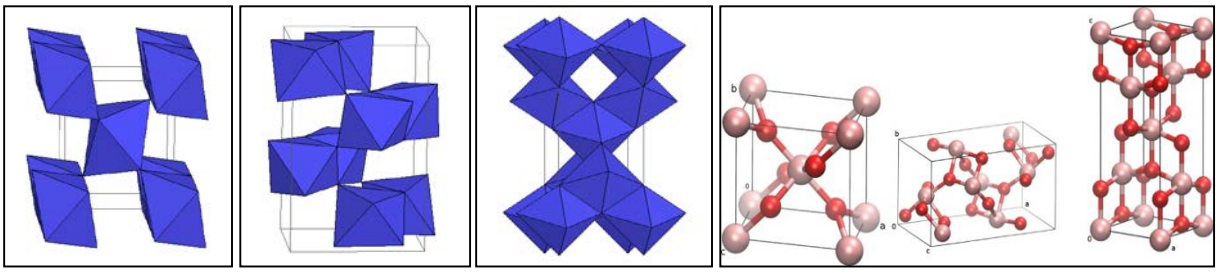

(a). ***(b)*** ***(c)*** ***(d)***

Figure 2.17: The crystal structure of (a) Rutile, (b) Brookite, (c) Anatase (Smyth and Bish, 1988) and (d) Unit cell 3D-balls of the same crystal structure (Moellmann et al., 2012).

The position of oxygen ions on the exposed crystal surface of anatase is a triangular arrangement, allowing effective absorption of organics, where the position of titanium ions creates a favorable reaction condition with the absorbed organics (Thiruvekatachari et al., 2008). Thiruvekatachari et al. (2008) acknowledges that the anatase favorable structure arrangement is not available for rutile. Rutile type of TiO_2 also has a tetragonal crystal structure with prismatic habit as shown in figure 2.17 *(a)* and it is mainly used as white pigment in paint (Johnson et al., 1997). Brookite has an orthorhombic crystalline structure as shown in figures 2.17 *(c)*. Figure 2.17 *(d)* shows the 3D-ball structures of Rutile, Brookite and Anatase respectively.

2.8.1 Production of Titanium Dioxide.

Titanium dioxide either in a form of anatase or rutile is manufactured using two commercial processes that are either sulphate or chloride process routes (Gázquez et al., 2014). Both processes start with an impure titanium dioxide feedstock. The main feedstocks used in the production of titanium dioxide are tabulated in table 2.7, where in general the chloride process uses a higher grade (% TiO_2) than the sulphate process (McNulty, 2007, Gázquez et al., 2014).

Table 2.7: Main feedstocks used for production of TiO_2 (McNulty, 2007)

Process	Feedstocks	TiO_2 (%)
Chloride process	Rutile	93 - 96.5
	Synthetic Rutile	88 - 95.5
	Chloride Slag	85 - 86
Sulphate process	Sulphate Slag	79 - 86
	Ilmenite	45 - 65

Rutile is considered a natural high-grade type of titanium dioxide mineral, while Ilmenite also called iron titanium oxide is a naturally occurring titanium or iron oxide found either in rock form or as a heavy mineral sand (McNulty, 2007). Synthetic Rutile is produced by reducing the iron oxide in ilmenite to metallic iron using carbon monoxide, followed by re-oxidation and separation from the TiO_2 rich fraction (Becher process) or leaching with hydrochloric acid (Benelite process) (McNulty, 2007). The smelting of ilmenites with coal at high temperature produces slag feedstocks (Chloride and Sulphate). The process is adjusted to produce the different particle size requirements for sulphate or chloride use (McNulty, 2007).

The feedstocks in table 2.7 is used in the process routes in figure 2.18 to convert it into the pure white TiO_2 pigment (McNulty, 2007). According to McNulty (2007) the processes sound very simple but to achieve pure white TiO_2 pigment, it is necessary to chemically convert the impure TiO_2 into another chemical, separate out the impurities then convert back to pure TiO_2. These processes are in effect a chemical purification. McNulty (2007) and Gázquez et al. (2014) clarified the Chloride and Sulphate process routes in figure 2.18 as conveyed in sections 1.8.1.1 and 1.8.1.2.

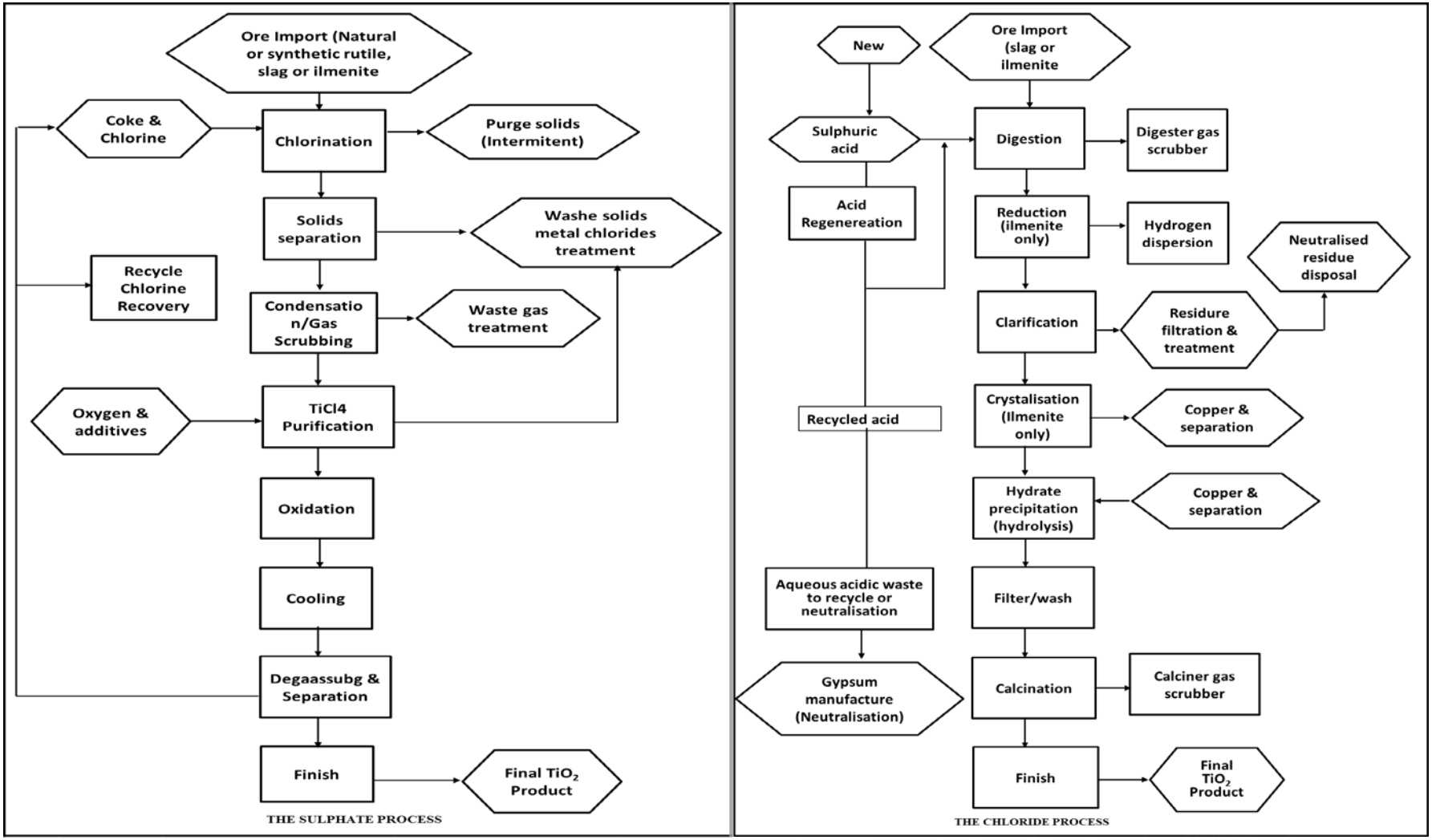

Figure 2.18: The Chloride and Sulphate Process TiO_2 Production Routes (McNulty, 2007).

2.8.1.1 The chloride process route

The overall chemistry of this commercial process can be represented by equation 2.1 and 2.2 as follows:-

$$2TiO_2 + 3C + 2Cl_2 \rightarrow 4TiCl_4 + 2CO + CO_2 \quad 2.1$$

$$TiCl_4 + O_2 \rightarrow TiO_2 + 2Cl_2 \quad 2.2$$

In the unit operation process involved, the chlorine released during the formation of the titanium dioxide is recycled back to the beginning of the process so that the only chlorine consumed is that which reacts with impurities. Chlorination is carried out in the presence of coke at a temperature as high as around 1000 ^{o}C in a fluidised bed reactor. The gas stream contains titanium tetrachloride, oxides of carbon and all metal impurities from the feedstock in the form of metal chlorides. The gas stream is passed through the recycled liquid $TiCl_4$ which cools the gas stream to a level at which the other metal chlorides separate out as solids (McNulty, 2007, Gázquez et al., 2014).

The $TiCl_4$ condensed as a liquid by further cooling and then fed to a high temperature oxidation reactor, where it is reacted with oxygen in a plasma reactor or toluene burner to restore titanium dioxide. The chlorine released in a plasma reactor or toluene burner is recycled back to the beginning of the reaction. This pure titanium dioxide is then exposed to a range of chemical surface treatments, milling and drying operations. This is done to give a range of TiO_2 products with particular properties in terms of dispersion and durability, suitable for particular end use applications. The metal chloride impurities removed during processing are typically neutralised with lime or limestone and sent for disposal via landfill (McNulty, 2007, Gázquez et al., 2014).

2.8.1.2 The sulphate process route

The overall chemistry of the sulphate process route can be represented by equations 2.3 - 2.5 as follows:-

$$FeTiO_3 + 2H_2SO_4 \rightarrow TiOSO_4 + FeSO_4 + 2H_2O \quad 2.3$$

$$TiOSO_4 + H_2O \rightarrow TiO_2n.H_2O + H_2SO_4 \quad 2.4$$

$$TiO_2n.H_2O \rightarrow TiO_2 = n.H_2O \quad 2.5$$

According to McNulty (2007) the sulphate process is more complicated in terms of the number of unit operations involved as shown in figure 2.18 than the chloride process. The feedstock in table 2.7 for sulphate process is first digested in strong sulphuric acid which converts the titanium components into titanyl sulphate and the iron into sulphates. Ilmenite based feedstock requires a reduction step in which iron is added to convert any ferric iron to the ferrous form to aid separation later in the process. A clarification step follows to remove any undigested material from the liquor. Crystallisation typically follows for ilmenite based feedstock, which separates out co-product ferrous sulphate heptahydrate (copperas), although it is also possible to extract copperas later in the process. The separated copperas is sold for a range of applications including water treatment, agriculture and also used in cement (Gázquez et al., 2014).

The liquor is sent to a hydrolysis stage where the oxysulphate is reacted with water to produce a hydrated titanium dioxide product and releases sulphuric acid (McNulty, 2007). The hydrated TiO_2 goes to a rotary kiln where it is calcined to produce the anhydrous titanium dioxide product. Further processing (finishing), is then similar to the chloride process involving chemical surface treatments (coating), milling and drying operations (Gázquez et al., 2014). The sulphuric acid released at hydrolysis is not strong enough to be recycled directly back to the digestion unit, therefore it is sent to one of two processes. These two processes are either acid concentration; or neutralisation to produce gypsum. Firstly, the acid is typically subjected to a number of heating, concentration and filtration cycles to increase the strength of the acid to a level allowing reuse in the process or sale. The process also concentrates residual iron that is separated as a ferrous sulphate monohydrate co-product. The alternative process, of gypsum production, treats the acid with a calcium salt to give gypsum which is used in plasterboard manufacture, agriculture and cement (McNulty, 2007, Kuznesof, 2006, Gázquez et al., 2014).

2.8.2 Mechanism of TiO_2 Photocatalytic Chemistry

The particles of TiO_2 as a photocatalyst have been strongly studied in photo-physics and photochemistry (Thiruvekatachari et al., 2008, CHLÁDOVÁ et al., 2011). The particle of TiO_2 works as a Photocatalytic oxidant (oxidizing-agent) in the present of the UV light (Gaya and Abdullah, 2008). The TiO_2 particles are recognized as photocatalyst because of its lone electron properties in the particle outer orbital (Gaya and Abdullah, 2008).

When the TiO_2 particle is illuminated with UV light with energy greater or equals to a band gap of the particle (Band-gap energies of common semiconductors are given in Table 2.8), it generates an electron and a hole (Malato et al., 2009).

Table 2.8: Band-gap energy for some common semiconductor materials at 0K (Thiruvekatachari et al., 2008).

Semi-Conductors	Bandgap Energy (Ev)	Semi-Conductors	Bandgap Energy (Ev)
Diamond	5.4	**WO_3**	2.76
CdS	2.42	**Si**	1.17
ZnS	3.6	**Ge**	0.744
ZnO	3.436	**Fe_2O_3**	2.3
TiO_2	3.03	**PbS**	0.286
CdS	2.582	**PbSe**	0.165
SnO_2	3.54	**ZrO_2**	3.87
CdSe	1.7	**Cu_2O**	2.172

The electron-hole generate on the valence band of the particle. The electron becomes excited and form energy. The excited electron will gain excess energy and move to the conductive band of the particle creating a negative-electron (e^-) on the conductive band and positive-hole (h^+) on the valence band (Malato et al., 2009).

The electron on the conductive band is then released to the adsorbed O_2 to form a super oxide anion O_2^- and the surface of the TiO_2 particle is left positively charged. The positively charged surface particle accepts an electron from the moisture (H_2O) to become neutral. The moisture (H_2O) loses an electron to the positively charged surface particle to become a hydroxyl radical (OH^-) (Thiruvekatachari et al., 2008).

The chain oxidative-reductive reactions that occur at the photon-activated surface as stipulated by Chong et al. (2010) and Malato et al. (2009) illustrated it in figure 2.19 are as follow:

Photo excitation:

$TiO_2 + h\nu \rightarrow e^- + h^+$ 2.6

Change carrier-trapping e^-:

$e_{CB}^- \rightarrow e_{TR}^-$ 2.7

Change carrier-trapping e^-:

$h_{VB}^+ \rightarrow h_{VB}^+$ 2.8

Photo excited e— scavenging:

$O_2 + e^- \rightarrow O_2^-$ 2.9

h^+ scavenging:

$H_2O + h^+ \rightarrow OH^\bullet + H^+$ 2.10

Photo degradation by O_2^- and OH•:

$OH^\bullet$ + Organic $\rightarrow CO_2$ 2.11

h^+ + Organic $\rightarrow CO_2$ 2.12

O_2^- + Organic $\rightarrow CO_2$ 2.13

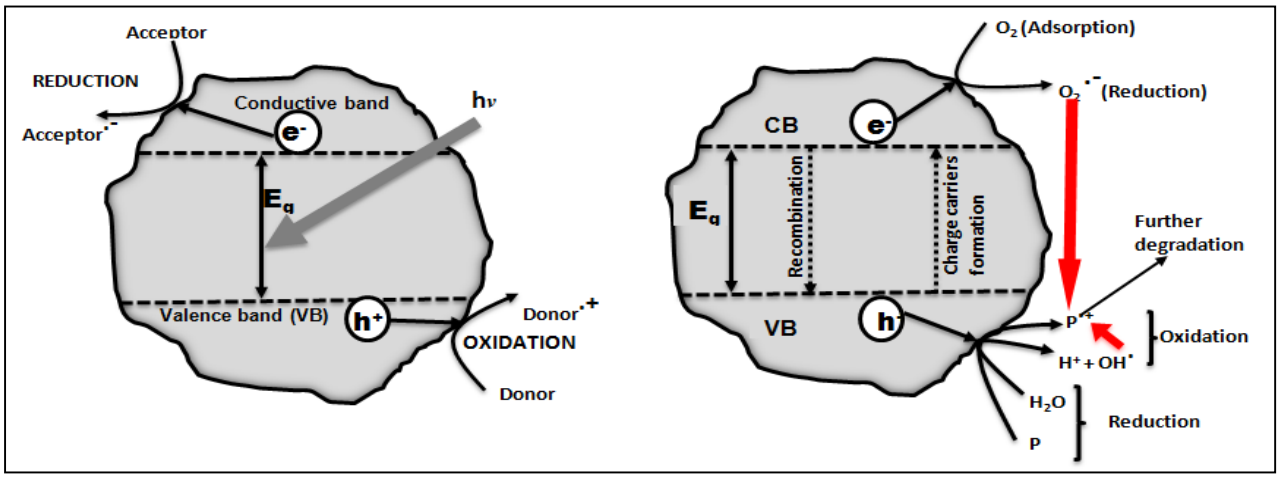

Figure 2.19: Energy band diagram and fate of electrons and holes in a semiconductor particle in the presence of water containing a pollutant (Malato et al., 2009).

The hydroxyl radical and super oxide anion have the power of oxidizing destruction that decomposes organics, harmful bacteria and odour in water to harmless substances (Carbon dioxide, water and

inorganic salts) (Chong et al., 2010). One of the advantages of using the photocatalyst in water disinfection is the mitigation of the sludge formation, which requires further handling or dumping when formed.

2.8.3 Factors Affecting Photocatalytic degradation

The factors that affect the performance of the photocatalyst (TiO_2) are temperature, initial pH, UV light intensity and wavelength, treatment time, dissolved oxygen, photocatalyst concentration and bacterial concentration (Chong et al., 2010).

2.8.3.1 Light Source (UV light intensity and wavelength)

TiO_2 absorbs radiation below the visible range of light spectrum, whereby, photo activation of TiO_2 requires radiation with light of a wavelength less than or equal to 384 nm, with an absorbance maximum at approximately 340 nm (Thiruvekatachari et al., 2008). Majority of research studies have been carried out using UV-A radiation, which is wavelength between 320- 380 nm provided by fluorescent low-pressure mercury lamps emitting low intensity (Hoffmann et al., 1995, Legrini et al., 1993, Thiruvekatachari et al., 2008). According to Thiruvekatachari et al. (2008) medium pressure mercury lamps for UV-A have also been used, which emit high intensity UV light in the short, medium and long UV spectrums. Thiruvekatachari et al. (2008) also mentioned that the short (UV-C; 200-280 nm) and medium (UV-B; 280-320nm) UV radiation emitted by the mercury is usually cut-off by the photocatalytic reactor material, unless it is made of quartz.

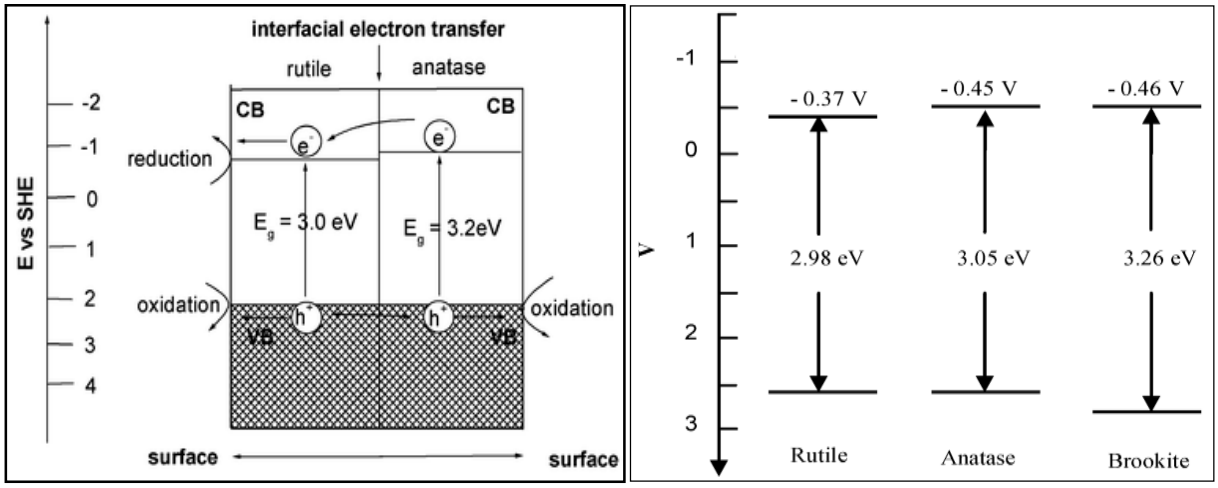

Figure 2.20: The band gap of the Anatase and Rutile (Yu et al., 2002, Di Paola et al., 2013)

According to most researchers, anatase has a larger band gap than rutile TiO_2 as shown in figure 2.20. While this reduces the light that can be absorbed, it may raise the valence band maximum to higher energy level relative to redox potentials of adsorbed molecules (Yu et al., 2002). This increases the oxidation 'power' of electrons and facilitates electron transfer from the TiO_2 to adsorbed molecules (Yu et al., 2002).

2.8.3.2 Temperature

The photocatalytic reactors are mostly operated at room temperature because the system do not require heating (Shivaraju, 2011). Chong et al. (2010) reported that heat energy is inadequate to activate the TiO_2 surface and the understanding on such dependency could be extrapolated when operating the process under natural sunlight illumination. Most research recommend the photocatalytic reactor to be operated at temperatures between 20 and 80 ^oC (Herrmann, 1999, Gogate and Pandit, 2004, Herrmann, 2005, Mozia, 2010). An increase in photocatalytic reaction temperature (>80 ^oC) promotes recombination of charge carriers and disfavor the adsorption of pollutants onto TiO_2 surface (Herrmann, 2005, Gaya and Abdullah, 2008, Chong et al., 2010). On the other hand, very low temperatures (<0 ^oC) decreases the photocatalytic activity and results in desorption of the final product from the catalyst surface (Mozia, 2010, Chong et al., 2010).

2.8.3.3 Initial pH

The initial pH of the solution is more significant on the electrostatic charge of the TiO_2 surface (Shivaraju, 2011). This determines the density of $TiOH^+$ groups, which results in the adsorption of bacteria on TiO_2 (McCullagh et al., 2007). McCullagh et al. (2007) stated that the microbial growth is also pH dependent, with a decrease in the growth rate that is observed when the pH is changed in either direction away from the optimum pH. Shivaraju (2011) evaluated the effect of initial pH (2 to 12) on degradation of organic pollutant in the sewage water. The findings showed the degradation efficiency decreasing with an increasing initial pH from 2 to 6.3 and the degradation efficiency also increased significantly with increasing initial pH from 7 to 12 as illustrated in figure 2.21.

Shivaraju (2011) revealed that any variation in the operating pH affects the isoelectric point or the surface charge of the photocatalyst more especially the TiO_2 due to its nature. The point of zero charge (PZC) has been used by most research to study the effect of pH on the photocatalytic oxidation performance (Bayarri et al., 2005, Chin et al., 2006, Chong et al., 2009, Chong et al., 2010). The PZC is the position at which the surface charge of the photocatalyst is zero or neutral and for TiO_2 it ranges between 4.5 and 7 (Chong et al., 2010). At PZC, there is minimal photocatalytic performance due to the absence of any electrostatic force (Chong et al., 2010). McCullagh et al. (2007) stated that vast majority of human pathogens prefer a neutral pH.

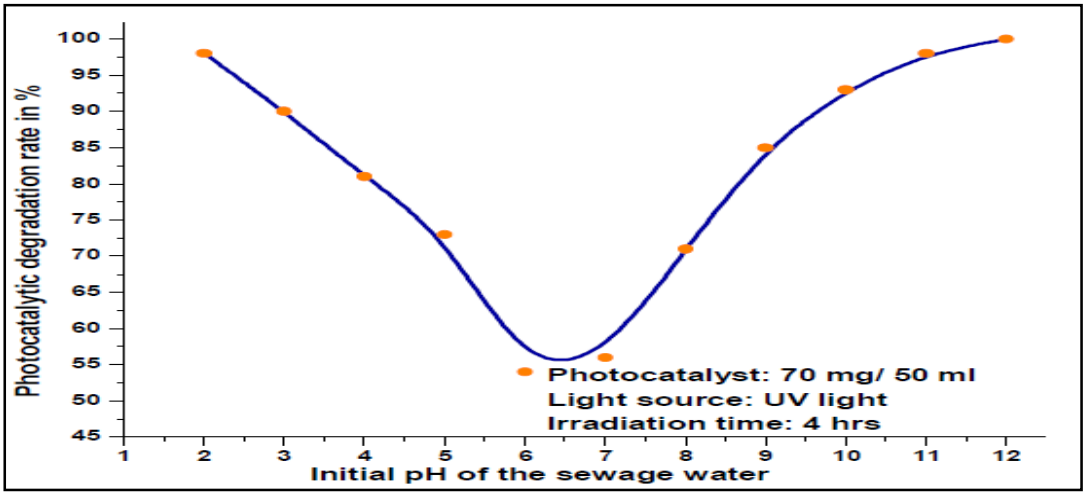

Figure 2.21: Effect of initial pH on the photocatalytic degradation efficiency of organic pollutants in the sewage water (Shivaraju, 2011)

Depending on the pH, the catalyst surface can be positively charged (pH < PZC), negatively charged (pH > PZC) or neutral (pH = PZC) (Bayarri et al., 2005).

2.8.3.4 Photocatalyst loading

The main reason for investigating the effect of photocatalyst loading is to find the optimum amount for efficient photocatalytic degradation. An excess amount of photocatalyst in a solution tends to reduce the photodegradation rate due to the excess amount that leads to scattering and reduction in light penetration through a suspension. Shivaraju (2011) investigated the effect of photocatalyst loading on the photocatalytic degradation efficiency of sewage water. The trend showed a significant increase until the photodegradation rate became constant at photocatalyst loading of 70 mg as shown in figure 2.22.

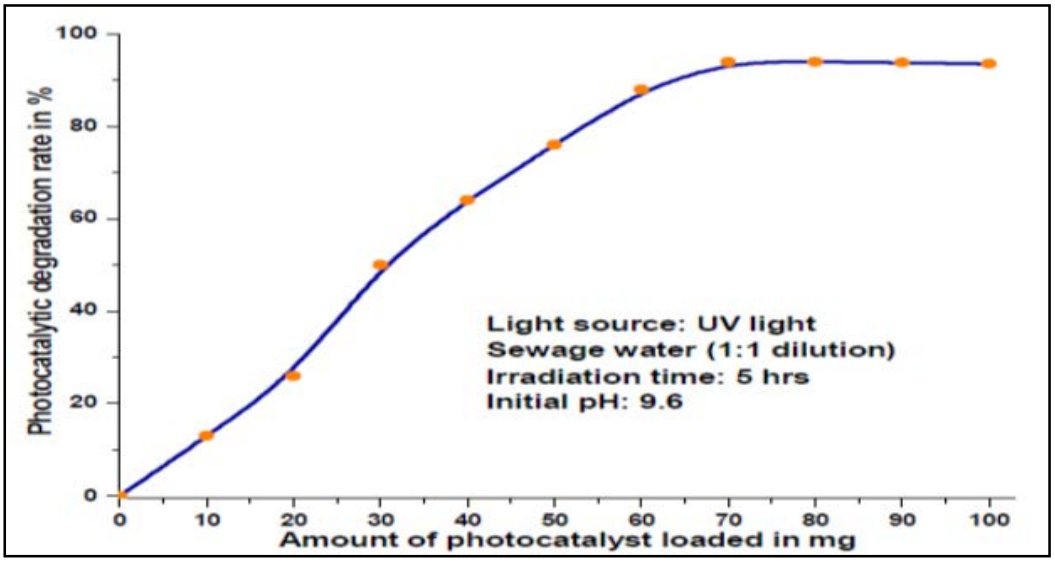

Figure 2.22: Effect of photocatalyst loading on the photocatalytic degradation efficiency of organic pollutants in the sewage water (Shivaraju, 2011)

A further increase beyond 70 mg shows a considerably reduced photodegradation rate due to the large amount of photocatalyst load in solution leading to light scattering and reduction in light penetration through the aqueous medium because of the decrease in transparency of sewage water (Shivaraju, 2011).

2.8.3.5 Dissolved Oxygen

In a photodegradation process, oxygen is considered as an electron scavenger to trap the excited conduction-band electron from recombination (Shivaraju, 2011). Kabra et al. (2004) found that the presence of oxygen might hinder when in excess or improve the photodegradation rate and this is depending on the mechanism of the degradation of the pollutant.

2.9 DESIGN OF EXPERIMENTS (DOE)

Experimentally, DOE is defined as the systematic procedure carried out under controlled conditions in order to obtain unknown effects, to test or establish a hypothesis or to illustrate a known effect. **DOE** is also referred to as **Designed Experiments** or **Experimental Design**; where all of the terms are considered to have the same meaning (MoreSteam.com, 2015).

Engineering perspective on the use of experimentation is to reduce time to design/develop new products & processes, improve performance of existing processes, improve reliability and performance of products, achieve product & process robustness, perform evaluation of materials, design alternatives, setting component & system tolerances, etc. (PennState, 2015).

The DOE has been used to efficiently carry out experiments and analysis of results. The main use of DOE is to determine simultaneously the individual and interactive effects of input factors that affect the output results in any design.

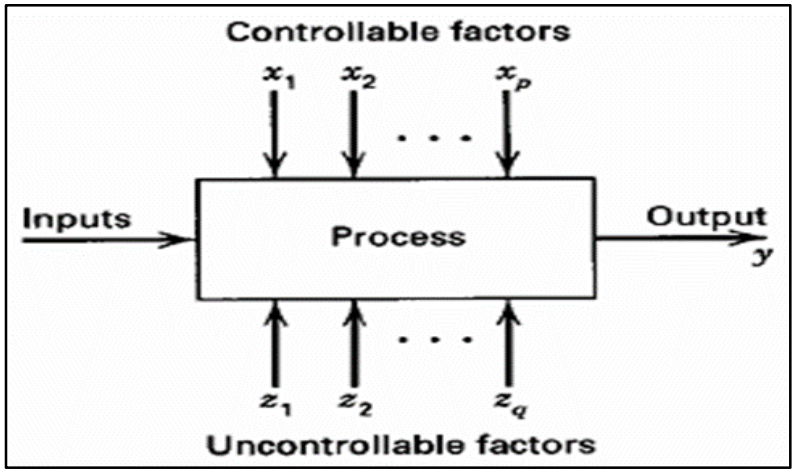

Figure 2.23: A general model of system variables (Montgomery, 2009)

An experiment has inputs and factors, some of which can be controlled and others cannot be controlled. The selection of factors affecting the output is of vital importance. Figure 2.23 is a presentation of a model of the process or system. The objectives of conducting the experiment on the system in figure 2.23 may include the following (Montgomery, 2009):

- Determining which variables are most influential on the response *y*.
- Determining where to set the influential *x*'s so that *y* is almost always near the desired nominal value.
- Determining where to set the influential *x*'s that variability in *y* is small.
- Determining were to set the influential *x*'s so that the effects of the uncontrollable variables $z_1, z_2, \ldots, z_q$ are minimized.

The selection of an experimental design mostly depends on the objectives of the experiment and factors to be investigated as illustrated in table 2.9 and 2.10.

Table 2.9: Description of experimental objectives (Nist/SEMATECH, 2012, Filliben and Heckert, 2012).

Objective	Description
Comparative objective	The primary goal of the experiment is to make a conclusion about one a-priori important factor if there is one or several factors under investigation in the presence of and/or in-spite of the existence of the other factors. The question of interest is whether that factor is "significant", (i.e., whether there is a significant change in the response for different levels of that factor), then is a *comparative problem* and a *comparative design* solution is needed.
Screening objective	The primary purpose of the experiment is to select or *screen out* the few important main effects from the many less important ones. These *screening designs* are also termed main effects designs.
Response Surface (method) objective	The experiment is designed to allow researchers to estimate interaction and even quadratic effects, and therefore gives an idea of the (local) shape of the response surface being investigated. For this reason, they are termed *response surface method (RSM) designs*. RSM designs are used to: ✓ Find improved or optimal process settings ✓ Troubleshoot process problems and weak points ✓ Make a product or process more *robust* against external and non-controllable influences. "Robust" means relatively insensitive to these influences.
Optimizing responses when factors are proportions of a mixture objective	If factors are proportions of a mixture and the "best" proportions of the factors are so as to maximize (or minimize) a response, then a *mixture design* is required.
Optimal fitting of a regression model objective	To model a response as a mathematical function (either known or empirical) of a few continuous factors and desires a "good" model parameter estimates (i.e., unbiased and minimum variance), then a *regression design* is needed.

Table 2.10: Design Selection Guideline (Nist/SEMATECH, 2012, Filliben and Heckert, 2012).

Number of Factors	Comparative Objective	Screening Objective	Response Surface Objective
1	1 factor completely randomized design		
2 to 4	Randomized Block Design	Full or Fractional Factorial	Central Composite or Box-Behnken
5 and more	Randomized Block Design	Fractional Factorial or Plackett-Burman	Screen first to reduce number of factors.

2.9.1 One Factor At- a Time (OFAT) Design

OFAT is the most popular method used extensively for every experiment design situation. OFAT depends on selecting a starting point, for each factor, and then successively varying each factor over its range with the other factors held constant at the baseline level. The main well-known disadvantage is that it does not take into consideration any possible interaction between factors.

However, Milani et al. (2008) briefly mentions in general the various types of one-factor-at-a-time DOE approaches as distinguished by Robinson (2000) as shown in table 2.11. Milani et al. (2008) investigated the OFAT strategy when it is used within a DOE approach (i.e., with predefined discrete levels of factors), the task was to evaluate the response at each new design point by varying only one factor and keeping the rest at fixed levels from previous runs. The main reasoning to use this method is its simplicity and sometimes its speed (Milani et al., 2008). Frey et al. (2003) showed that for a number of complex engineering problems with low to medium noise levels and moderate to large interactions, OFAT generally outperforms other optimisation methods with similar resource demands such as Taguchi methods (Milani et al., 2008).

Table 2.11: In general, the various types of OFAT DOE approaches (Milani et al., 2008).

One-Factor-At-a-Time DOE.	Description
"Strict" OFAT method.	Varies one factor solely from the preceding trial.
"Standard" OFAT.	Varies one factor each time from a standard (nominal) level combination defined at the beginning of a design. This is not always useful because the nominal design might not be feasible or it may not be estimated around the actual optimal solution.
"Free" OFAT.	A succeeding run can be made using any level combinations from a study of previous runs.
"Adaptive" OFAT	Succeeding run is made from the study of all preceding runs but always at the best previously observed levels. It is known that adaptive OFAT can perform better than the strict type in the presence of interactions.
"Nested" or "Curved" OFAT method.	The new runs are produced in sets that include several combinations for one-easy-to-vary factor.

There are also advantages that Milani et al. (2008) pointed out as previously reported by other researchers where Frey and Wang (2006) came with the proof of theorems. The advantages are reported by Milani et al. (2008) as follows:

- The expected number of experiments to arrive at chosen factor levels is smaller, particularly when the number of factors is large.
- It can be adapted to provide large improvement gains in the early stages of the experimentation process.
- The expected improvement is higher on average than that of saturated resolution III fractional factorial experiments.
- OFAT is capable of exploiting the largest effects among given interactions with a high probability in the early stages of the search and this is sustained and improves as the search proceeds.
- Figure 2.24 shows one of the OFAT used within the DOE approach, where Frey and Wang (2006) applied the adaptive OFAT to a system with three factor at two levels.

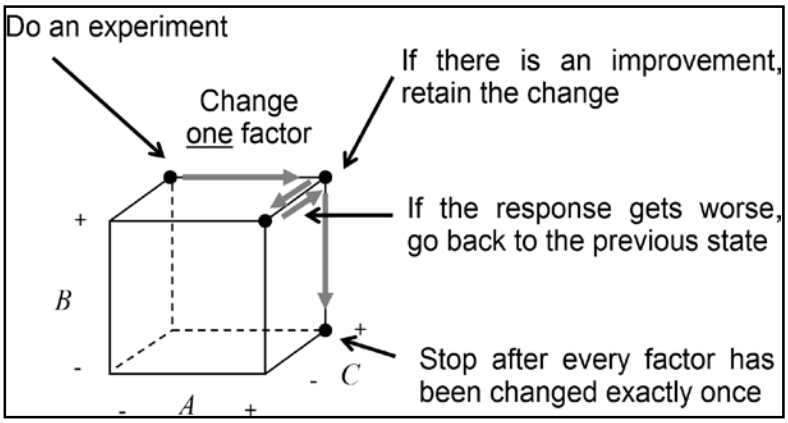

Figure 2.24: Adaptive OFAT as Applied to a System With Three Two-Level Factors (A, B, and C) (Frey and Wang, 2006).

2.9.2 Factorial Design

The approach deals with several factors in which all factors are varied simultaneously; therefore, it reduces the number of experiments to be performed. The design takes into account the interactions between factors that may affect the yield or response. The factorial design can be classified in two

categories, which are full factorial designs and fractional designs. A common factorial design is with all input factors set at two levels each. The levels are called 'high' and 'low' or '+1' and '-1' respectively. Therefore, a full factorial design is the one with all possible combinations of all the input factors. A full factorial design with *k (2)* number of factors and N (2) levels is represented as N^k (2^2) and with three factors at two levels is 2^3. Therefore, full factorial is not suitable for a high number of factors because it requires a large number of runs or experiments, which is not economical and feasible see table 2.12. The number of runs do not take into account the center points in a two level factorial, and replicates on two and three level factorials.

Table 2.12: Number of Runs for a Two Level (n^k) and Three Level Full Factorial

Number of Factors (*k*)	Two level Factorial	Three level Factorial
	Number of Runs	Number of Runs
2	4	9
3	8	27
4	16	81
5	32	243
6	64	729
7	128	2187

A full factorial design is then deemed unsuitable when the number of factors are equals or greater than 5. A solution to a large number of runs of the full factorial design is to carefully select a fraction of a full factorial in order to reduce the number of runs. When a fraction of a full factorial is conducted, it is then referred to as a fractional factorial design and it is expressed as N^{k-p}, where N is the number of levels of each factor investigated, *k* is the number of factors investigated and *p* describes the size of the fraction of the full factorial used. In general, *p* represent the fraction used for instance ½ is $p = 1$, ¼ is $p = 2$ and 1/8 is $p = 4$.

The regression model statement for a simple 2 level factorial design is as follows:

$$y_i = \beta_0 + \beta_1 Z_{1i} + \beta_2 Z_{2i} + \beta_3 Z_{1i} Z_{2i} + \varepsilon_i \qquad 2.14$$

Where:

y_i = Output/Response for the i^{th} unit.

β_0 = Coefficient for the intercept

β_1 = Mean difference on factor 1.

β_2 = Mean difference on factor 2.

β_3 = Interaction of factor 1 and factor 2.

Z_{1i} = Dummy variable for factor 1

Z_{1i} = Dummy variable for factor 2

ε_i = residual for the i^{th} unit.

The factorial design is used to decide which of these factors is important and thereafter, decide what level of the factors gives the optimal response (finding the optimal level of the important factors).

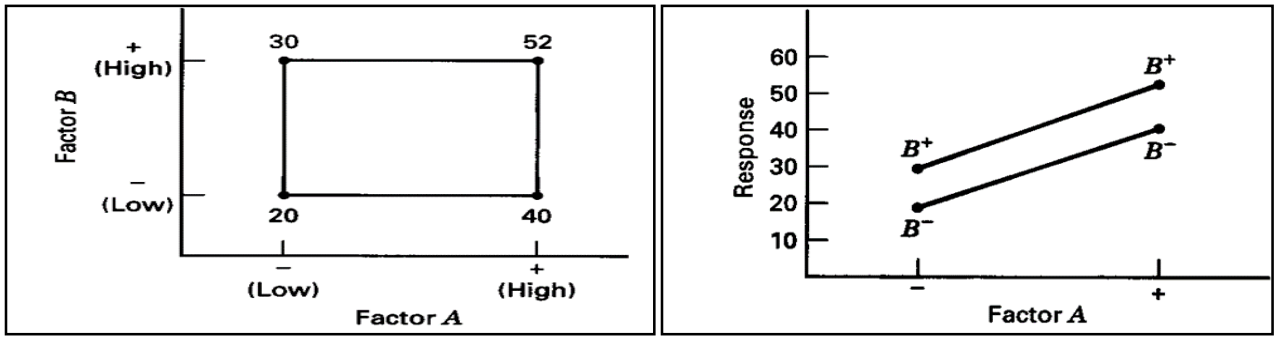

(a) . (b)

Figure 2.25: A two-factor factorial experiment (a) with the response (y) shown at the corners (b) without interaction (Montgomery, 2009).

Figure 2.25 (a) shows the response on factor A and B, which suggest that there is no interaction between the factors in figure 2.25 (b).

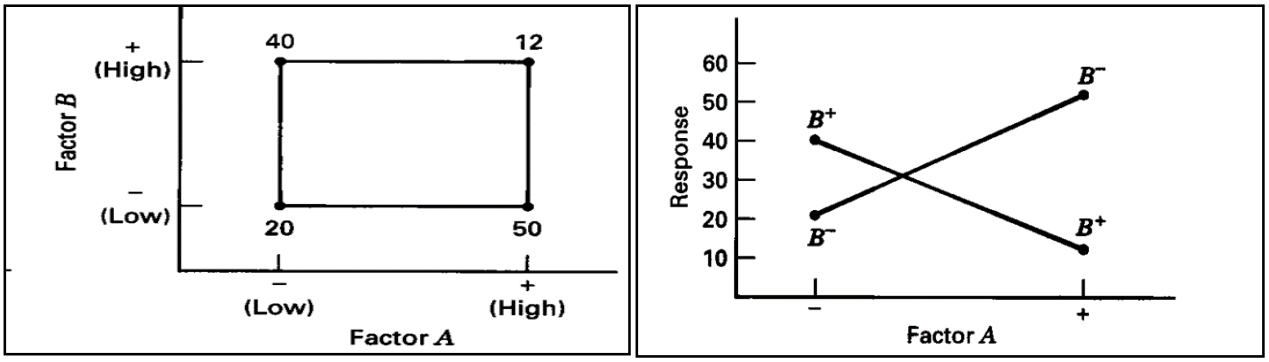

(a) . (b)

Figure 2.26: A two-factor factorial experiment (a) with the response (y) shown at the corners (b) with interaction (Montgomery, 2009).

On the other hand, figure 2.26 shows that there is an interaction between factors.

2.9.3 Response Surface Methodology Design

Many have described the response surface methodology (RSM) as a method that involves a group of mathematical and statistical practices in the development of the most functional relationship between a response (y) and control variables (x_i) (Khuri and Mukhopadhyay, 2010). The relationship between the response and control variables can be estimated using a low-degree polynomial model of the form (Khuri and Mukhopadhyay, 2010):

$$y = f'(x)\beta + \varepsilon \qquad 2.15$$

Where:

y	=	Response of interest
x	=	Control variables/factors
$f'(x)$	=	Vector function consists of powers and cross-products of powers of x.
β	=	Constant coefficient term
ε	=	Represent the noise or error observed in the response (y).

This model is considered to establish a relationship to be used to predict response values for the control variables, to determine the significance of the factors whose levels are represented by x, and to determine the optimum settings of x that result in the maximum (or minimum) response over a certain region of interest (Khuri and Mukhopadhyay, 2010).

The main goal of using RSM is for process optimization fitted on a three-dimensional response surface showing the expected response as a function of control variables (Montgomery, 2009). The first step in most RSM problems is the screening of the variables in order to select the few important main effects from the many less important variables (Khuri and Mukhopadhyay, 2010). Therefore, the response can be well modeled by a linear function of the independent variables using the function in the first order model as follows:

$$y = \beta_0 + \beta_1 x_1 + \beta_2 x_2 + ... + \beta_k x_k + \varepsilon \quad 2.16$$

This model is similar to the model eq 2.14, which also shows the interaction of the variables. If the model ignores the cross products or interaction component that gives an indication of the curvature of the response surface that has to be fitted in RSM, the model becomes eq 2.16 called the steepest ascent model. This first order model, which is the steepest ascent model, shows the hill at which the new variable ranges for the second order model to be investigated to find optimums as illustrated in figure 2.27.

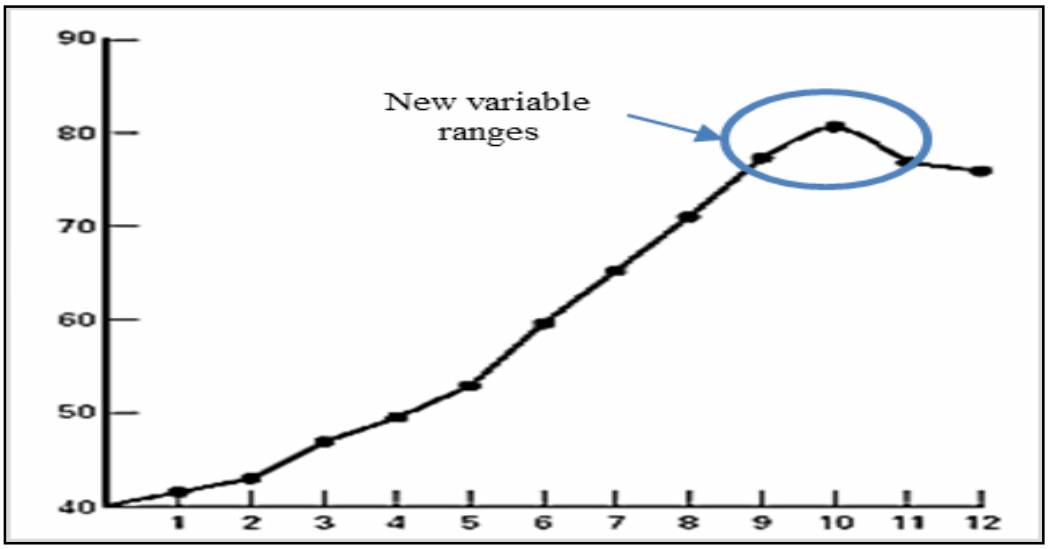

Figure 2.27: Response along the path of steepest ascent (Montgomery, 2009)

The choice of experimental design to generate a second order polynomial, which incorporates curvature to approximate the response in the RSM is generally as follows:

$$y = \beta_0 + \beta_1 x_1 + \beta_2 x_2 + \beta_{12} x_1 x_2 + \beta_{11} x_1^{\ 2} + \beta_{22} x_2^{\ 2} + \varepsilon \quad 2.17$$

The second order model contains the linear terms, cross product terms and second order terms as demonstrated in eq 2.17. The second order polynomial model requires a response surface design that has more runs than the first order designs. This is accomplished by adding center points to the first order design (N^k). These response surface designs include the central composite design (CCD), the Box-Behnken design (BBD) and the Doehlert design (DD) are commonly used.

2.9.3.1 The Central Composite Design (CCD)

It contains an entrenched factorial or fractional factorial design with center points that is augmented with a group of 'star points' that allow estimation of curvature as illustrated in figure 2.28 (a). This simply means that the CCD has five levels per factor (-α, -1, 0, +1 and +α). The star points represent new extreme values (low and high) for each factor in the design. There are three types of CCD that can be used when selecting a design, which are Circumscribed (CCC), Face-Centered (CCF) and Inscribed (CCI) as shown in figure 2.28 (b). It can be designed in two ways, which is orthogonal block where the model terms and block effects can be estimated independently and to minimize the variation in the regression coefficients. The second way is the rotatability design where Rotatable designs provide constant prediction variance at all points that are equidistant from the design center.

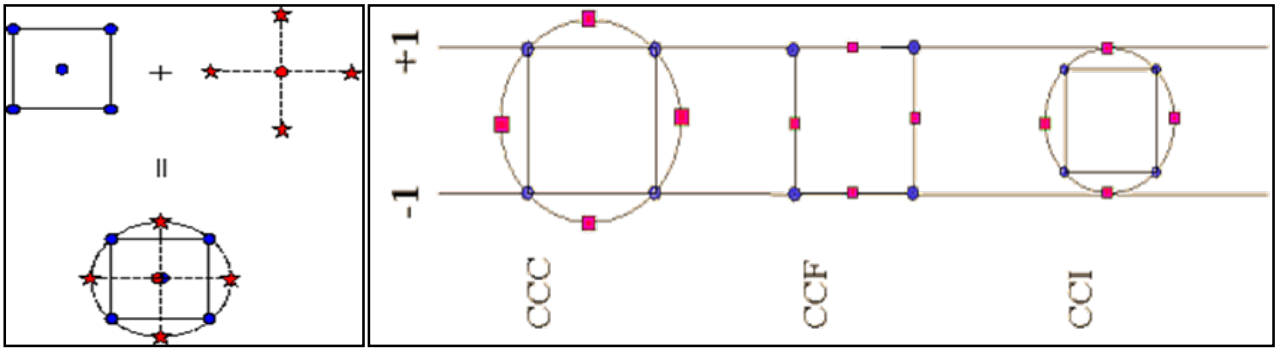

(a) . (b)

Figure 2.28: Central Composite Design (a) Generation of a CCD, (b) Illustrative representation of where the star points are placed for the 3 types of CCD.

CCD can be used to efficiently estimate first and second order terms and to model a response variable with curvature by adding center and axial points to a previously done factorial design.

2.9.3.2 The Box-Behnken Design (BBD)

BBD does not contain an embedded factorial or fractional factorial design. The design points fall at combinations of the high and low factor levels and their midpoints as illustrated in figure 2.29. BBD has a limited capability for orthogonal blocking compared to the CCD.

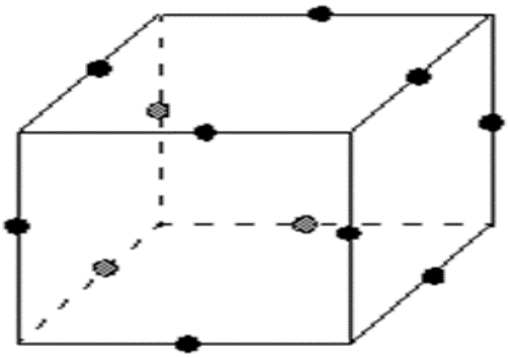

Figure 2.29: Box-Behnken Design for three factors.

It allows efficient estimation of the first- and second-order coefficients and the design is not suitable for sequential experiments because it does not have an embedded factorial design. This design proves to be useful when the process cannot be operated beyond the safe operating limits.

2.9.4 Analysis of Design Model

The first analysis is considering the region of exploration for fitting the first-order model with the approximating function in eq 2.16 for a well-modeled response. When the RSM shows a little curvature in the system for the first-order model to indicate the region of the optimum, a more elaborate model can be used. The more elaborate model is the second-order model in eq 2.17 to perform an analysis to locate optimum.

2.9.4.1 Model Adequacy Checking for first-order regression

The relationship between the response and independent variables is assumed to be a purely algebraic relationship. The error term ε has zero mean with a constant variance σ^2 and errors are normally distributed. Therefore, the model adequacy cannot rely on the analysis of variance until the validity of these mentioned assumptions has been checked by the examination of residuals.
The definition of the residual is as follows:

$$e_i = y_i - \hat{y}_i , \qquad i = 1, 2, \dots, n \tag{2.18}$$

Where:

y_i = An observation

$\hat{y}_i$ = The corresponding fitted value.

The residuals have several important properties with zero mean, and their approximate average variance is estimated by:

$$\frac{\sum_{i=1}^{n}(e_i - \bar{e})^2}{n-p} = \frac{\sum_{i=1}^{n} {e_i}^2}{n-p} = \frac{SS_{Res}}{n-p} = MS_{Res} \qquad 2.19$$

$n - p$ is degrees of freedom associated with them.

The model is said to be adequate when the residuals are structureless, meaning that, there should be no obvious patterns. A more useful procedure is the use of a normal probability plot of the residuals. For a normal underlying error distribution, the plot resemble a straight line (Montgomery, 2009). Substantial departures from a straight line indicate that the distribution is not normal see illustration in figure 2.30.

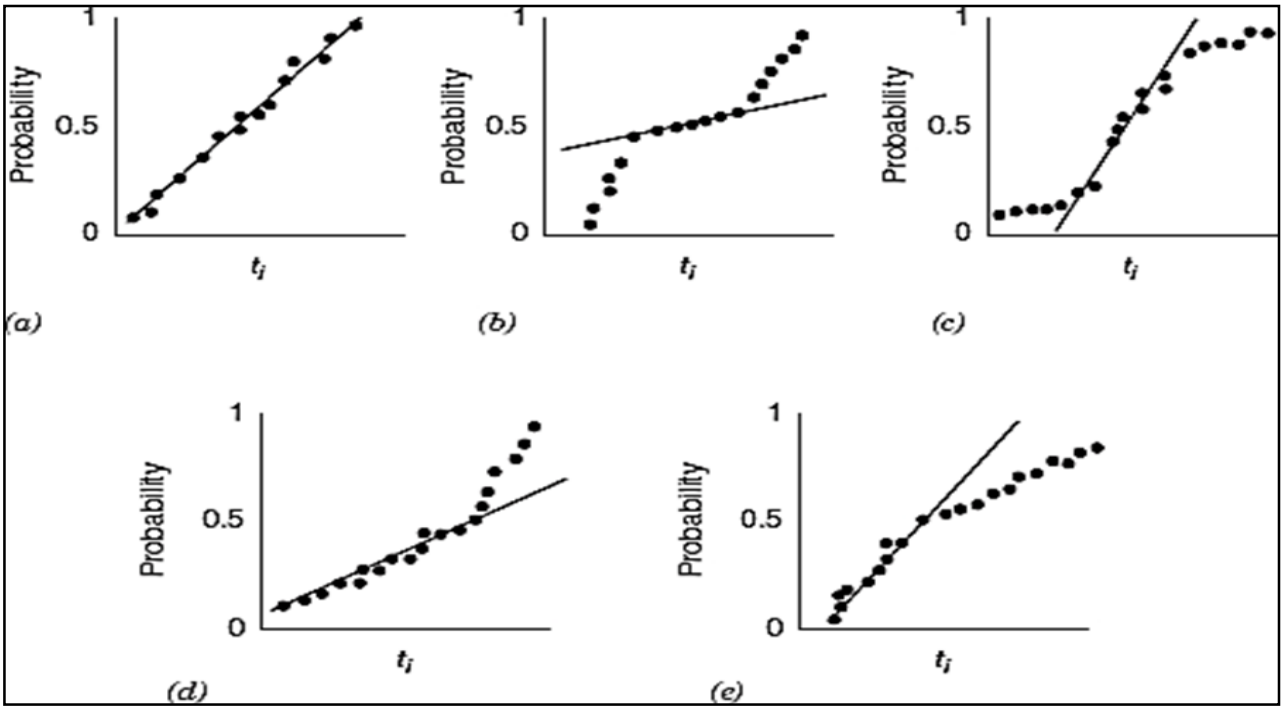

Figure 2.30: Normal probability plots: (*a*) ideal; (*b*) light-tailed distribution; (*c*) heavy-tailed distribution; (*d*) positive skew; (*e*) negative skew (Montgomery et al., 2012).

Observations that are outliers, or extreme values, which are said to be separated in some fashion from the rest of the data are dealt with using scaled residuals. Methods of scaled residuals are Standardized

Residuals, Studentized Residuals, PRESS Residuals and R-Student. An example of a normal probability plot of the external studentized residual is shown in figure 2.31. Figure 2.31 shows that the residuals do not lie exactly along the straight line. This is an indication that there may be outlier/s in the data, which is a problem with the normality assumptions.

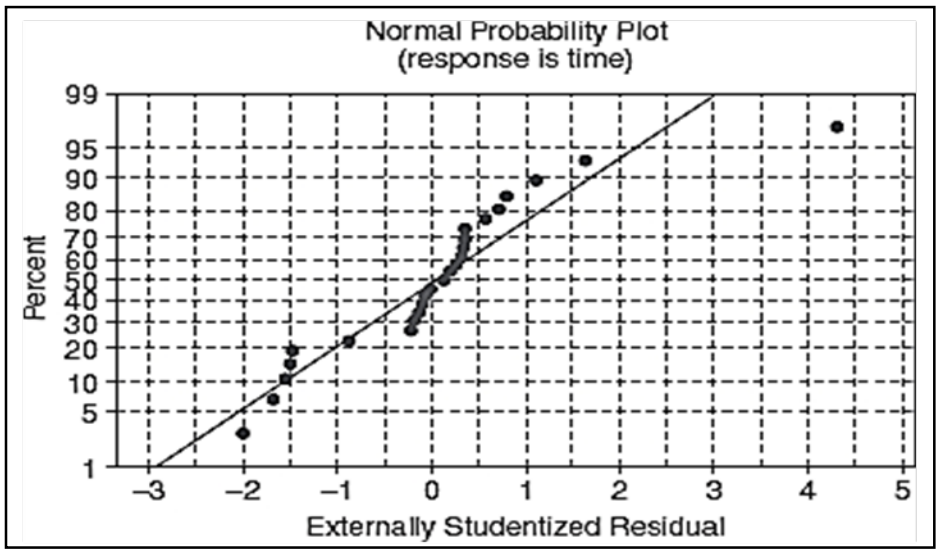

Figure 2.31: Normal probability plot of the externally studentized residuals for the delivery time data (Montgomery et al., 2012)

In order to detect several common types of model inadequacies, a plot of the externally studentized residuals t_i versus the corresponding fitted values $\hat{y}_i$ is used.

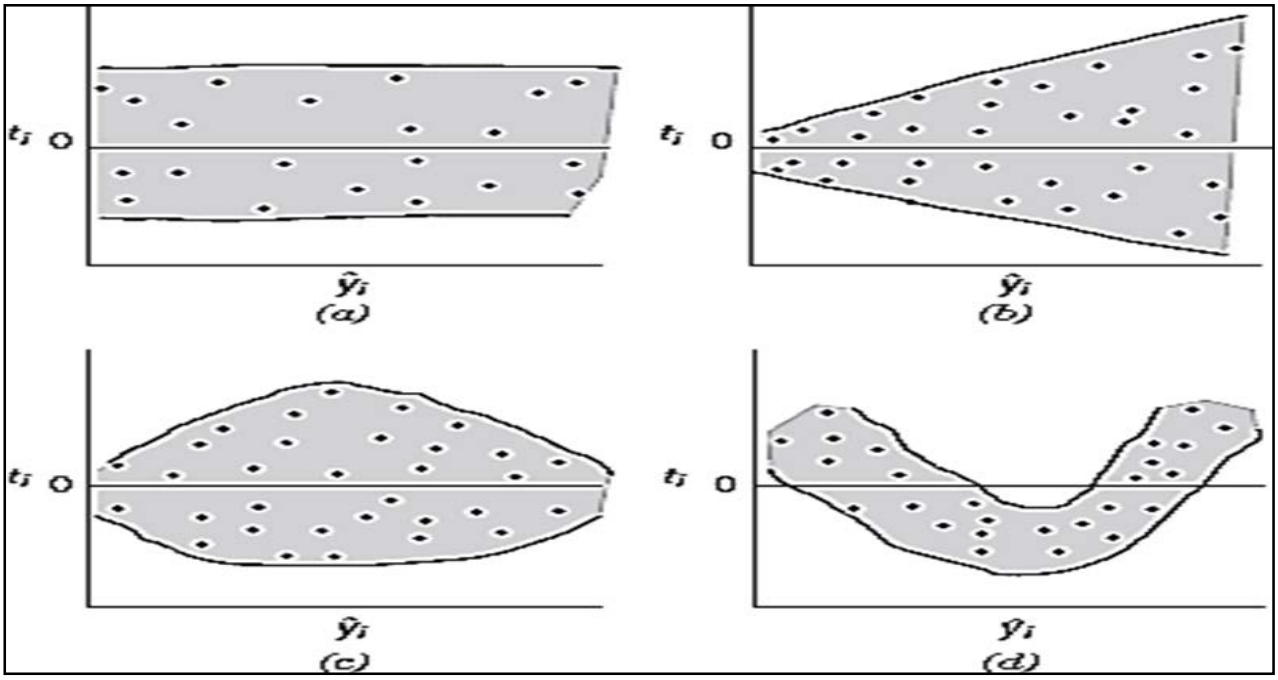

Figure 2.32: Patterns for residual plots: (*a*) satisfactory; (*b*) funnel; (*c*) double bow; (*d*) nonlinear (Montgomery et al., 2012).

A model with no obvious defects follows a pattern of residual on figure 2.32 (a). The plots of the patterns in figure 2.32 (b), (c) and (d) show symptoms of model deficiencies, where the variance of the errors in figures 2.32 (b) and (c) is not constant and in figure 2.32 (d) is a nonlinear curve. Figure 2.32 (d) may mean that other regressor variables are required in the model e.g. a squared term may be necessary and a transformation may be effective in this case (Montgomery et al., 2012).

Another potential violation of the basic regression assumptions is the presence of autocorrelation. Autocorrelation is the correlation between model errors at different time periods.

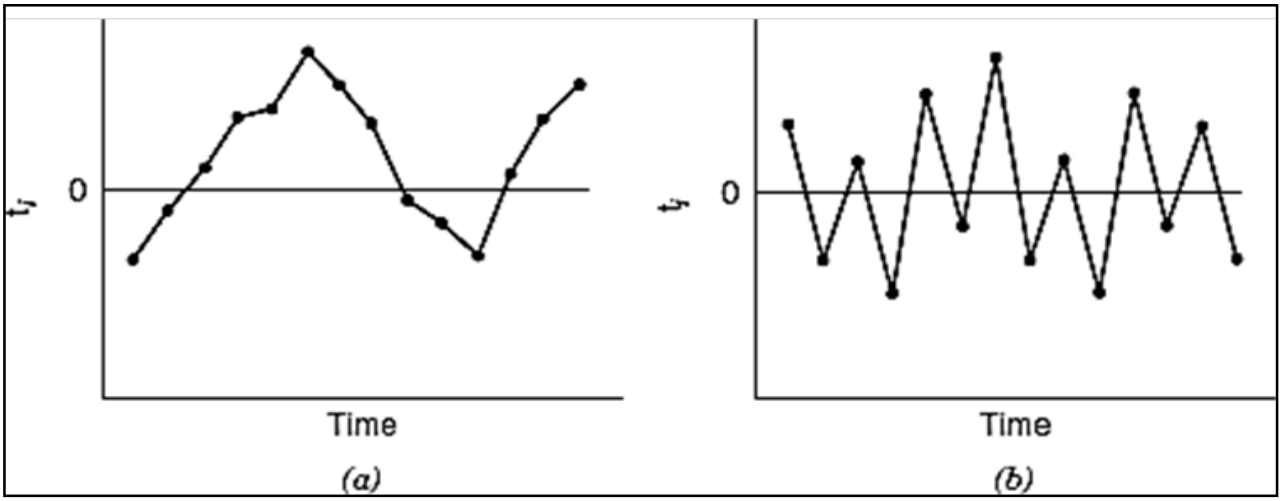

Figure 2.33: Prototype residual plots against time displaying autocorrelation in the errors: (*a*) positive autocorrelation; (*b*) negative autocorrelation (Montgomery et al., 2012)

2.9.4.2 Polynomial Regression Models in Two or More Variables

The regression function for fitting a second-order model such as eq 2.17 is called response surface. Table 2.13 shows the analysis of variance for the Chemical Process example. The example in table 2.13 indicates the lack of fit for the quadratic model shown by the *P* value ($P = 0.8120$) that is large, implying that the quadratic model is adequate.

Table 2.13: Analysis of Variance for the Chemical Process Example (Montgomery et al., 2012).

Source of Variation	Sum of Squares	Degrees of Freedom	Mean Square	F_0	*P* Value
Regression	1733.6	5	346.71	58.86	<0.0001
SS_R (β_1, β_2, β_0)	(914.4)	(2)	(457.20)		
SS_R (β_{11}, β_{22}, β_{12}, β_0, β_1, β_2)	(819.2)	(3)	(273.10)		
Residual	35.3	6	5.89		
Lack of fit	(8.5)	(3)	(2.83)	0.3176	0.8120
Pure error	(26.8)	(3)	(8.92)		
Total	1768.9	11			
$R^2 = 0.9800$		$R^2_{adj} = 0.9800$			PRESS = 108.7

The significance of regression is shown by the F value (58.86) with a P value of <0.0001 which signify that the quadratic model is significant and some of the coefficient parameters are nonzero. The R^2 and adjusted R^2 values for the model are satisfactory to fit the full quadratic model since the differences between the full and reduced model are not large. The $R^2_{prediction}$ is calculated as shown in eq 2.20 and it is an indication that the model can explain about 94 % of the variability in new data.

$$R^2_{prediction} = 1 - \frac{PRESS}{SS_T} = 1 - \frac{108.7}{1768.9} = 0.9385 \qquad 2.20$$

The studentized residuals or the values of R-student are not large to indicate any potential problems with outliers as shown in table 2.14 of the chemical process example.

Table 2.14: Observed Values, Predicted Values, Residuals, and Other Diagnostics for the Chemical Process Example (Montgomery et al., 2012)

Observed Value	Actual Value	Predicted Value	Residual	h_{ii}	Studentized Residual	Cook's D	R-Student
1	43.00	43.96	-0.96	0.625	-0.643	0.115	-0.609
2	78.00	79.11	-1.11	0.625	-0.745	0.154	-0.714
3	69.00	67.89	1.11	0.625	0.748	0.155	0.717
4	73.00	72.04	0.96	0.625	0.646	0.116	0.612
5	48.00	48.11	-0.11	0.625	-0.073	0.001	-0.067
6	76.00	75.90	0.10	0.625	-0.073	0.001	-0.067
7	65.00	63.54	1.46	0.625	0.982	0.268	0.979
8	74.00	75.46	-1.46	0.625	-0.985	0.269	-0.982
9	76.00	79.75	-3.75	0.250	-1.784	0.177	-2.377
10	79.00	79.75	-0.75	0.250	-0.357	0.007	-0.329
11	83.00	79.75	3.25	0.250	1.546	0.133	1.820
12	81.00	79.75	1.25	0.250	0.595	0.020	0.560

The plots in figure 2.34 show no sign of model defect. The example in figure 2.34 (a) and (b) show a horizontal line around the residuals of approximately zero, which suggests that the model fits the data well and the variances of the error terms are equal. The normal probability plot in figure 2.34 (c) suggests that the error terms are normally distributed (Montgomery et al., 2012).

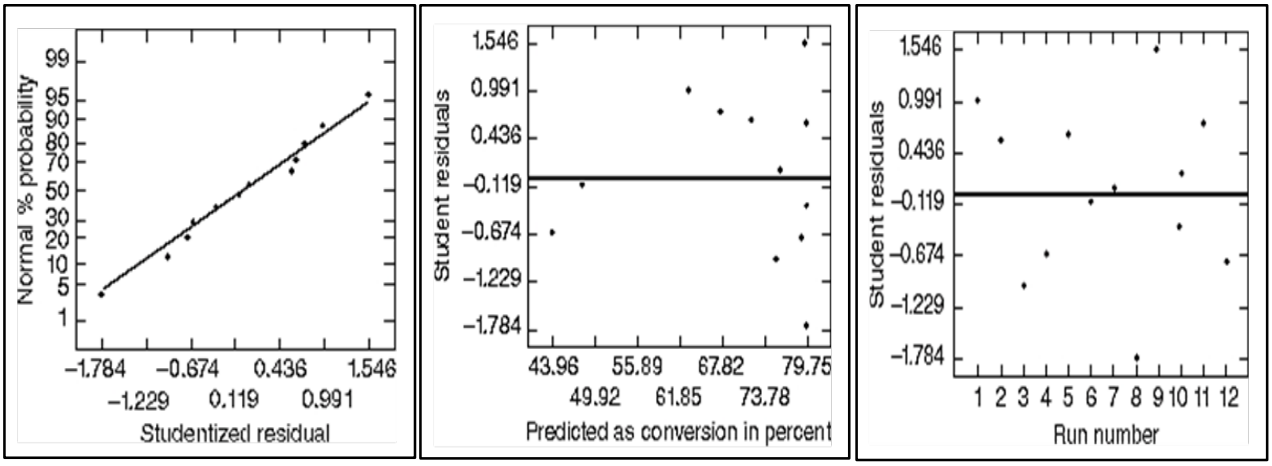

(a) . (b) (c)

Figure 2.34: (a) Normal probability plot of the studentized residuals, (b) Studentized versus predicted conversion, (c) Studentized residuals run order (Montgomery et al., 2012).

A response surface and contour plots in figure 2.35 will then indicate the maximum response with its corresponding independent variables.

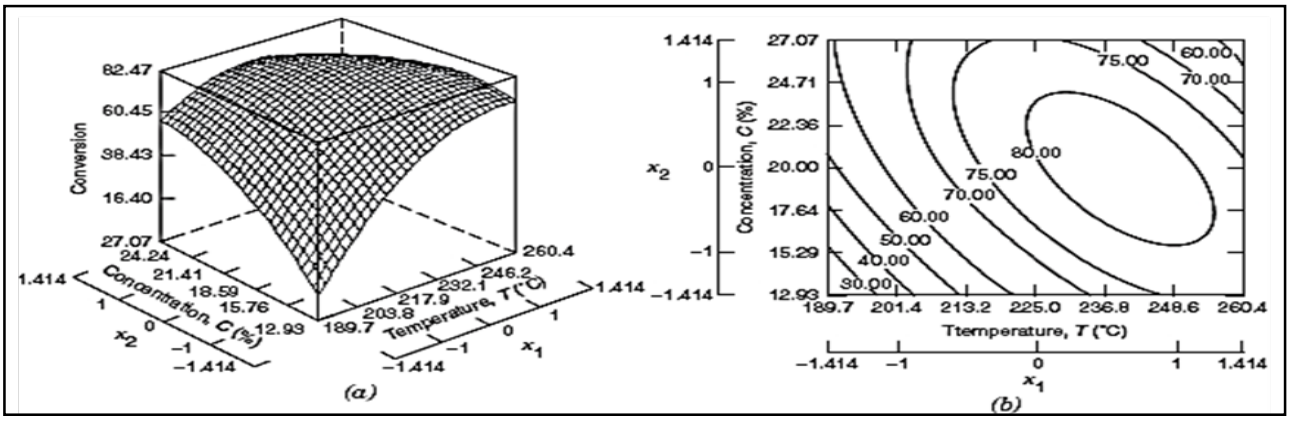

Figure 2.35: (a) Response Surface of predicted conversion, (b) Contour plot of predicted conversion (Montgomery et al., 2012).

The example of the response surface plot and contour plot indicate the maximum percent conversion at about 245 ˚C and 20 % concentration. The interest for using response surface and contour plot is in predicting the response (y) by estimating the mean response at a particular point in the process variable space.

2.10 SUMMARY

An increase in demand in potable water from industrial sector, agriculture and communities for human consumption is putting more stress in conventional treatment systems. The conventional treatment systems also require investment to keep up with the change in feed water contaminations. This leaves less investments on designing, installing and operation of more such treatment systems to deal with the demands. Small, footprint and decentralized treatment systems that are cheap, easy to operate and regenerate, and robust in producing water that is suitable for drinking need to be researched and practically applied. These systems must be for treating natural water resources that are contaminated and to treat wastewater that can be reused to oppress the exacerbated physical water scarcity due to climate change.

This study is evaluating the micro scaled particles of grades of TiO_2 locally produced as paint pigment for potable water production. The $mTiO_2$ is readily available, cheap and has no toxicity levels documented, therefore regarded as safe for consumption. The micro particles of TiO_2 are removable from treated water when a suitable separation process is used, which is a major setback with the practical application of nano particles of TiO_2 in water treatment. The literature shows that TiO_2 degrade organics and bacteria by mitigating the formation of sludge, whereby other processes are accumulation a sludge that need to be dealt with after water treatment. Further in this study, the recovered of the $mTiO_2$ from treated water was carried out using a locally manufactured PWFMF membrane.

The OFAT is the traditional method mostly used to carry out experiments. There are other methods that have more advantages on number of experiments, showing interactions between the factors, and giving high precision and predictions over the design limits for all the outputs of the system. The Central Composite design and Box-Behnken design were selected for this study because of the reliability of predictions on the number of factors selected when both designs were having same number of experiments.

CHAPTER 3

RESEARCH DESIGN AND METHODOLOGY

3.1 GENERAL INTRODUCTION

This chapter presents the materials used with the description of the sampling of the $mTiO_2$ grades from the simplified Sulphate Process are discussed, the experimental methods and analytical technique used in this study are also covered.

3.2 MATERIALS AND METHODS

3.2.1 Materials and Chemicals

The grades of $mTiO_2$ were sourced from Huntsman Tioxide SA. The four grades investigated are grade 1: Anatase, grade 2: Anatase with additions (Calciner feed), grade 3: Rutile (Calciner discharge) and grade 4: Coated Rutile (final product) as shown and presented in figure 3.1 and table 3.1 respectively.

The local river water used for the experiments was sourced from Umgeni and uMzinyathi Rivers. The turbidity ranged between 10-30 NTU and 50-80 NTU for Umgeni and uMzinyathi rivers respectively.

The starting pH of the water being treated was adjusted using sodium hydroxide (NaOH) 1 N/1 M prepared solution with pallets from Capital laboratory and Hydrochloric acid (HCl) 1 N/1 M solution H5800 from Minema. The pH meter Sension 1 with a temperature indicator from HACH was used to measure the pH and temperature. The temperature of the system was controlled using a low temperature water bath 3095U/CPM 50 5035U from Labcon which was connected to the copper cooling coil that was immersed in the solution.

The aeration was measured using the Kytölö MUURAME Air flowmeter EK-4AR-H from Finland. The air was supplied by the Oil-less air compressor.

The separation of treated water and $mTiO_2$ was carried out using PWFMF. PWFMF is a locally manufactured material by Galvenor Consolidated Fabrics PTY LTD located in Hammarsdale, SA.

The membrane is uncharacterized, therefore particle size ranges that have a potential of going through the membrane are not yet known.
The UV-light source was the F8T5/BL 8 Watt T5 Black Light Fluorescent of 30 cm long with wavelength range of 320-400 nm (UV-A).

3.2.1.1 Sampling of the grades of $mTiO_2$ for the Research Project.

In this project, $mTiO_2$ was used as the photocatalyst to degrade and mineralize bacterial pollutants in the river water to produce drinking water. Huntsman Tioxide SA produces their final product, which is coated rutile through the Sulphate process. In this Sulfate process as illustrated in figure 3.1 and 7.1 of the appendices, samples were taken at different points in the process and used for the investigation. The leaching of anatase type of TiO_2 from the Titania slag and heating it at 900 ^oC through a calciner to form rutile which is further processed to final product which is coated rutile motivated the sampling of the grades. The types of TiO_2 perform differently in the purification of water and air, therefore, an opportunity was taken to investigate these different grades.

The grades were sampled as follows; The Titania slag is first digested in a strong sulphuric acid and the clarified liquor is then hydrolyzed, pre-leach washed, leached and post-leach washed to produce hydrated titanium dioxide. The first grade (hydrated titanium dioxide, $hTiO_2$) is taken after post-leach washing. Chemicals that are referred to as additions are added to the hydrated TiO_2 to promote crystal growth, influence millability, acts as a rutile inhibitor and to improve durability with a balance charge, and then the second grade (hydrated titanium dioxide with additions, $ahTiO_2$) is taken just before entering the Calciner. The calcined product, which is anhydrous titanium dioxide ($anTiO_2$) is taken as the third grade. The $anTiO_2$ goes through further processing of drying and milling, screening and then coating with additions to have a pigment slurry. The pigment slurry is then washed with water, filtered and sent to a drier to produce a dried pigment titanium dioxide ($apTiO_2$). The $apTiO_2$ is sampled as the fourth grade.

The first two grades were predominantly in an Anatase form and were dried and milled before use as photocatalyst. The third sample was a Calciner discharge, which was in a rutile form because

grade 2 was subjected to high temperatures of up to 900 ^{o}C in the Calciner to change from Anatase to Rutile.

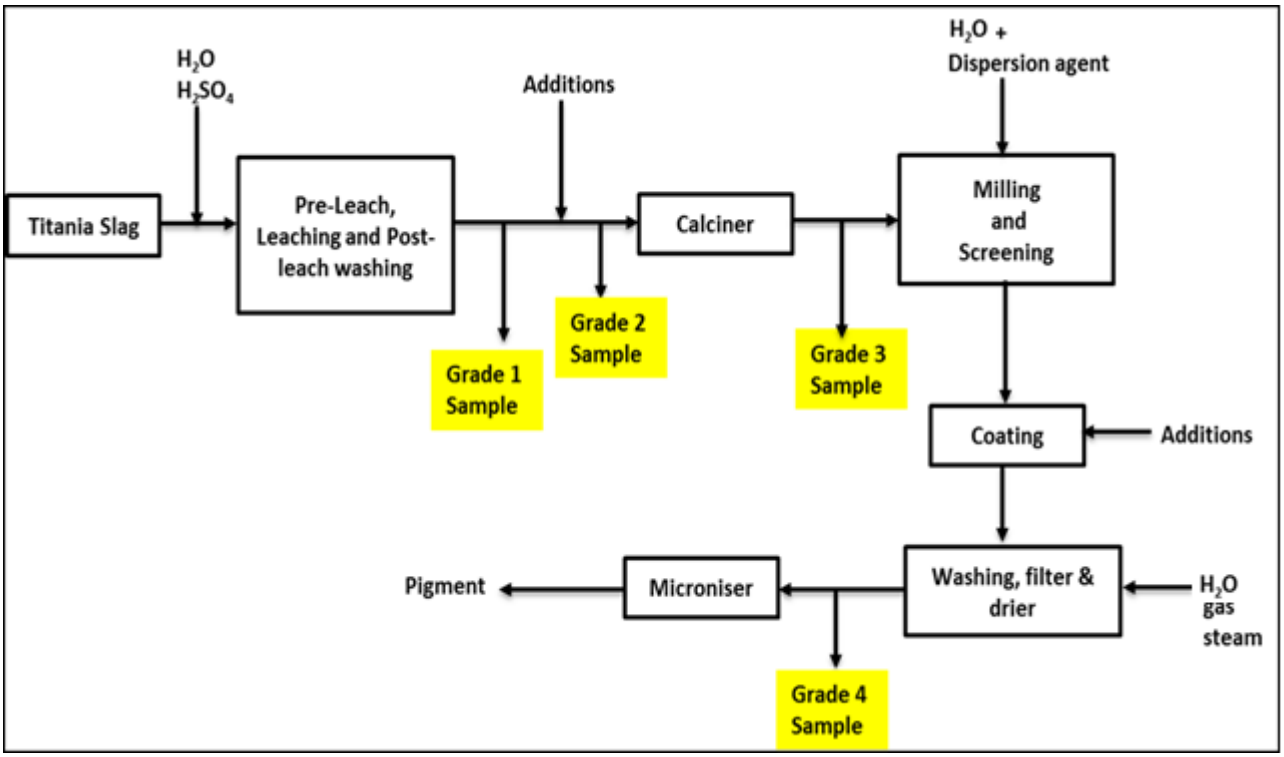

Figure 3.1: Tioxide Sulphate Process with sampling of the grades of $mTiO_2$.

The last sample was the final product of coated Rutile before milling it to its commercial size of 0.2-0.4 µm. All these samples of $mTiO_2$ are referred to as **GRADES of $mTiO_2$** in this study. The grades of $mTiO_2$ are shown as grade 1-4 sample in figure 3.1 and the simplified description tabulated in table 3.1.

Table 3.1: The description of the grades of $mTiO_2$ used in this project.

$mTiO_2$ Grades	Abbreviation	Description of the Grades
Grade 1	$hTiO_2$	Hydrated Titanium dioxide (Predominantly Anatase)
Grade 2	$ahTiO_2$	Hydrated Titanium dioxide with additions (anatase: Calciner feed)
Grade 3	$anTiO_2$	Anhydrous Titanium dioxide (Rutile: Calciner discharge)
Grade 4	$apTiO_2$	Anhydrous Titanium dioxide coated with additions (Rutile: final product)

3.3 EXPERIMENTAL SET-UP

Preliminary experimental process was conducted to give the most suitable limits and products to use for further research. This also assisted when the information on the subject is not currently available. The preliminary work for this study was carried out to support the selection of parameters, variables and materials to be used.

Since the $mTiO_2$ pigment from Huntsmen Tioxide RSA has not been used as a photocatalyst, preliminary experiments were conducted to investigate the photocatalytic activity of the product and the effect of particle size range and concentration on degradation of organics in river water. This lead to further study being done to investigate the best performing grade and to use the information to find the optimum value for the most important variables.

3.3.1 Photocatalytic activity of the $mTiO_2$ pigment using the Batch process.

The bench scale experiments were conducted in the laboratory to investigate photocatalytic activity of the locally produced $mTiO_2$. Umgeni river water with turbidity ranging between 10-30 NTU was used for the investigation. A randomly selected grade of the photocatalyst was used, which was $ahTiO_2$ as described in table 3.1 to degrade the organic pollutant in river water. The experiment conditions kept constant were the photocatalyst concentration of 2.5 g/L, irradiation time of 6 hours, particle size range of 0.2-53 µm and room temperature. The experiments were done using four beakers at a time with 8W UV light above the beakers as shown in figure 3.2. The suspension of the $mTiO_2$ particles in the beakers was ensured by using the SONIC 9905 aquarium air pump. The set-up was cover with a cloth to prevent the exposure of eyes and skin to the UV light. The samples for the analysis of organic pollutant in water were taken every hour for 6 hours.

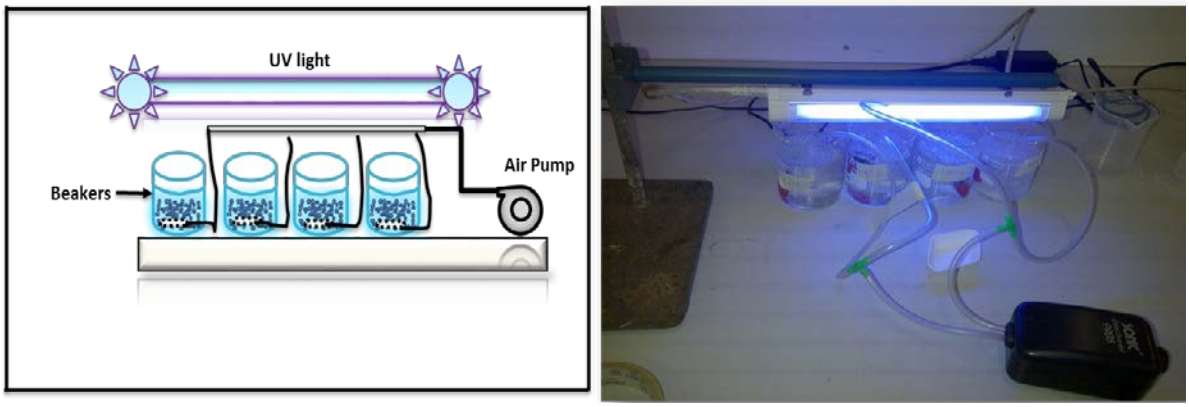

Figure 3.2: Schematic image for the investigation of Photocatalytic activity of the $mTiO_2$ pigment.

The second set of experiments were to investigate the effect of particle size range and photocatalyst concentration on the degradation of organic pollutant in river water. The same bench scale set-up was used. The experiments were conducted at room temperature for constant irradiation time of 3 hours. The variables investigated for this set of experiments were the size range of 0.2-53µm and 54-75µm, and the $mTiO_2$ concentrations of 2.5, 3.75, 5 and 7.5 g/L for each size range.

3.3.2 Photocatalytic activity using the Continuous Tubular Reactor.

These experiments were to investigate the effect of UV light without the $mTiO_2$ and the introduction of $mTiO_2$ on the degradation of organic pollutant in river water. The continuous tubular reactor used is as shown in figure 3.3 (a), and 3.3 (b) for the flow diagram.

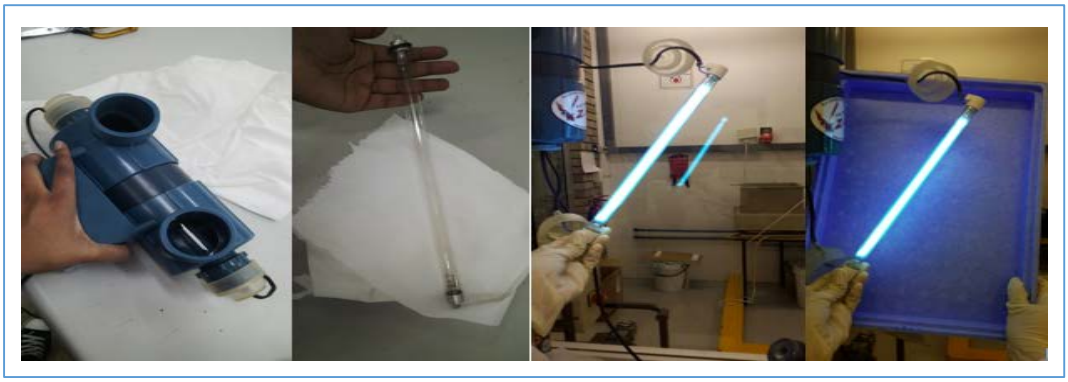

Figure 3.3 (a): The image of the Ultra Zap UV sterilizer with the UV light fitted inside.

The equipment consisted of the feed tank of 10 L feeding the Ultra Zap UV sterilizer, which is a 1.5 L reactor fitted with 8W UV-C light (100-280nm). The HPE60 peristatic pump was used to pump the solution. The flow was controlled and indicated using a 1 inch ball valve and water flowmeter respectively as shown in the flow diagram in figure 3.3 (b).

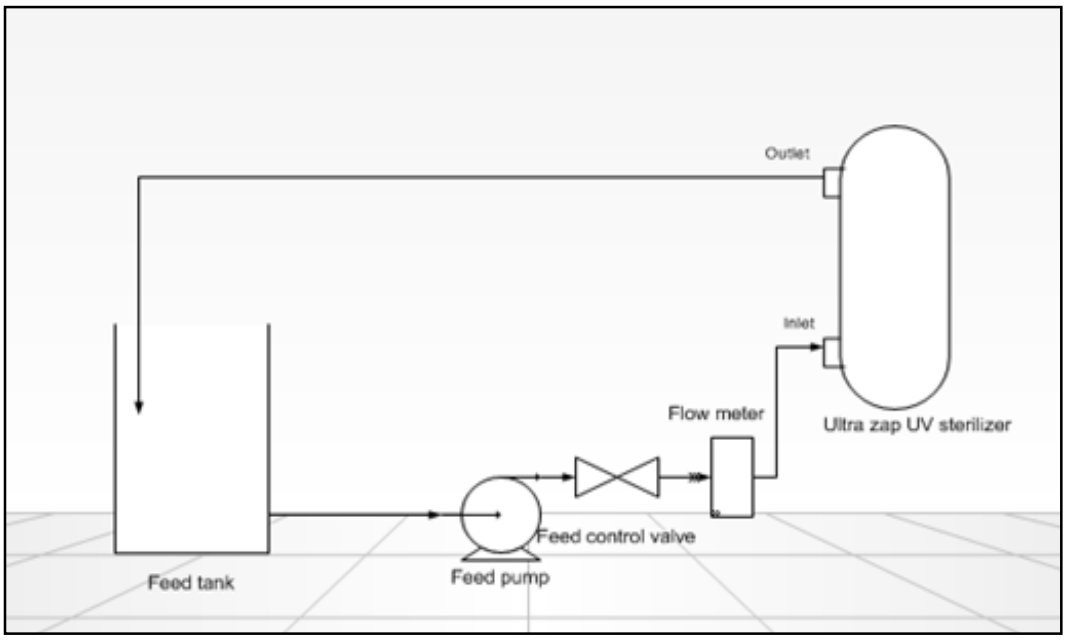

Figure 3.3 (b): The schematic diagram of the Continuous tubular reactor.

The experiments were conducted at room temperature and particle size range of 53-63 µm for constant irradiation time of 4 hours. The variables investigated for this set of experiments were the UV light with 0 g/L $mTiO_2$ and the $mTiO_2$ concentrations of 2, 5, 6, 7, 8 and 10 g/L.

3.3.3 Evaluation of the PWFMF on recovery of the photocatalyst ($mTiO_2$).

The recovery of the photocatalyst from treated water has been the major setback on the practical application of the photocatalytic systems. The uncharacterized PWFMF membrane was evaluated for the removal of the $mTiO_2$ from treated water. The experiments were carried out in the 17 L photocatalytic reactor, with 15 L $mTiO_2$ solution. To ensure suspension of the $mTiO_2$ particles in order to be exposed to the UV-A light (320-400 nm), the SONIC 9905 aquarium air pump was used.

The UV lights were placed on the outside on either side of the reactor and the experiments were conducted at room temperature.

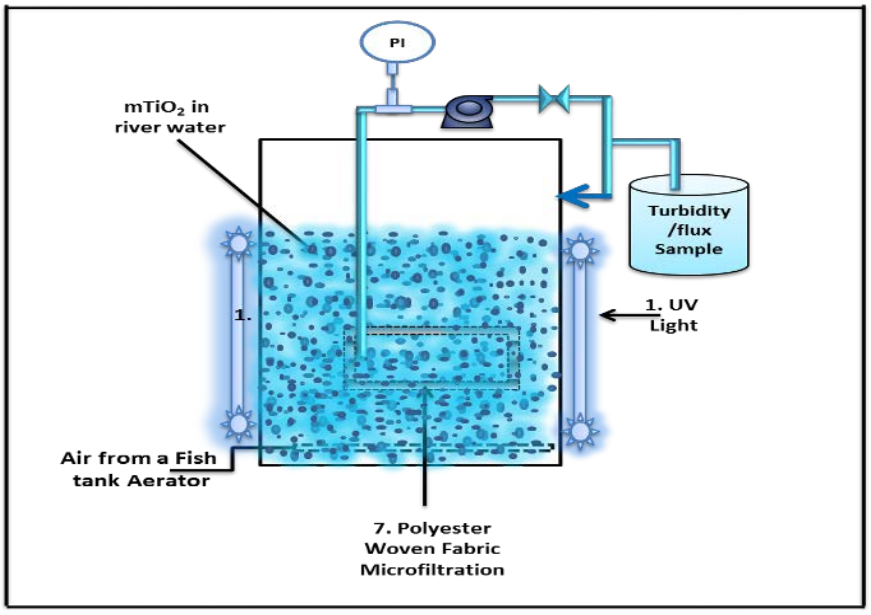

Figure 3.4: The experimental schematics for evaluation of PWFMF on Recovery of the $mTiO_2$ particle.

The PWFMF membrane was immersed in the solution as illustrated in figure 3.4 and a peristaltic pump was used to draw permeate from the membrane to the permeate tank. Permeate flowed through the walls of the membrane from the outside to the inside. In this way, contaminants and $mTiO_2$ particles accumulated in the reactor and on the outer wall of the membrane, forming a fouling layer which increase the hydrodynamic resistance to permeate flow.

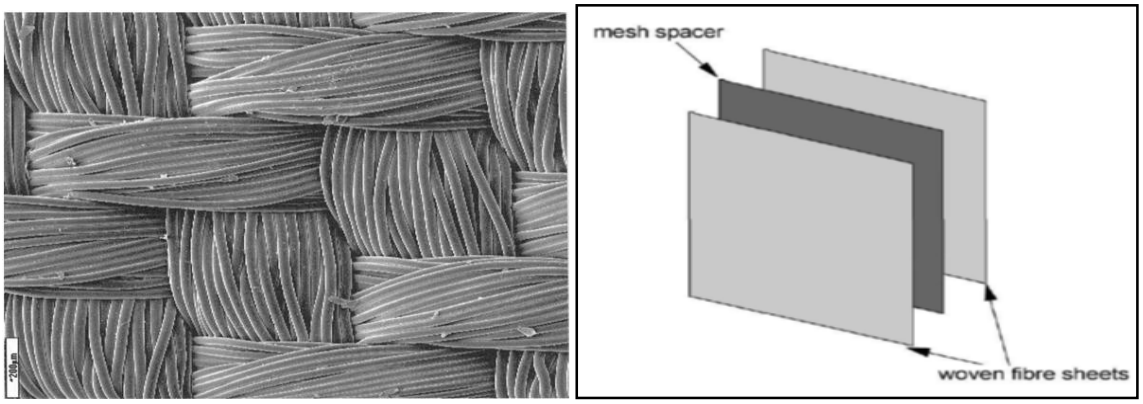

(a). **(b)**

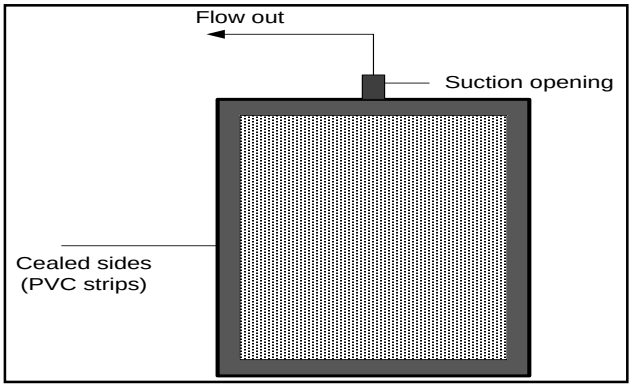

(c)

Figure 3.5: Polyester Woven Fabric Micro-Filtration membrane design, (a) Woven Fabric, (b) Flat sheet design, and (c) Final PWFMF membrane (Pillay and Jacobs, 2005, Pikwa et al., 2009).

Figure 3.5 shows the membrane design, where two woven fibre are separated by a sheet of flat mesh to create space between the woven sheets for a free movement of permeate. This approach is the same as that used in existing flat sheet immersed membranes (e.g. Kubota Membrane), with the difference that the woven fibre fabric is used instead of a flat sheet membrane (Pillay and Jacobs, 2005). The turbidity of permeate was measure every 5 minutes for 2 hours.

3.3.4 Optimization of the system by DOE.

This is the experimental apparatus used to obtain experimental data for the DOE to optimize the system. The uMzinyathi river water with TiO_2 in suspension was irradiated with UV light for 4 hours and samples were taken in 30 minutes, 2 hours and 4 hours to analyze gram –ve bacteria of *E. coli*. The optimization experiments were carried out in a 17 L photocatalytic reactor, with 10 L $mTiO_2$ solution. The samples to analyze E-coli were taken inside the suspension, and the turbidity and flux were measured after the membrane filtration. The oil-less air compressor was used to supply air in the tank and to keep the $mTiO_2$ particles in suspension. The air flowmeter was used to measure the air flowrate into the reactor. The cooling or heating coil was immersed in the suspension to control the temperature of the solution using the low temperature water bath.

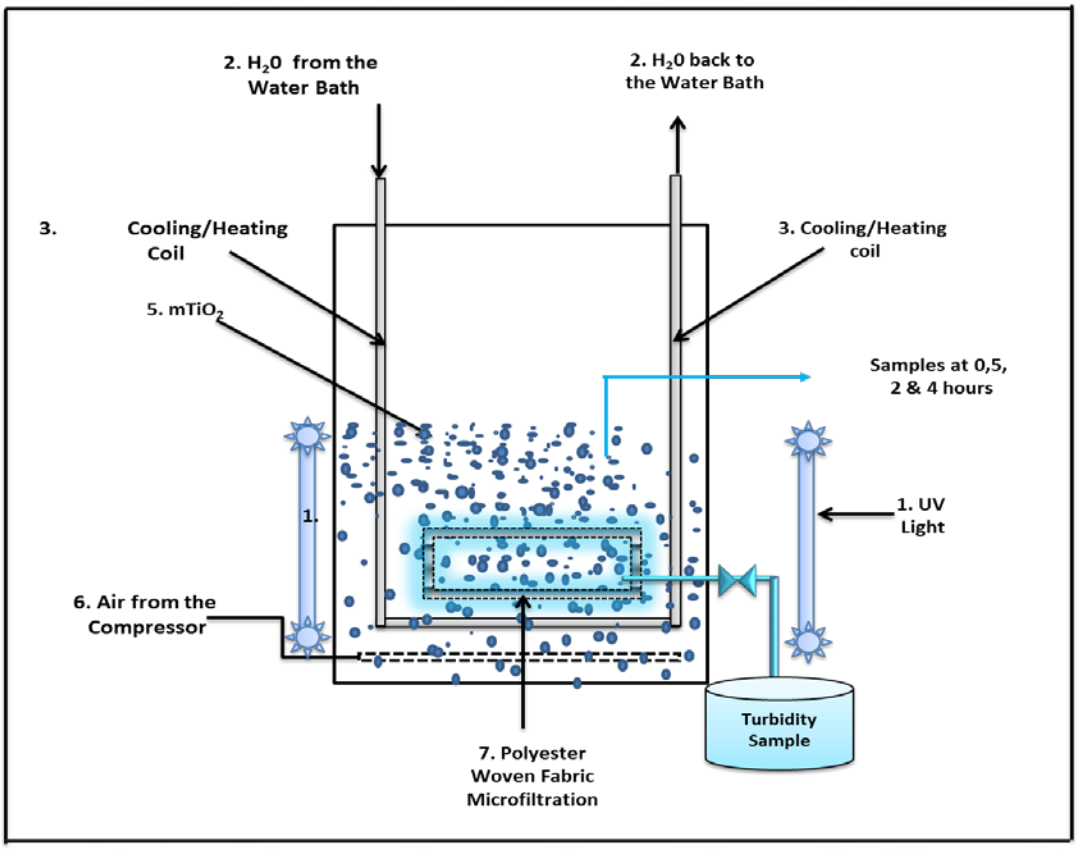

Figure 3.6: The experimental Apparatus for the degradation of bacteria and Separation of the catalyst from treated water.

The initial pH of the solution was adjusted using sodium hydroxide (NaOH) 1 N/1 M prepared solution and Hydrochloric acid (HCl) 1 N/1 M solution. The PWFMF membrane was submerged in the suspension in order to separate the $mTiO_2$ from treated water using gravity head as a driving force.

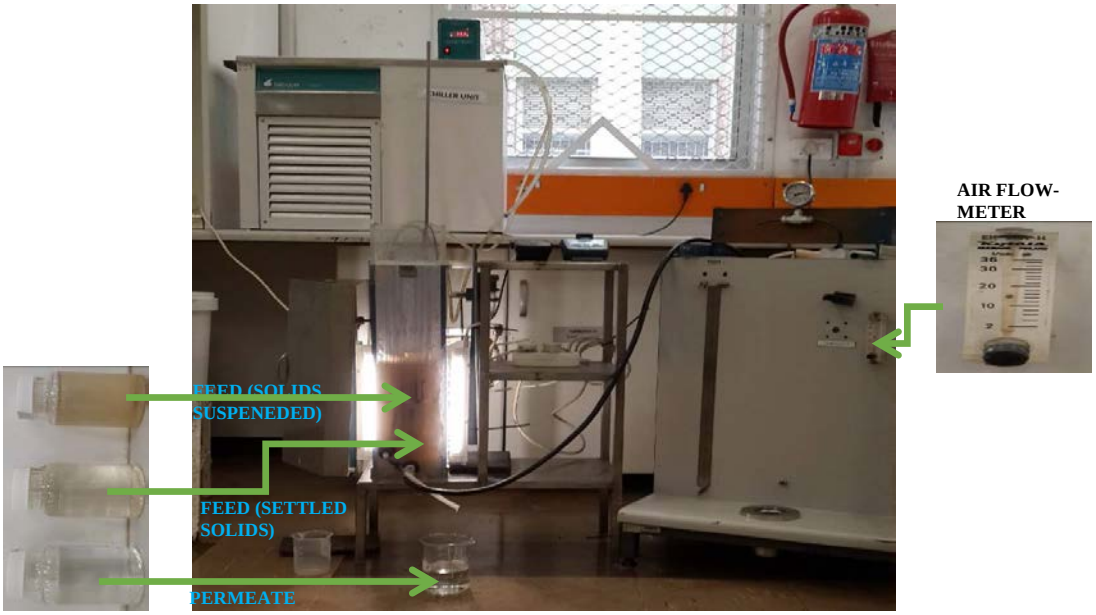

Figure 3.7: The set-up to optimize the system of the degradation of bacteria.

Permeate was basically drawn from the outside of the membrane into the membrane leaving the contaminants and mTiO_2 particles within the suspension. The optimization experimental set-up is as illustrated in figure 3.6 and 3.7.

3.4 SELECTED METHODS OF ANALYSIS.

3.4.1 Turbidity

Suspended matters in water were measured using the 2100Q HACH potable turbidity meter (cat No.: 2100 Q 01) as illustrated in figure 3.8 and the specification of this meter is in table 3.2.

Figure 3.8: The schematic image of the turbidity meters (grey and blue, grey and black), and pH meter (black).

Table 3.2: The turbidity meter's specification

Parameter	Specification
Measurement method	Ratio Nephelometric signal (90˚) scatter light ratio to transmitted light.
Range	0 – 1000 NTU (automatic); 0 – 9.99 NTU (manual)
Accuracy	± 2% of reading plus stray light from 0 – 1000 NTU
Resolution	0.01 NTU on lowest range
Repeatability	± 1% of reading or 0.01 NTU
Response time	6 seconds for full step change
Stray light	< 0.02 NTU

The initial sample (feed sample) measures the turbidity of the feed and the final samples measure the turbidity of treated water (samples after PWFMF). The percentage recovery of the $mTiO_2$ was then calculated as follows:

$$\%\ \text{Recovery} = \frac{(T_{\text{Initial}} - T_{\text{Final}})}{T_{\text{Initial}}} \times 100 \qquad 3.1$$

Where T_{Initial} is the feed turbidity and T_{Final} is the turbidity of treated water that has been passed through the membrane.

The calibration of the turbidity meter was carried out with the supplied standards to ensure the accuracy of the results. This must be conducted as often as required or as indicated by the equipment. For this study, the turbidity meter was calibrated every day before use.

A set of stablCal primary standards are provided in sealed vials each containing the solutions which read; <0.1 NTU, 20 NTU, 100 NTU, 800 NTU.

To calibrate the equipment, switch the meter on, and push the CAL button, the screen will display the CAL and S1 icons as well as the turbidity reading of one of the required primary standard stated above. Insert the required standard and push the READ button. The screen will now display the next primary standard required, insert the standard and push read. Repeat this until all the primary

standards have been inserted and read. The meter is now ready for use. Sources of error that might affect reading of the results are as follow:

- When taking the reading place the meter on a stationary and level surface, do not hold in hand.
- Always close the compartment lid during sample reading.
- Ensure that the sample cell is not scratched or dirty, these factors may influence the accuracy of measurements.
- Avoid settling of sample before measurement.

3.4.2 *E. coli* or total coliform

E. coli and total coliform were measured using the most probable number (MPN) technique, which estimate microbial population. The MPN method used for this study is IDEXX Colilert-18 procedure. The 100 ml samples of solution before filtration was sampled for *E. coli* and total coliform tests. The content of Colilert powder (one pack) was added to the 100 ml sample and shaken. The sample was then poured into a Quanti-Tray or Quanti-Tray®/2000. Sealed Quanti-trays were placed in an incubator for 18 hours and results were read thereafter.

Figure 3.9: Quanti-trays after incubation (initial and treated water samples)

According to IDEXX procedure, Colilert-18 detects both total coliforms and *E. coli* or fecal coliforms in water. When the total coliforms metabolize, the sample turns yellow and when E.coli metabolize, the sample fluoresces as shown in figure 3.9. The bacterial pollutant in river water before

and after degradation was quantified as the percentage degradation (DE) using the following equations.

$$\mathrm{DE} = \frac{\left(E.coli_{\mathrm{Initial}} - E.coli_{\mathrm{Final}}\right)}{E.coli_{\mathrm{Initial}}} \times 100 \qquad 3.2$$

$$\mathrm{DE} = \frac{\left(\mathrm{T.coliform}_{\mathrm{Initial}} - \mathrm{T.coliform}_{\mathrm{Final}}\right)}{\mathrm{T.coliform}_{\mathrm{Initial}}} \times 100 \qquad 3.3$$

E. coli, Initial and T. coliform, Initial are the bacteria before water treatment, and *E. coli*, Final and T. coliform, Final are the bacteria in water after it has been irradiated with UV light.

3.4.3 COD

COD measures the oxygen equivalent consumed by organic matter in a sample during strong chemical oxidation. COD were measured using USEPA Reactor Digestion Method. Samples of solution are taken and 2 ml are then transferred into the Dichromate Low Range Reagent vials as shown in figure 3.10 (a). The vial is placed for 2 hours into the COD Digester which is pre-heated to 150 ^{0}C. The vials are removed from the COD Digester and allowed to cool to room temperature and the COD results in mg/ L are determined using a spectrophotometer in figure 3.10 (c). According to (Agrawal, 2009), the drinking water specification of COD should not be more than 10 ppm (10mg/L).

(a) (b) (c)

Figure 3.10: (a) COD vials ready for digestion, (b) COD digesters, (c) The spectrophotometer.

The organic pollutants in river water before and after degradation was quantified as the percentage degradation (DE) as follow:

$$DE = \frac{(COD_{Initial} - COD_{Final})}{COD_{Initial}} \times 100 \qquad 3.3$$

$COD_{, Initial}$ is the bacteria before water treatment and $COD_{, Final}$ is the bacteria in water after it has been irradiated with UV light.

Precautions to be taken when doing this analysis are as follows (James, 2015):

- When inverting the vial before placing in the digester, hold vial at cap only, the contents of the vial may become very hot once the sample is added.
- At least one reagent blank must be used with each set sample vials.
- The vials may shatter if dropped or rapidly cooled, after reaction contents of the vials may be carcinogenic.

Sources of error that must be taken into account are:

- Mercury vials containing low and high range COD reagents are formulated to withstand interferences of up to 2000 ppm chloride, high range plus COD reagent can withstand up to 20000 ppm chloride. Samples with higher chloride concentrations require dilution.
- Also, samples that contain high levels of chloride (>1000 ppm) and low levels of COD (<30 % of the product range) will give false positive readings and in this case, sample requires dilution.

Table 3.3: COD Vial types and ranges

Range name	Range (mg/L)
Low range (LR)	0 – 150
High range (HR)	0 – 1500
High range plus (HR+)	0 – 15000

3.5 DESIGN OF EXPERIMENTS (DOE) EXPERIMENTAL MATRIX.

A Central Compose Design (CCD) and the Box-Behnken design (BBD) were used in this project to generate the experimental matrix for the four factors. The Design Expert software 9.0 was used to generate and optimize the experimental data. The experimental design for this work was a second order factorial design required to determine the optimum values of $mTiO_2$ loading or concentration, temperature, aeration and initial pH. These four factors affect the photocatalytic activity of the TiO_2. The response variable for the project is the photocatalytic degradation of bacteria in river water.

The ranges chosen for the optimization experiments were based on literature and preliminary experiments. The $mTiO_2$ loading was based on preliminary experiments of this study with the low-level of 3 g/L and the high level of 8 g/L, where both *E. coli* and total coliform met the drinking water specification at TiO_2 concentration of 5 g/L. The low-level temperature was 20 ^oC and the high level of 40 ^oC were used for the study because the TiO_2 apparent activation energy is between 20 and 80 ^oC (Malato et al., 2009). The high level temperature of 40 ^oC was selected for the rural communities with poor or no working infrastructure because heating beyond this point will require cooling before drinking. The pH of the solution was adjusted to a lower level of pH 3 to a high level of pH 8 (Ku et al., 1996, Vasiliev, 2008).

A 2^4 factorial design chosen was used to study the variables at two levels by conducting sixteen experiments (e.g.2^4 =16) (Korus et al., 1993). Tables 3.4 (a) and (b) show variables with levels coded in such a way that minus one (-1) represents the low level and plus one (+1) represents the high level. A level of zero (0) is the average of the low and high levels, which is added in the experiments. The zero level was added to provide a measure of process stability and inherent variability, and to check for curvature in the surface response.

Table 3.4 (a): Experimental Range and Levels of the four Variables or Factors for the CCD

Variables	Symbols	Ranges and Levels				
		-α	-1	0	1	+α
TiO_2 Loading (g/L)	X_1	0.5	3	5.5	8	10.5
Temperature (^{0}C)	X_2	10	20	30	40	50
Starting pH	X_3	2	4	6	8	10
Aeration (l/min)	X_4	2	6	10	14	18

There were six (6) experiments for the system-recommended center points. The center point runs were dispersed throughout the design matrix as shown in table 3.5 and 3.6. The CCD generates new extremes for all factors to create the star points (-α and +α). The star points consisted of eight (8) experiments, which made up thirty (30) experimental runs for the CCD design.

Table 3.4 (b): Experimental Range and Levels of the four Variables or Factors for the BBD

Variables	Symbols	Ranges and Levels		
		-1	0	1
TiO_2 Loading (g/L)	X_1	3	5.5	8
Temperature (^{0}C)	X_2	20	30	40
Starting pH	X_3	4	6	8
Aeration (l/min)	X_4	6	10	14

The Design expert software generates 24 experiments for the BBD based on the combination of the low, mid and high levels, plus 6 center points intentionally selected instead of 5 default center points, see figure 3.4 (b). Therefore, the total experiments for the BBD was 30 runs.

The total number of experiments for both CCD and BBD were 60 runs. Each run was irradiated for 4 hours and the samples were taken in 0.5, 2 and 4 hours.

Table 3.5: The Central Composite Design Matrix for Four Factors.

Std. Order	Run Order	Coded Process Factors				Actual Process Factors				Response
		X_1	X_2	X_3	X_4	C (g/L)	T (^{O}C)	pH	Air (L/min)	Y
1	8	-1	-1	-1	-1	3	20	4	6	
2	26	1	-1	-1	-1	8	20	4	6	
3	27	-1	1	-1	-1	3	40	4	6	
4	20	1	1	-1	-1	8	40	4	6	
5	9	-1	-1	1	-1	3	20	8	6	
6	10	1	-1	1	-1	8	20	8	6	
7	12	-1	1	1	-1	3	40	8	6	
8	25	1	1	1	-1	8	40	8	6	
9	13	-1	-1	-1	1	3	20	4	14	
10	19	1	-1	-1	1	8	20	4	14	
11	2	-1	1	-1	1	3	40	4	14	
12	3	1	1	-1	1	8	40	4	14	
13	18	-1	-1	1	1	3	20	8	14	
14	14	1	-1	1	1	8	20	8	14	
15	29	-1	1	1	1	3	40	8	14	
16	1	1	1	1	1	8	40	8	14	
17	22	-2	0	0	0	0.5	30	6	10	
18	23	2	0	0	0	10.5	30	6	10	
19	7	0	-2	0	0	5.5	10	6	10	
20	21	0	2	0	0	5.5	50	6	10	
21	15	0	0	-2	0	5.5	30	2	10	
22	6	0	0	2	0	5.5	30	10	10	
23	30	0	0	0	-2	5.5	30	6	2	
24	5	0	0	0	2	5.5	30	6	18	
25	4	0	0	0	0	5.5	30	6	10	
26	16	0	0	0	0	5.5	30	6	10	
27	17	0	0	0	0	5.5	30	6	10	
28	24	0	0	0	0	5.5	30	6	10	
29	11	0	0	0	0	5.5	30	6	10	
30	28	0	0	0	0	5.5	30	6	10	

Tables 3.5 and 3.6 were generated using the Design expert software 9.0. The experiments were conducted by randomized run order instead of standard order to minimize variability of the response variable (Zhang et al., 2010).

Table 3.6: The Box-Behnken Design Matrix for Four Factors.

Std. Order	Run Order	Coded Process Factors				Actual Process Factors				Response
		X_1	X_2	X_3	X_4	C (g/L)	T (^{O}C)	pH	Air (L/min)	
1	22	-1	-1	0	0	3	20	6	10	
2	20	1	-1	0	0	8	20	6	10	
3	18	-1	1	0	0	3	40	6	10	
4	5	1	1	0	0	8	40	6	10	
5	1	0	0	-1	-1	5.5	30	4	6	
6	10	0	0	1	-1	5.5	30	8	6	
7	13	0	0	-1	1	5.5	30	4	14	
8	3	0	0	1	1	5.5	30	8	14	
9	7	-1	0	0	-1	3	30	6	6	
10	14	1	0	0	-1	8	30	6	6	
11	25	-1	0	0	1	3	30	6	14	
12	17	1	0	0	1	8	30	6	14	
13	29	0	-1	-1	0	5.5	20	4	10	
14	16	0	1	-1	0	5.5	40	4	10	
15	8	0	-1	1	0	5.5	20	8	10	
16	9	0	1	1	0	5.5	40	8	10	
17	19	-1	0	-1	0	3	30	4	10	
18	2	1	0	-1	0	8	30	4	10	
19	26	-1	0	1	0	3	30	8	10	
20	21	1	0	1	0	8	30	8	10	
21	27	0	-1	0	-1	5.5	20	6	6	
22	6	0	1	0	-1	5.5	40	6	6	
23	4	0	-1	0	1	5.5	20	6	14	
24	11	0	1	0	1	5.5	40	6	14	
25	30	0	0	0	0	5.5	30	6	10	
26	24	0	0	0	0	5.5	30	6	10	
27	28	0	0	0	0	5.5	30	6	10	
28	23	0	0	0	0	5.5	30	6	10	
29	15	0	0	0	0	5.5	30	6	10	
30	12	0	0	0	0	5.5	30	6	10	

CHAPTER 4

RESULTS AND DUSCUSSION

4.1 GENERAL INTRODUCTION

This chapter presents the experimental results for the optimization of the photocatalytic degradation of bacteria in river water to produce potable water. Firstly, the $mTiO_2$, which is a commercial product produced locally as pigment for paint was evaluated for photocatalytic activity. Four grades of $mTiO_2$ were sampled at different points from the sulphate process and the best performing grade on the degradation of gram –ve bacterial (i.e. *E. coli* and total coliform) was further investigated.

4.2 PHOTOCATALYTIC ACTIVITY OF $mTIO_2$ PIGMENT

4.2.1 The effect of reaction time on degradation efficiency of organics

This was essentially a screening process to determine if the particles produced as pigment for paint have any photocatalytic activity in degrading organic matters present in river water. The arbitrarily selected $hTiO_2$ (Grade 2: Hydrated Titanium dioxide with additions) was used to evaluate the photocatalytic activity for the effect of irradiation time and particle size on degradation of organics as presented in figure 4.1. The experiments were carried out under constant conditions such as $ahTiO_2$ concentration (2.5 g/L), irradiation time (6 h), particle size range of 0.2–53 μm, and room temperature (23-25 ^oC) depending on the weather.

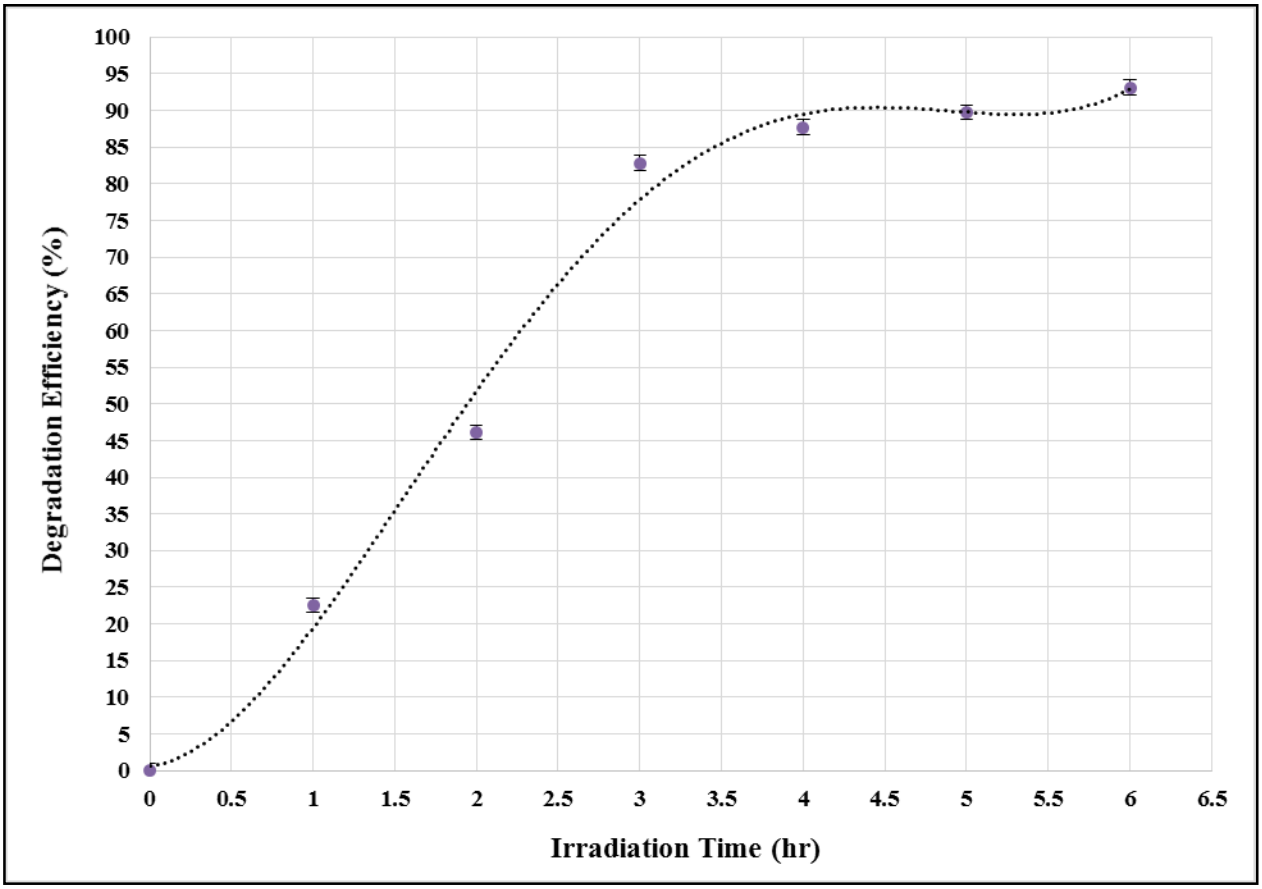

Figure 4.1: Effect of Irradiation Time on degradation of organics

The results show a rapid increase in degradation of organics from 0 to 88 % in the first four hours of irradiation and thereafter, the degradation only increased by 5 % to 93 % in two hours. The degradation of organic pollutant slows down after four hours. The errors were significantly small, which indicated that the data points were closer to the mean where 95 % of the data points were within the 1st standard deviation. This industrial locally produced grade of ahTiO_2 is photocatalytic, and suitable to be used for further investigation.

4.2.2 The effect of particle size and catalyst loading of ahTiO_2 on degradation efficiency of organics

The loading of ahTiO_2 with the particle size range was also investigated on the degradation of organics in river water as presented in figure 4.2. Two-particle sizes of range of 0.2-53 µm and 54-

75 µm were investigated. The reaction time for this investigation was 3 hours of irradiation based on figure 4.1 that showed a more economical irradiation time in 3 hours for the degradation of organics in river water.

The results for the particle sizes of range of 0.2-53 µm and 54-75µm both show similar trend. An increase in ahTiO_2 concentration from 0 to 5 g/L shows a significant increase in degradation efficiency from 0-90 and 0-77% for the mTiO_2 of range of 0.2-53µm and 54-75µm respectively. A similar trend was obtained by Shivaraju (2011). The trends indicate that the optimum concentration of mTiO_2 is between 5 and 7.5 g/L, and a further increase in concentration to 7.5 g/L makes no significant impact on the degradation and this is due to excess catalyst particles that scatter and reduce UV light penetration. The excess particles also shadow the contaminants from being degraded, which results in decreased photodegradation. The results obtained by Jain et al. (2012) indicated a decrease in *E. coli* degradation of the sewage samples when degradation was carried out over 6 hrs.

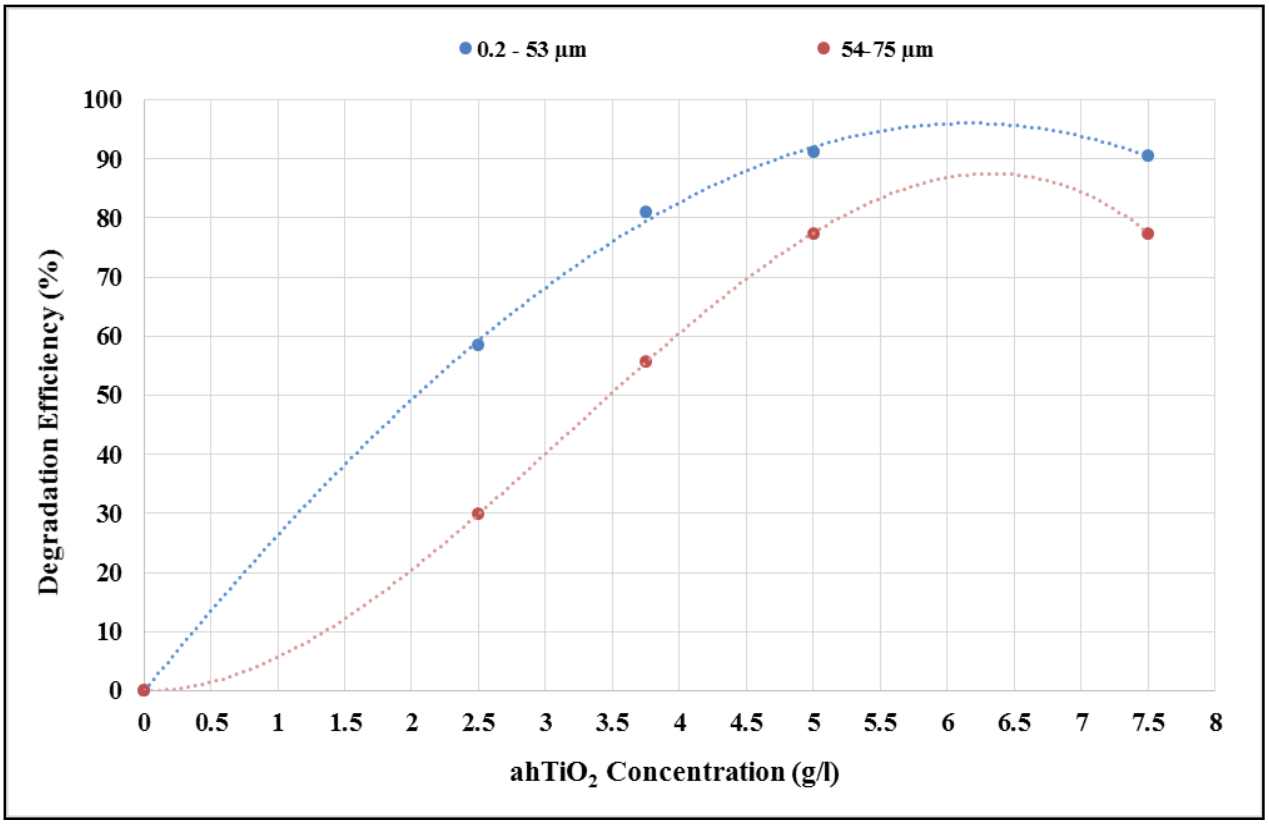

Figure 4.2: Effect of particle size and catalyst loading on degradation of organics.

The particle size range of 0.2 – 53 µm shows a better performance than the bigger particle size range of 54 – 75 µm as supported by Porter et al. (1999) results that show that an increase in particle size shows a reduced surface area which reduces the photocatalytic activity.

4.2.3 Photocatalytic activity using the Continuous Tubular Reactor.

Another preliminary study carried out on the continuous tubular reactor for the degradation of organics from Isipingo river water showed that the UV light had little effect on degradation in the absence of the catalyst. Table 4.1 shows the effect of concentration on degradation of organics in Isipingo river water where each run was irradiated for 4 hours at room temperature. The first run with 0 g/L TiO_2 concentration was illuminated with UV light for 4 hours and the degradation after that 4 hours was only 7 %. In the absence of $mTiO_2$ there was low degradation by UV light.

Table 4.1: Effect of concentration on degradation efficiency of organics in Isipingo river water

TiO_2 (53-63 µm)	COD (mg/l)		Degradation Eff.
g/L	Initial	final (4 hrs)	(%)
0	117	109	7
2	117	77	34
4	117	58	50
5	117	52	56
7	117	38	68
8	117	57	51
10	117	80	32

The degradation increased with an increased concentration until 7 g/L where the maximum degradation achieved was 68 %, and the degradation decreased with increased catalyst loading. A decreased degradation with increased $mTiO_2$ concentration indicated excess $mTiO_2$ particles that caused insufficient exposure to the UV light of both particles and contaminants. Jain et al. (2012) investigated degradation E. coli by TiO2 in the dark (absence of UV light), which also indicated that there was degradation although lower than in the presence of UV irradiation.

4.2.4 Recovery of TiO_2 from treated water.

A calibration curve was obtained, which best fitted a linear curve as shown in figure 4.3. The catalyst loading of 5g/l and particle size range of 0.2 – 53 µm was then filtered using a PWFMF. A calibration curve was developed and in a simple linear regression, the model is as shown in figure 4.3 that was used to quantify the amount of $ahTiO_2$ in the permeate.

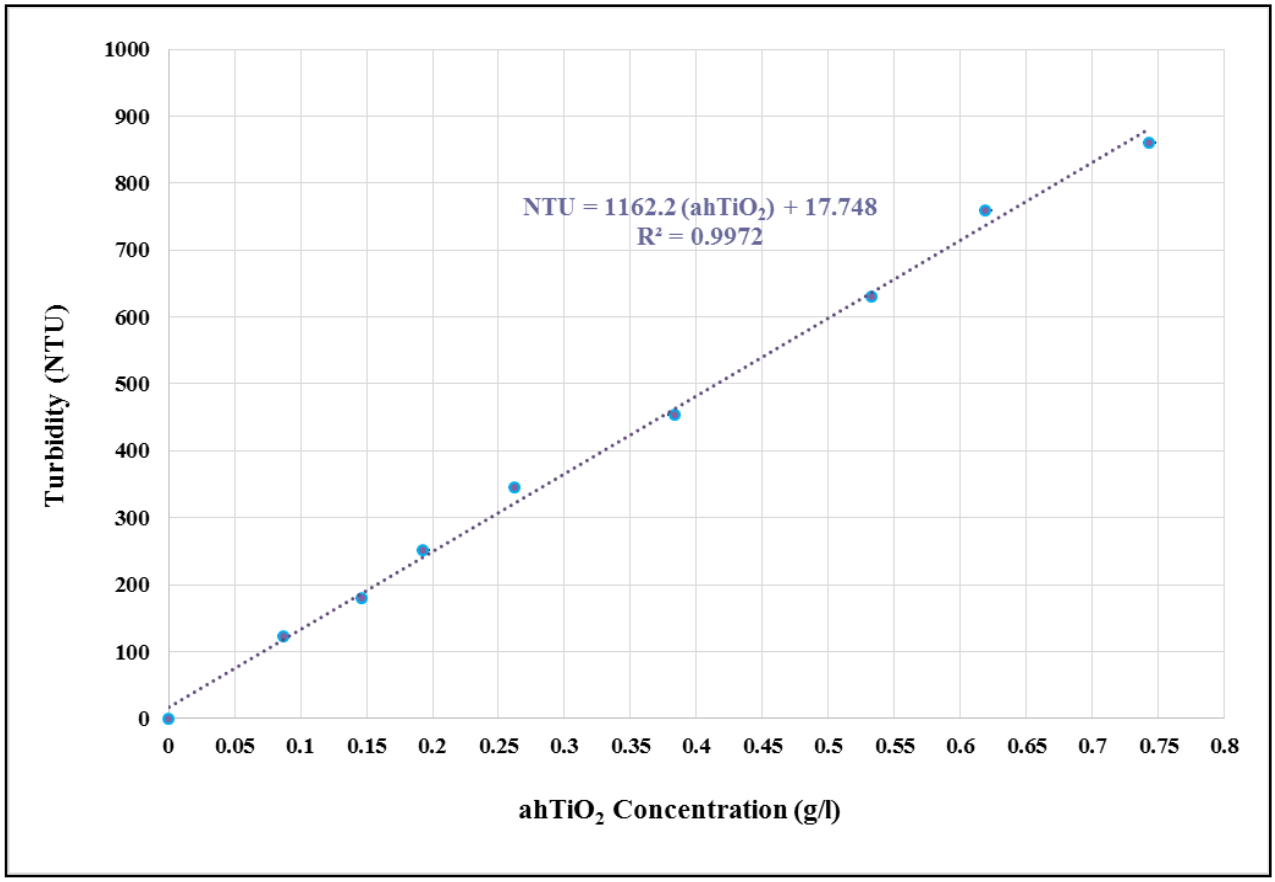

Figure 4.3: The Calibration Curve for the $mTiO_2$ concentration

Therefore, figure 4.4 shows that the concentration of $ahTiO_2$ in permeate measured a single digit (<10 mg/l) in just 5 minutes of filtering from the initial concentration of 354-380 mg/l as presented in tables A-7.5 - A-7.7 in the appendices. The percentage recovery of all three trials (each with three runs) were above 97 % as shown in figure 4.4. The turbidities in all three trials and all the runs were <1 NTU after 20 minutes. The assumption made was that, other suspended solids in water are negligible although river water has suspended matters. Trial 3, which was a membrane that had been

used for other two trials and washed with tap water and a brush, shows the best recovery of 98.97 % in 2 hours. The best recovery was due to the possibility that some of the particles blocked the pores of the membrane or rested on the membrane surface, which reduced the membrane pores thus smaller particles were retained.

The permeate flux and ahTiO$_2$ percentage recovery in figure 4.4 show that an increase in resistance due to cake thickness, the flux decreases with time until 40 min. The cake thickness was indicated by the ahTiO$_2$ recovery. The cake thickness became constant after 40 min because of the aeration that minimized the build-up of cake thickness. This resulted in constant permeate flux after 40 min. The theory indicates that an increase in resistance due to increase in cake thickness decreases flux with time (Pillay and Jacobs, 2005).

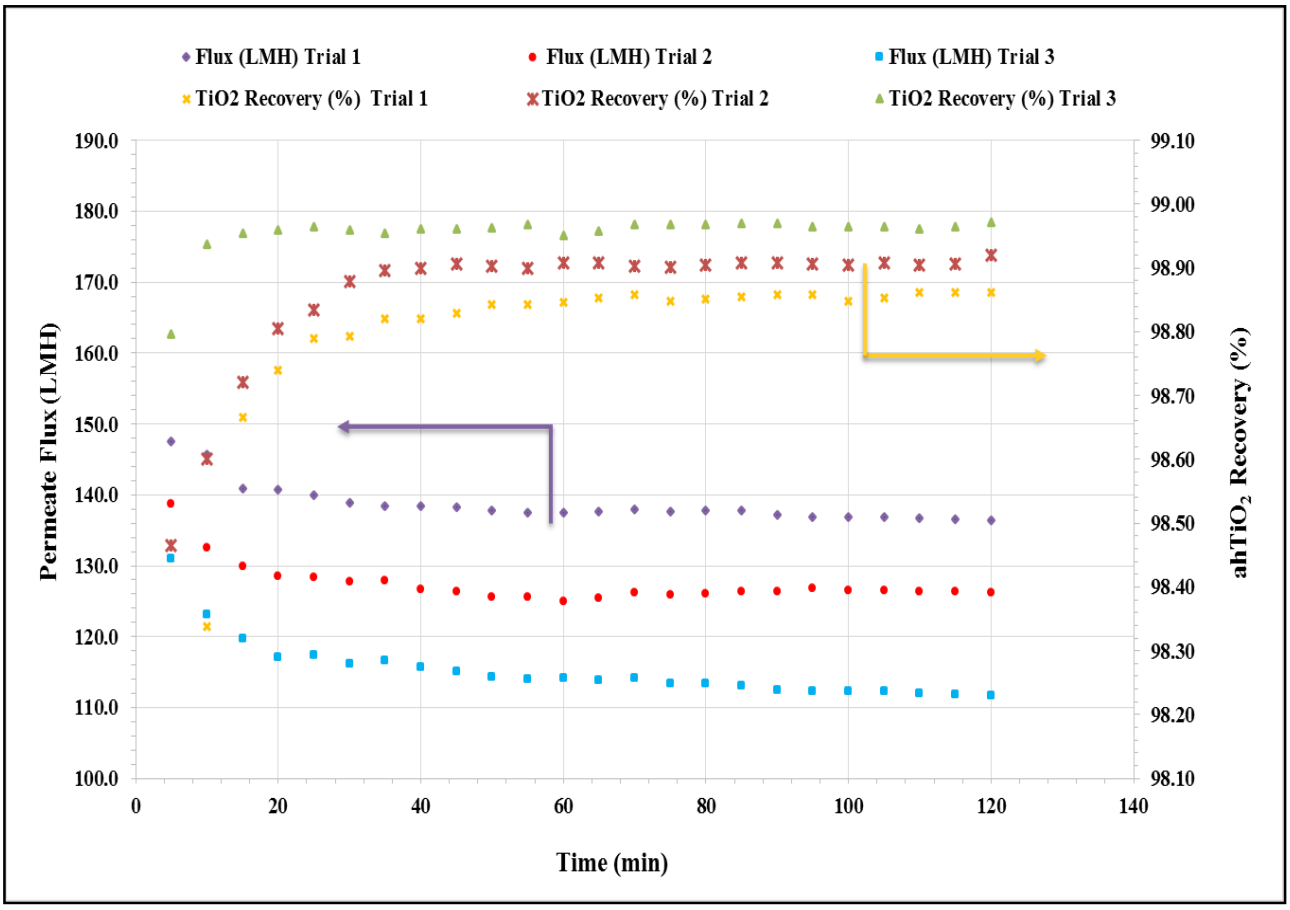

Figure 4.4: Evaluation of PWFMF on Recovery of particle size range of 0.2 – 53 µm

When the permeate flux is constant, the TMP across the membrane increases with time until it reaches a high value, therefore, the membrane requires cleaning to restore lower TMP (Pillay and Jacobs, 2005). Figure 4.5 shows that with the permeate flowrate maintained between 10-15 L/h, the TMP increased from 10 to 26 kPa.

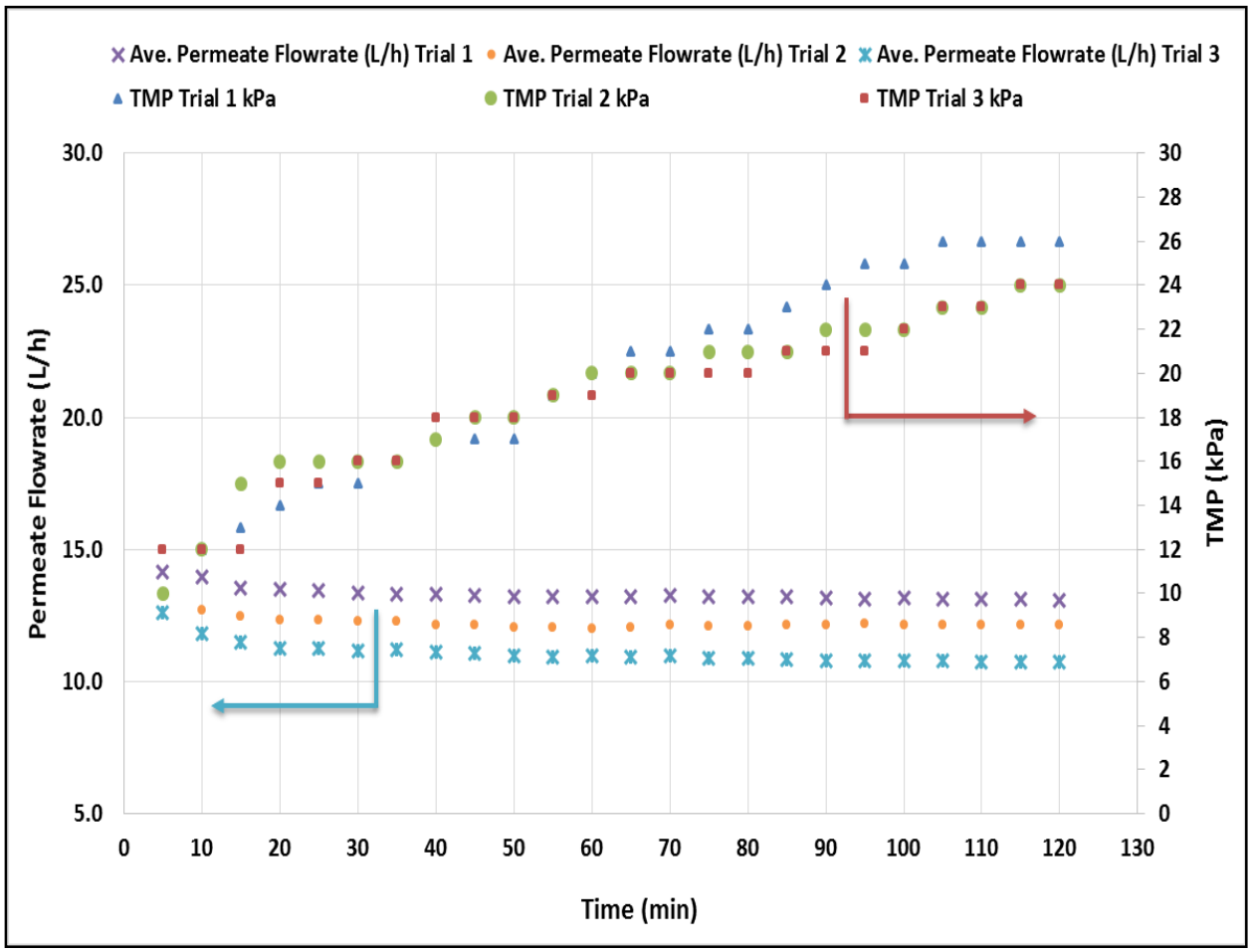

Figure 4.5: Differential pressures and Permeate flowrate changes with time.

The results shown in figures 4.4 and 4.5 agree with theory, which indicate that mechanical cleaning of the membrane was very effective in removing the fouling layer and to restore the permeability of the membrane. The rate of increase in deferential pressure after the membrane cleaning is very similar to that before the cleaning.

4.3 PERFORMANCE OF THE FOUR GRADES OF MTIO$_2$.

The four grades of mTiO$_2$ were evaluated to select the best performing grade for further experimentation. The concentration of mTiO$_2$ of 2, 5 and 7 g/l were investigated on the degradation of bacteria in river water.

Table 4.2: The effect of 2 g/l of mTiO$_2$ on degradation of bacteria in river water

Time hr	E-coli (count/100 ml)			
	Grade 1	Grade 2	Grade 3	Grade 4
0	**205**	**205.5**	**205.5**	**205.5**
0.5	27.1	16.4	32.4	22.2
2	13.7	8.7	27.1	9.9
4	12.4	3.1	15	8.7

Table 4.3: The effect of 5 g/l of mTiO$_2$ on degradation of bacteria in river water

Time hr	E-coli (count/100 ml)			
	Grade 1	Grade 2	Grade 3	Grade 4
0	**205.5**	**205.5**	**205.5**	**205.5**
0.5	5.3	2	7.5	3.1
2	4.2	0	5.3	2
4	3.1	0	4.2	1

Table 4.4: The effect of 7 g/l of mTiO$_2$ on degradation of bacteria in river water

Time hr	E-coli (count/100 ml)			
	Grade 1	Grade 2	Grade 3	Grade 4
0	**205.5**	**205.5**	**205.5**	**205.5**
0.5	3.1	0	4.2	2
2	2	0	3.1	1
4	1	0	2	0

Table 4.2 to 4.4 present the effect of concentration on degradation of E.coli bacteria in river water for a feed *E. coli* bacteria exceeding 205.5 count/100 ml. Based on the South African National Standard (2011) and World Health Organisation (2011), potable water should be free of *E. coli* (count/100 mL). The results clearly demonstrate that all grades performed remarkably well since <10

count /100mL were observed in 0.5 hrs for concentrations of 5 and 7 g/L. Grade 2 obtained the drinking water specification in 2 hours when 5 g/l was used and in less than an hour at a concentration of 7 g/l. Grade 4 obtained the drinking water specification in 4 hours of irradiation when the concentration was 7 g/l.

The influence of the anatase and rutile grades of $mTiO_2$ on the degradation of gram –ve bacteria namely *E. coli* and total coliform are presented in figures 4.6 (a) and (b).

The first three columns were the total coliform for 2, 5 and 7 g/L respectively and the last three were the *E. coli*. Figure 4.6 (a) shows that the 2 g/L of grade 1 has a poor performance on degradation of total coliform, which increased with increased concentration to > 80 % in 2 hrs for a concentration of 7 g/L. Grade 2 shows a vast improvement in degradation efficiency of total coliform for the two higher concentrations in just 0.5 hrs. The remarkable performance of grade 2 on total coliform degradation efficiency may be attributed to the additions that were used to promote crystal growth, improve durability with a balance charge.

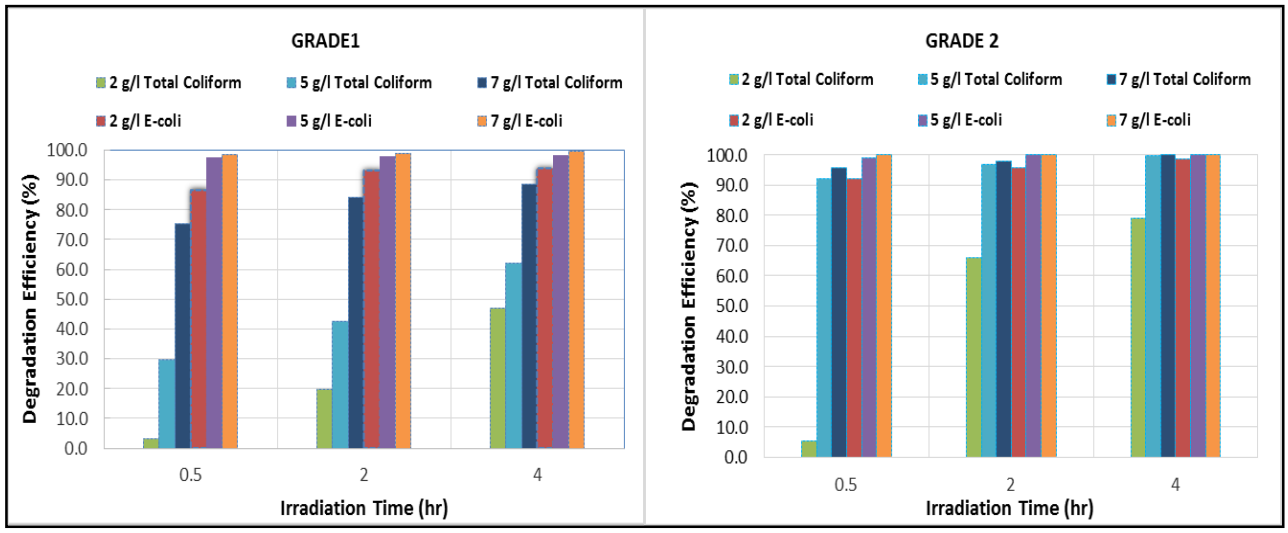

Figure 4.6 (a): Effect of Anatase grades of mTiO2 on degradation efficiency of *E. coli* and total coliform in river water.

Figure 4.6 (b) shows the performance of rutile grades on degradation efficiency of E. coli and total coliform. Grade 3 poorly performed in all three concentrations investigated over a period of 4 hrs.

However, grade 4 shows a remarkable improvement of degradation efficiency of total coliform for the two highest concentrations investigated. The remarkable performance of grade 4 compared to grade 3 on degradation of total coliform may be attributed to the coating of grade 4 particles with additions.

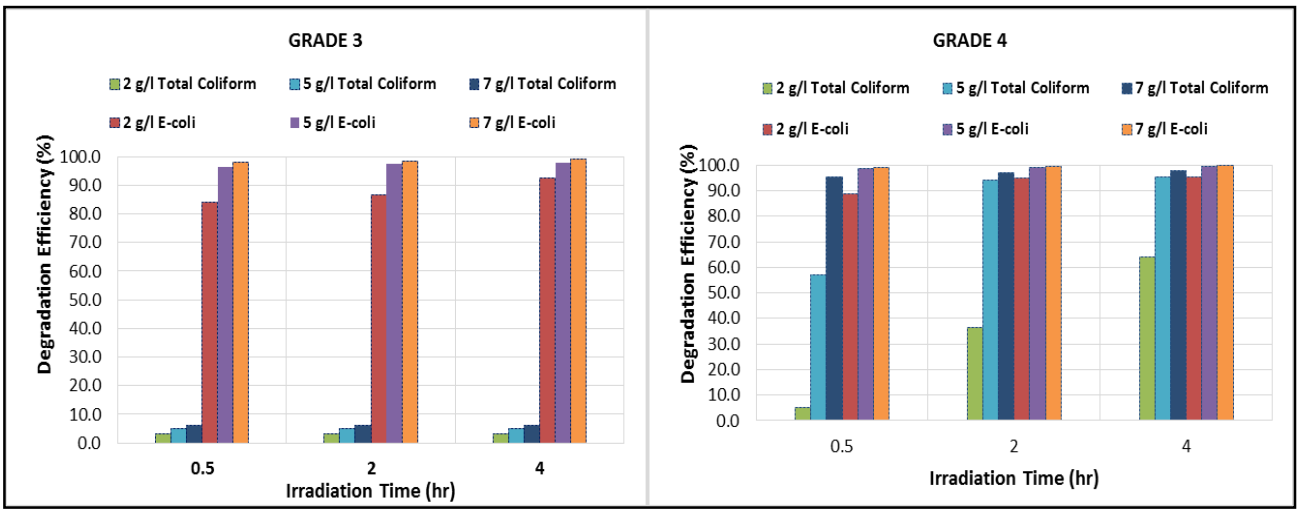

Figure 4.6 (b): Effect of the Rutile grades of mTiO$_2$ on degradation efficiency of *E. coli* and total coliform in river water

The additions on grades 2 and 4 appear to have an impact on the TiO_2 performance regardless of the type. The influence these additions have may be due to a structural change of the particle or charge stabilization, which requires an intense study of the particle behavior when additions are present. Grade 2 emerged as the best performing grade to be further explored for statistical analysis and optimization of a photocatalytic reactor.

CHAPTER 5

OPTIMISATION OF THE PHOTOCATALYTIC REACTOR USING RSM

5.1 GENERAL INTRODUCTION

This chapter presents the application of CCD and BBD to optimize the independent variables of the photocatalytic reactor for the maximum degradation efficiency of *E. coli*. The experiments conducted according to the generated CCD and BBD matrix and optimization are discussed.

5.2 OPTIMIZATION OF THE $mTIO_2$ PHOTOCATALYTIC REACTOR SYSTEM USING DOE

The Design Expert Software 9.0 was used to find optimum values for independent variables to provide the maximum degradation efficiency (100% target) of gram –ve bacterial of *E. coli* in river water. Two RSM methods were evaluated for the optimization study, which are CCD and BBD. The reason to use both RSM methods that were compared to each other was to evaluate the accuracy of the predictions to the actual experimental response. The CCD that is circumscribed as illustrated in figure 2.28 of Chapter 2 of this dissertation indicates that CCC should provide high quality predictions over the entire design space because the limits of the factors are set outside the range of the factors in the factorial part (Filliben and Heckert, 2012, Nist/SEMATECH, 2012). The BBD proves to be advantageous when the optimums are within the safe operating zone for a process. There were four independent variables represented as X_1, X_2, X_3 and X_4 with one output or dependent variable, which was degradation efficiency (Y) as illustrated in table 5.1.

Table 5.1: Manipulated variables and output for this study

Variables	Unit	Symbols
TiO_2 Loading	**g/L**	X_1
Temperature	**^0C**	X_2
Starting pH		X_3
Aeration	**L/min**	X_4
Output	**Unit**	**Symbols**
Degradation Efficiency	**%**	Y

The experiments conducted in a random approach of the run order instead of the standard order to avoid biases gave the degradation efficiency for CCD and BBD as shown in tables 5.2 (a) and (b).

Table 5.2 (a): The CCD experimental matrix results

Std. Order	Run Order	Actual Process Factors				Response
		C (g/L)	T (^{O}C)	pH	Air (L/min)	Y
1	8	3	20	4	6	62
2	26	8	20	4	6	90
3	27	3	40	4	6	60
4	20	8	40	4	6	75
5	9	3	20	8	6	49
6	10	8	20	8	6	66
7	12	3	40	8	6	49
8	25	8	40	8	6	55
9	13	3	20	4	14	79
10	19	8	20	4	14	100
11	2	3	40	4	14	89
12	3	8	40	4	14	99
13	18	3	20	8	14	50
14	14	8	20	8	14	60
15	29	3	40	8	14	78
16	1	8	40	8	14	74
17	22	0.5	30	6	10	50
18	23	10.5	30	6	10	78
19	7	5.5	10	6	10	95
20	21	5.5	50	6	10	95
21	15	5.5	30	2	10	65
22	6	5.5	30	10	10	25
23	30	5.5	30	6	2	62
24	5	5.5	30	6	18	94
25	4	5.5	30	6	10	95
26	16	5.5	30	6	10	99
27	17	5.5	30	6	10	99
28	24	5.5	30	6	10	96
29	11	5.5	30	6	10	98
30	28	5.5	30	6	10	97

The results in table 5.2 (a) show a maximum degradation of 99 to 100 % which correspond to the variables manipulated. This means different combination and interaction of the manipulated variables produced the same degradation efficiency.

Table 5.2 (b): The BBD experimental matrix results

Std. Order	Run Order	Actual Process Factors				Response
		C (g/L)	T (^{O}C)	pH	Air (L/min)	
1	22	3	20	6	10	82
2	20	8	20	6	10	90
3	18	3	40	6	10	79
4	5	8	40	6	10	98
5	1	5.5	30	4	6	91
6	10	5.5	30	8	6	50
7	13	5.5	30	4	14	100
8	3	5.5	30	8	14	55
9	7	3	30	6	6	75
10	14	8	30	6	6	80
11	25	3	30	6	14	78
12	17	8	30	6	14	97
13	29	5.5	20	4	10	99
14	16	5.5	40	4	10	98
15	8	5.5	20	8	10	60
16	9	5.5	40	8	10	61
17	19	3	30	4	10	85
18	2	8	30	4	10	99
19	26	3	30	8	10	45
20	21	8	30	8	10	61
21	27	5.5	20	6	6	83
22	6	5.5	40	6	6	82
23	4	5.5	20	6	14	98
24	11	5.5	40	6	14	95
25	30	5.5	30	6	10	95
26	24	5.5	30	6	10	99
27	28	5.5	30	6	10	99
28	23	5.5	30	6	10	96
29	15	5.5	30	6	10	98
30	12	5.5	30	6	10	97

Similar to the CCD results, the BBD obtained numerous efficiencies of 99 % and a 100 % at different combination of manipulated variables.

The models were developed and inspected for the suitability to the experimental data, and used to navigate the design space for the optimization of the photocatalytic reactor. Once the models were verified for the suitability, the numerical optimization choice was then selected to generate one hundred (100-max) solutions of optimum conditions. The solution with the maximum degradation efficiency was selected to create figures of response surface, contour and overlay plots highlighting an area of operability. The solutions were streamlined by setting minimum and maximum limits for each variable and a response as presented in table 5.3. This technique was applied on both CCD and BBD.

Table 5.3: Minimum and maximum limits for the solutions of optimum conditions

Variables	Unit	Symbols	Minimum and maximum limits	
			-1	1
TiO_2 Loading	**g/L**	X_1	3	8
Temperature	**^0C**	X_2	20	30
Starting pH		X_3	6	8
Aeration	**L/min**	X_4	6	14
Output	**Unit**	**Symbols**	**Minimum and maximum limits**	
			-1	**1**
Degradation Efficiency	**%**	Y	98	100

The target for the degradation efficiency suitable for drinking water was 100 %. Therefore, the pH limits selected were fixed within the SANS (2011) and WHO Guidelines for drinking water as shown in table 2.3 of Chapter 2 of this dissertation. The temperature limits were targeting room temperatures and the concentration with the aeration were left the same as those used for the matrixes.

5.3 ANALYSIS USING THE CENTRAL COMPOSITE DESIGN

The ANOVA for Response Surface Quadratic model are shown in table 5.4. The results show a large F-value of 174.87 and a p-value less than 0.05 indicating that the model was significant. The most significant model terms were indicated by F-values and most importantly a p-values <0.05. Therefore, the results in table 5.4 show that all model terms were significant.

Table 5.4: ANOVA for Response Surface Quadratic model on the CCD

Analysis of variance table [Partial sum of squares - Type III]						
Source	**Sum of Squares**	**df**	**Mean Square**	**F Value**	**p-value Prob > F**	
Model	12170.14	14	869.3	174.87	< 0.0001	significant
A-TiO_2 Concentration	*1048.08*	*1*	*1048.08*	*210.84*	*< 0.0001*	
B-Temperature	*22.81*	*1*	*22.81*	*4.59*	*0.049*	
C-Starting pH	*2696.64*	*1*	*2696.64*	*542.47*	*< 0.0001*	
D-Aeration	*1463.28*	*1*	*1463.28*	*294.36*	*< 0.0001*	
AB	*155*	*1*	*155*	*31.18*	*< 0.0001*	
AC	*121*	*1*	*121*	*24.34*	*0.0002*	
AD	*55.5*	*1*	*55.5*	*11.17*	*0.0045*	
BC	*96.04*	*1*	*96.04*	*19.32*	*0.0005*	
BD	*390.06*	*1*	*390.06*	*78.47*	*< 0.0001*	
CD	*84.64*	*1*	*84.64*	*17.03*	*0.0009*	
A^2	*1852.74*	*1*	*1852.74*	*372.71*	*< 0.0001*	
B^2	*6.03*	*1*	*6.03*	*1.21*	*0.2882*	
C^2	*4613.17*	*1*	*4613.17*	*928.01*	*< 0.0001*	
D^2	*610.74*	*1*	*610.74*	*122.86*	*< 0.0001*	
Residual	74.57	15	4.97			
Lack of Fit	*63.23*	*10*	*6.32*	*2.79*	*0.1345*	*not significant*
Pure Error	*11.33*	*5*	*2.27*			
Cor Total	12244.71	29				

The LOF of p-values less than 0.05 (5%) is significant and it indicates that the model is not fitting an experiment data. The LOF for this study shows a p-value of 0.1345 which is greater than 0.05, signified that there was 13.45 % chance that the Lack-of-Fit (LOF) was due to noise, which makes

it insignificant; therefore, the model can fit any data. Noise refers to a certain amount of uncontrollable variation in the factors that affects the response, and some factors that cannot be controlled at all.

The suitability of the model was validated by evaluating the R squared presented in table 5.5. The R^2_{Pred} and R^2_{Adj} seem to be in reasonable agreement since the difference was less than 0.2.

Table 5.5: The R-Squared Results.

Std. Dev.	2.23	**R-Squared**	0.9939
Mean	76.07	**Adjusted R-Squared**	0.9882
C.V. %	2.93	**Predicted R-Squared**	0.9689
PRESS	380.54	**Adeq Precision**	47.733

The "Adeq Precision" which measures the signal to noise ratio and it was desirable to have a ratio greater than 4. The "Adeq Precision" for this study was 47.733, which represents the adequate signal. Therefore, the model was suitable to be used to navigate the design space.

Therefore, the fitted model for the degradation efficiency in terms of the actual factors or variables is as follows:

$$Y = -105.33 + 26.00X_1 - 0.91X_2 + 35.83X_3 + 6.90X_4 - 0.13X_1X_2 - 0.55X_1X_3 - 0.19X_1X_4 + 0.13X_2X_3 + 0.13X_2X_4 - 0.29X_3X_4 - 1.32X_1^2 - 4.69x10^{-3}X_2^2 - 3.24X_3^2 - 0.29X_4^2$$

The model reveals that the degradation efficiency mainly depends on the initial pH, TiO_2 concentration, temperature and aeration with the temperature being the least significant variable.

The plot of the degradation response surface indicates the presence of curvature where the maximum result may be obtainable as illustrated in figure 5.1. The flag indicates the maximum degradation efficiency with its corresponding optimum variables within the selected limits tabulated in table 5.3.

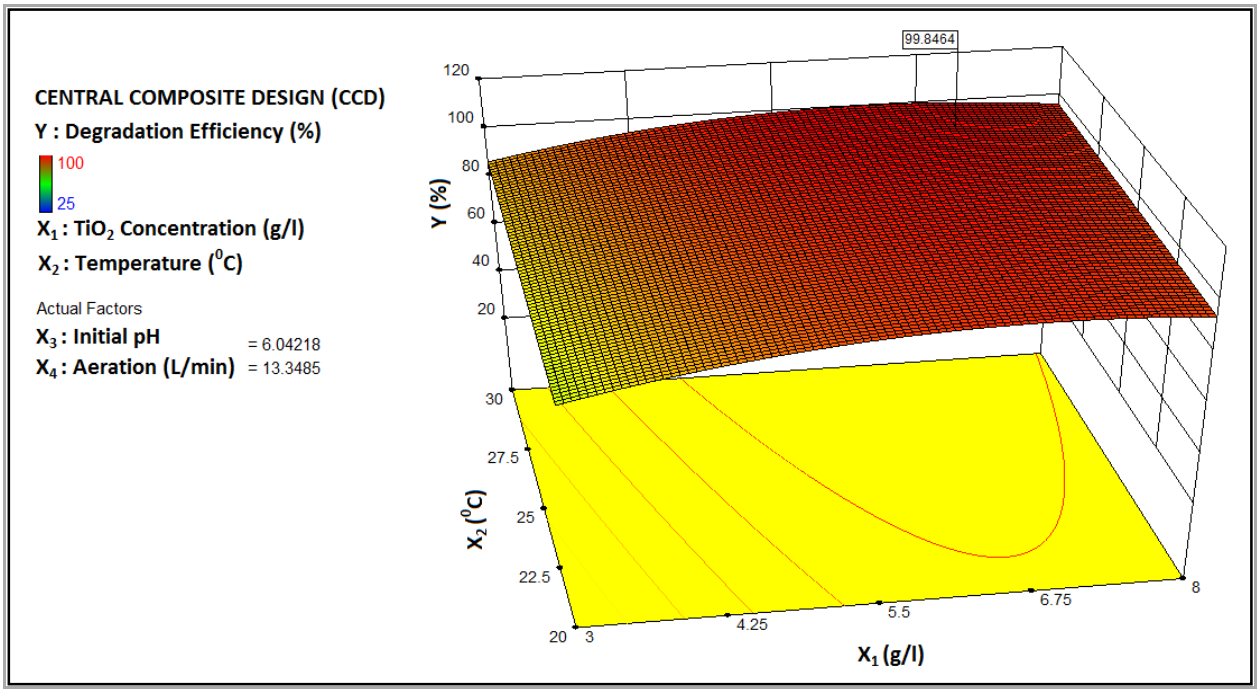

Figure 5.1: Response Surface of predicted degradation efficiency of *E. coli* in river water

The degradation response surface zoomed-in on the contour plot that shows the direction of the maximum efficiency within the limits of the variable as shown in figures 5.2 and 5.3.

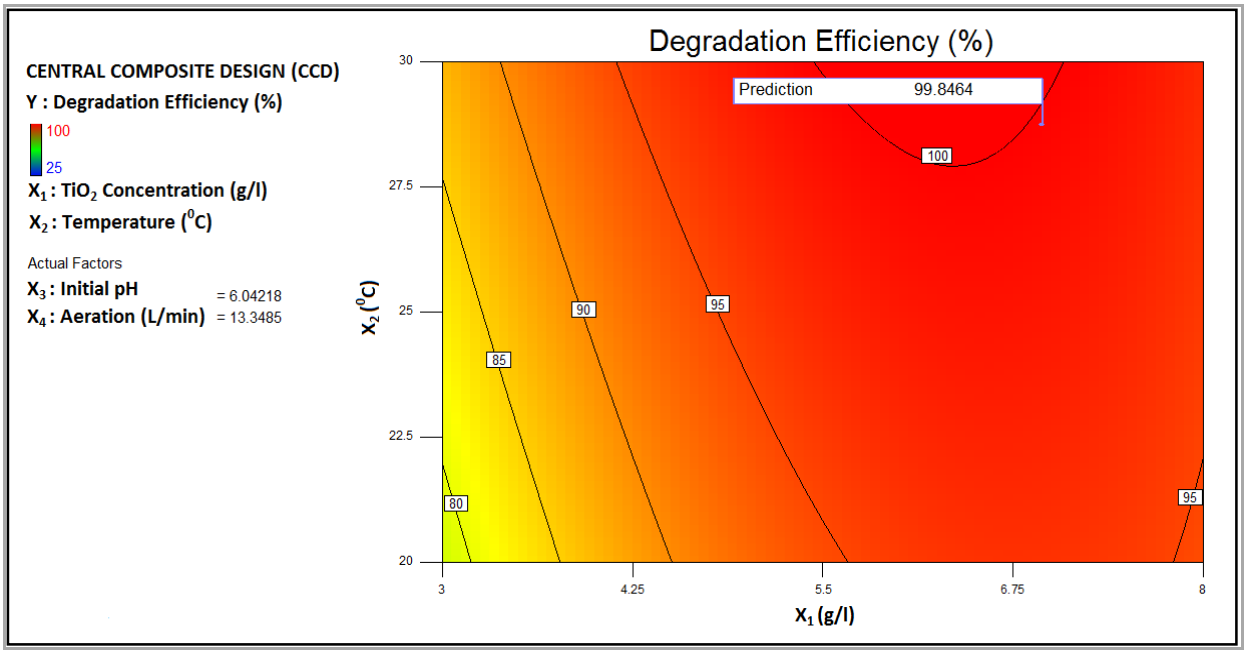

Figure 5.2: Contour plot of predicted degradation efficiency of *E. coli* in river water

Figure 5.2 and 5.3 indicate that the maximum efficiency of 99.85 % occurs at about 28.75 ^{O}C and 6.94 g/L concentration with an initial pH of 6.042 and aeration of 13.35 L/min.

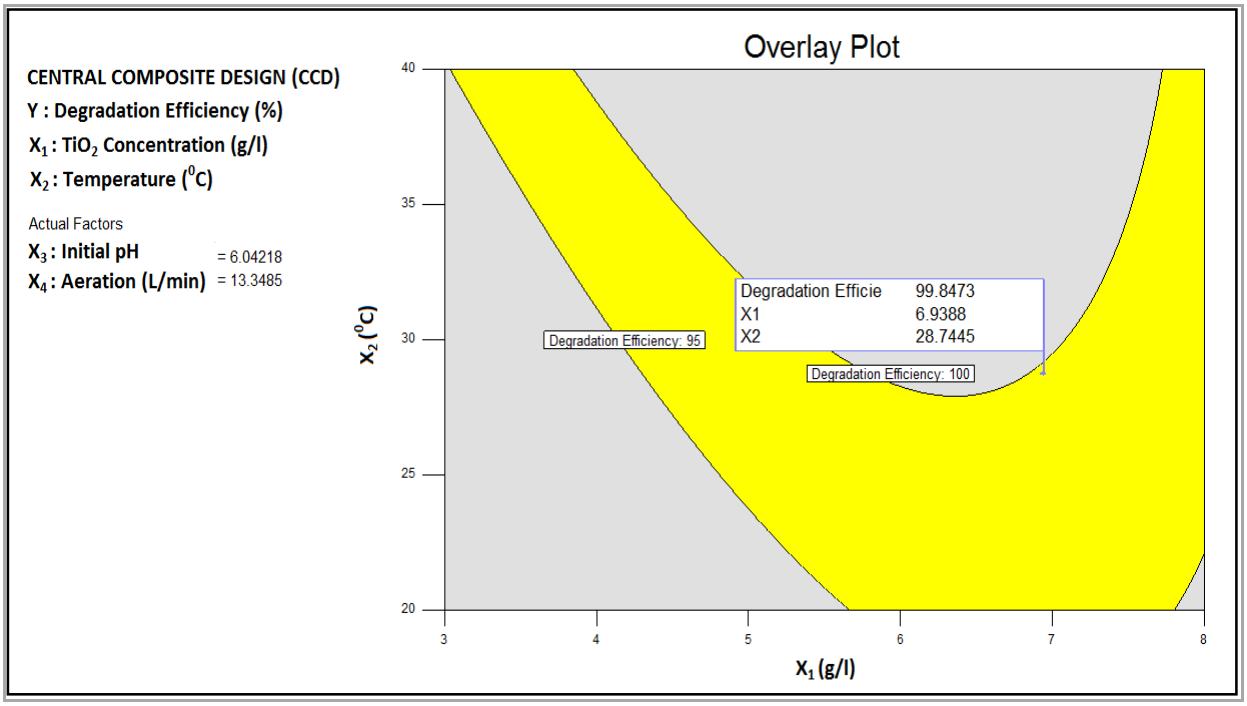

Figure 5.3: Overlay plot of predicted degradation efficiency of *E. coli* in river water

5.4 ANALYSIS USING THE BOX BEHNKEN DESIGN

The ANOVA for the Response Surface Quadratic model is presented in table 5.6. The model was significant due to the high F-value of 130.61 and the p-value of <0.0001. The F-value this large would have a 0.01 % chance that it was due to noise. The model shows a non-significant Lack-of-Fit (LOF) which represents the model that can fit any data. There was 17.47 % chance that the LOF was due to noise.

Table 5.6: ANOVA for Response Surface Quadratic model on the BBD

Analysis of variance table [Partial sum of squares - Type III]						
Source	Sum of Squares	df	Mean Square	F Value	p-value Prob > F	
Model	7974.55	14	569.61	130.61	< 0.0001	significant
A-TiO_2 Concentration	*546.75*	*1*	*546.75*	*125.37*	*< 0.0001*	
B-Temperature	*0.083*	*1*	*0.083*	*0.019*	*0.8919*	
C-Starting pH	*4800*	*1*	*4800*	*1100.64*	*< 0.0001*	
D-Aeration	*320.33*	*1*	*320.33*	*73.45*	*< 0.0001*	
AB	*30.25*	*1*	*30.25*	*6.94*	*0.0188*	
AC	*1*	*1*	*1*	*0.23*	*0.6389*	
AD	*49*	*1*	*49*	*11.24*	*0.0044*	
BC	*1*	*1*	*1*	*0.23*	*0.6389*	
BD	*1*	*1*	*1*	*0.23*	*0.6389*	
CD	*4*	*1*	*4*	*0.92*	*0.3534*	
A^2	*476.19*	*1*	*476.19*	*109.19*	*< 0.0001*	
B^2	*12.19*	*1*	*12.19*	*2.8*	*0.1153*	
C^2	*1857.44*	*1*	*1857.44*	*425.91*	*< 0.0001*	
D^2	*286.01*	*1*	*286.01*	*65.58*	*< 0.0001*	
Residual	65.42	15	4.36			
Lack of Fit	*54.08*	*10*	*5.41*	*2.39*	*0.1747*	*not significant*
Pure Error	*11.33*	*5*	*2.27*			
Cor Total	8039.97	29				

F-values greater than 0.100 indicate the model terms were not significant, therefore, A, C, D, AB, AD, A^2, C^2, D^2 were significant model terms for this study.

The suitability of the model was also validated by evaluating the R squared as presented in table 5.7. The R^2_{Pred} and R^2_{Adj} seem to be in reasonable agreement since the difference was less than 0.2.

Table 5.7: The R-Squared.

Std. Dev.	2.09		**R-Squared**	0.9919
Mean	84.13		**Adj R-Squared**	0.9843
C.V. %	2.48		**Pred R-Squared**	0.9592
PRESS	327.84		**Adeq Precision**	37.443

The "Adeq Precision" which measures the signal to noise ratio and desirable ratio should be greater than 4. The "Adeq Precision" for this study was 37.443, which represents the adequate signal. Therefore, the model was suitable to be used to navigate the design space.

The fitted model for the degradation efficiency in terms of the actual factors or variables is as follows:

$$Y = -77.72 + 9.97X_1 + 0.18X_2 + 39.33X_3 + 8.56X_4 + 0.11X_1X_2 + 0.1X_1X_3 + 0.35X_1X_4 + 0.025X_2X_3 - 0.013X_2X_4 - 0.13X_3X_4 - 1.33X_1^2 - 0.013X_2^2 - 4.12X_3^2 - 0.40X_4^2$$

The model also reveals that the degradation efficiency was mostly depended on the pH, TiO_2 concentration and aeration while temperature was insignificant.

The degradation response surface plot for the fitted model that shows the curvature is shown in figure 5.4. The flag emerged at the selected result of the maximum degradation efficiency with its corresponding optimum variables.

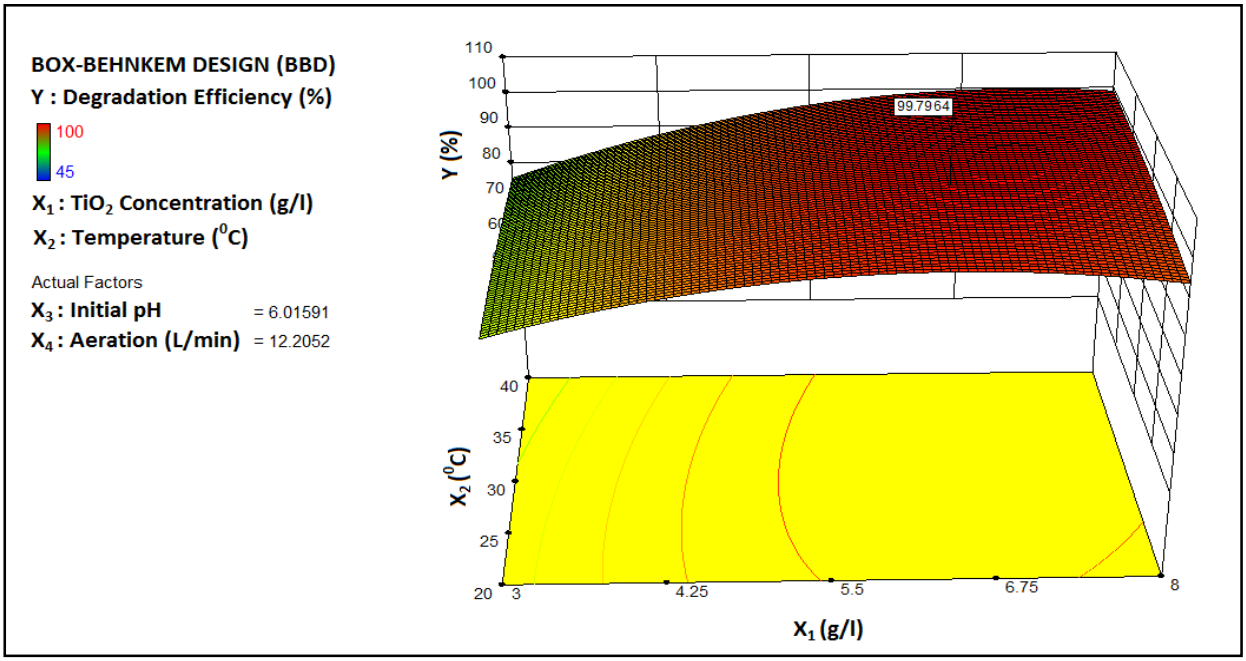

Figure 5.4: Response Surface of predicted degradation efficiency of *E. coli* in river water

The contour and overlay plots are shown if figures 5.5 and 5.6.

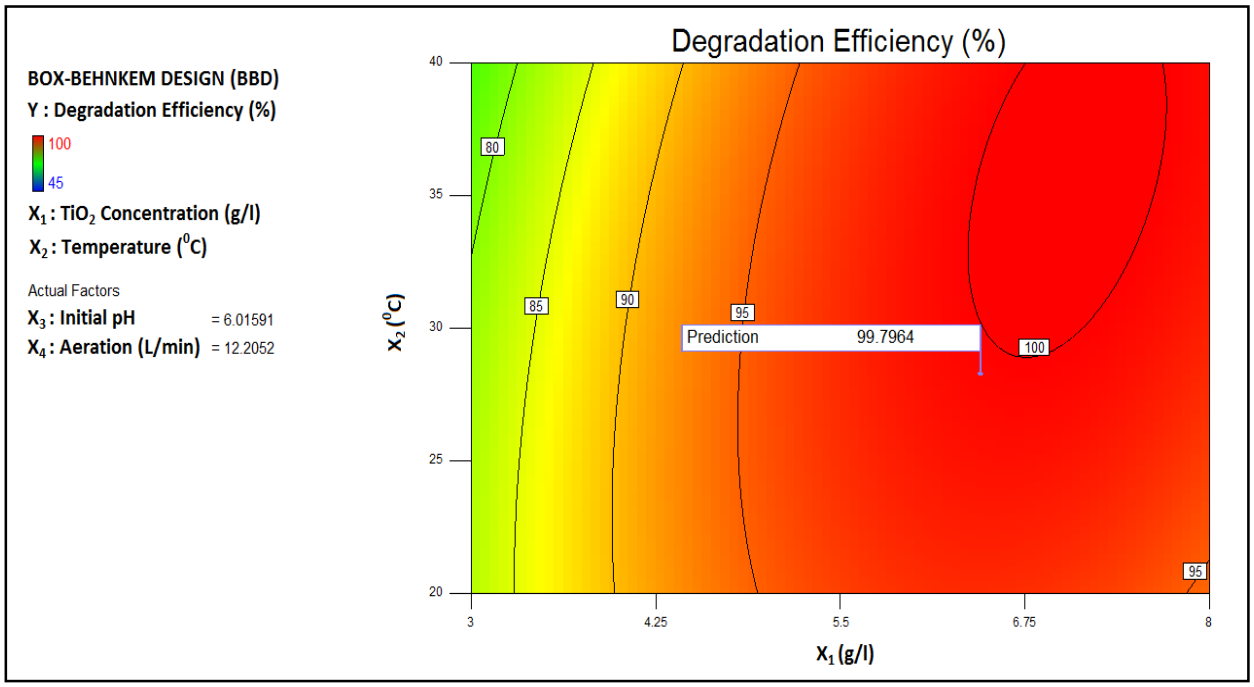

Figure 5.5: Contour plot of predicted degradation efficiency of *E. coli* in river water

The plots reveal that the maximum efficiency of 99.80 % occurs at about 28.28 ^{O}C and 6.45 g/L concentration with an initial pH of 6.02 and aeration of 12.21 L/min.

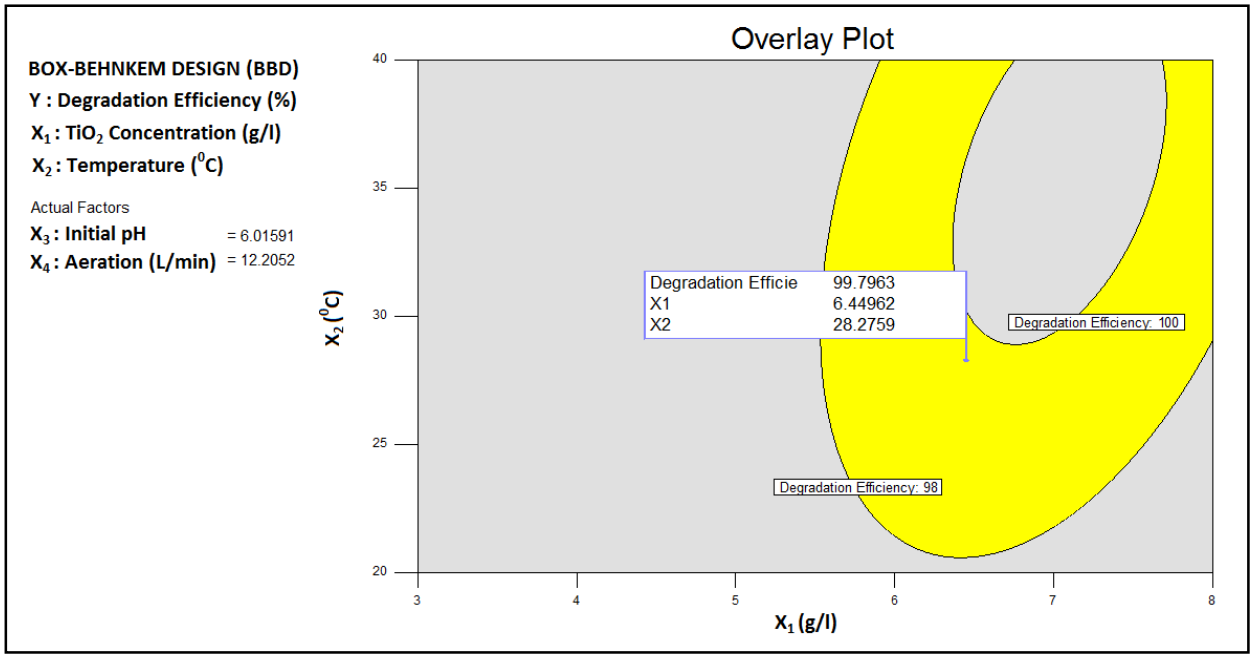

Figure 5.6: Overlay plot of predicted degradation efficiency of *E. coli* in river water

The results for the optimum values of the independent variables with the maximum degradation efficiency are tabulated in table 5.8 for both Box-Behnken and Central Composite Designs.

Table 5.8: The results of optimum Values

Parameter	Unit	Code	BBD	CCD
			Theoretical value	Theoretical value
Degradation Efficiency	%	Y	99.8	99.85
mTiO$_2$ Concentration	g/L	X_1	6.45	6.94
Temperature	^{0}C	X_2	28.28	28.75
Initial pH		X_3	6.02	6.04
Aeration	L/min	X_4	12.21	13.35

5.5 VERIFICATION OF THE DESIGN MODELS

The two designs (CCD and BBD) used to obtain the optimum values of the independent variables for the maximum degradation efficiency seems to validate each other's models. The two designs have approximately the same optimum values and maximum output as presented in table 4.9 which simple means that their models are valid. Thus, this is a theoretical validation, which is required to be verified by conducting a practical experiment.

Therefore, experiments were conducted using the optimum values of the independent variables and samples were taken after 4 hours for the analysis of maximum degradation efficiency. The results as presented in table 4.6 confirm the validity of both models.

Table 5.9: Verification of the design models.

Parameter	Unit	Code	Box-Behnken Design		Central Composite Design	
			Theoretical value	Experiment value	Theoretical value	Experiment value
Degradation Efficiency	%	Y	99.8	99.26	99.85	99.67
$mTiO_2$ Concentration	g/L	X_1	6.45	6.45	6.94	6.94
Temperature	^0C	X_2	28.28	28.3	28.75	28.8
Initial pH		X_3	6.02	6	6.04	6
Aeration	L/min	X_4	12.21	12	13.35	13

The experiments were repeated twice and the average degradation efficiency is then presented in table 5.9 alongside with the model value. The degradation efficiency by the models is comparable to the experimentally obtained values, which simple means that the models are effective.

CHAPTER 6

CONCLUSSIONS AND RECOMMENDATIONS

River water, also referred to as surface water was once naturally clean and safe as habitat for animals and plants, and been safely consumed by humans. The developments in an attempt to better our lives have left this precious source polluted with chemicals from chemical industries, farms and medical institutions, and biohazards from animal and human excretion due to lack of sanitation facilities. The conventional treatment systems were born to overcome the pollution, however, these systems are long, and expensive to design, install and operate. The primary concern presented by WHO and SANS 214-1 for drinking water quality was microbial hazards (Robertson et al., 2012). Therefore, a need to research a footprint and robust disinfection small treatment systems and methods to overcome the pollution of the receiving water is important.

Titanium dioxide (TiO_2) is one of the basic materials in our daily lives that has emerged as an excellent photocatalytic material for water and air purification. Nano-scaled particles of Anatase and Rutile types of TiO_2 are strong oxidizing agents. They have shown a great potential as a low-cost, environmental friendly and sustainable treatment technology, which produces less or zero waste. The main technical setback on the practical application is the post-recovery of the nano-particles of the catalyst after treatment.

The overall aim of this study was to evaluate the photocatalytic activity of the locally produced micro-scaled or micro-sized particles of TiO_2 ($mTiO_2$) pigment for paint on the destruction of bacteria from contaminated receiving water and hence, optimize the system. The results show that the $mTiO_2$ that is produced as pigment for paint has photocatalytic properties. The results also confirm the theory that an increase in particle size decreases the surface area of the particle and thereby decreases the photocatalytic activity. The particle size range of 0.2-53 µm was recovered using uncharacterized PWFMF membrane, which showed a good performance since a significant amount of particles of above 98 % was recovered.

Four grades of $mTiO_2$, which were basically two grades of anatase and two grades of rutile were sampled at different points in the sulphate process to investigate the best performing grade. Both grade 2 (anatase with additions) and grade 4 (Rutile coated with additions) showed a better performance that appear to be influenced by being exposed to additions. Grade 2 was the best performing grade since it achieved the drinking water specification for E coli and total coliform in 2 hours and it was further used in optimization process.

A comparative study between the Central Composite Design (CCD) and Box-Behnken Design (BBD), which are the Response Surface Methodology (RSM) were used to generate the model equations for the response variable. The optimum results for independent variables on the maximum degradation efficiency on both designs were approximately the same. The star points, which represent new extreme values for each factor in the CCD, did not add any significant effect since the optimum results were well within the limits. The results for both the designs can also be considered as a validation that the model is sustainable. Furthermore, experimental validation carried out for each design also showed models being viable.

Further work recommended on this study of locally produced $ahTiO_2$ is to use sunlight to photo activate the particles. UV from the Sunlight can be a great alternative to produce a low cost photodegradation technology for rural communities with no electricity infrastructure. The effect of additions should be studied on the structures or the charge stability of the two grades so that the additions can be optimized to produce a high photo active $mTiO_2$.

REFERENCES

About Civil.org. 2014. Civil Engineering. Available: http://www.aboutcivil.org/sources-quality-distribution-of-water.html (Accessed March 2014).

Achisa, M. C. 2013. Evaluation of Silver Nanoparticles Impregnated Woven Fabric Microfiltration Membrane for Potable Water Treatment. Master of Technology: Chemical Engineering, Durban University Of Technology.

Agrawal, R. 2009. study of physico-chemical parameters of groundwater quality of dudu town in rajasthan‖. Indian Journal of remote sensing, 2 (4): 969-971.

Baker, R. W. 2002. Membrane Technology. In: Encyclopedia of Polymer Science and Technology. John Wiley & Sons, Inc. Available: http://dx.doi.org/10.1002/0471440264.pst194 (Accessed February 2015).

Bayarri, B., Giménez, J., Curcó, D. and Esplugas, S. 2005. Photocatalytic degradation of 2,4-dichlorophenol by TiO2/UV: Kinetics, actinometries and models. Catalysis Today, 101 (3–4): 227-236.

Beydoun, D., Amal, R., Low, G. and McEvoy, S. 1999. Role of Nanoparticles in Photocatalysis. Journal of Nanoparticle Research, 1 (4): 439-458.

CHLÁDOVÁ, A., WIENER, J. and POLÁKOVÁ, M. 2011. Testing the Photocatalytic Activity of TiO2 Nanoparticles with Potassium Permanganate Solution. In: Proceedings of 3rd International Conference Nanocon.

Chin, S. S., Chiang, K. and Fane, A. G. 2006. The stability of polymeric membranes in a TiO2 photocatalysis process. Journal of Membrane Science, 275 (1–2): 202-211.

Chong, M. N., Jin, B., Chow, C. W. and Saint, C. 2010. Recent developments in photocatalytic water treatment technology: a review. Water Res, 44 (10): 2997-3027.

Chong, M. N., Lei, S., Jin, B., Saint, C. and Chow, C. W. K. 2009. Optimisation of an annular photoreactor process for degradation of Congo Red using a newly synthesized titania impregnated kaolinite nano-photocatalyst. Separation and Purification Technology, 67 (3): 355-363.

Craun, G. F. and Goodrich, J. A. 1999. Selecting residential or personal water treatment systems. Lewis Publishers, Washington, DC.

David, R. H., Ho, W. S. W. and Sirkar, K. K. 1992. Microfiltration Membane. In: Membrane Handbook. Kluwe Academic Publishers Group.

DeZuane, J. 1997. Handbook of drinking water quality. John Wiley & Sons.

Di Paola, A., Bellardita, M. and Palmisano, L. 2013. Brookite, the Least Known TiO2 Photocatalyst. Catalysts, 3 (1): 36-73.

Diersing, N. 2009. Water Quality: Frequently Asked Questions. Florida Brooks National Marine Sanctuary, Key West, FL.,

Filliben, J. and Heckert, A. 2012. Exploratory Data Analysis. NIST/SEMATECH eHandbook of statistical methods.

Frey, D. D., Engelhardt, F. and Greitzer, E. M. 2003. A role for" one-factor-at-a-time" experimentation in parameter design. Research in Engineering Design, 14 (2): 65-74.

Frey, D. D. and Wang, H. 2006. Adaptive one-factor-at-a-time experimentation and expected value of improvement. Technometrics, 48 (3): 418-431.

Fujishima, A., Rao, T. N. and Tryk, D. A. 2000. Titanium dioxide photocatalysis. Journal of Photochemistry and Photobiology C: Photochemistry Reviews, 1 (1): 1-21.

Gaya, U. I. and Abdullah, A. H. 2008. Heterogeneous photocatalytic degradation of organic contaminants over titanium dioxide: A review of fundamentals, progress and problems. Journal of Photochemistry and Photobiology C-Photochemistry Reviews, 9 (1): 1-12.

Gázquez, M. J., Bolívar, J. P., Garcia-Tenorio, R. and Vaca, F. 2014. A review of the production cycle of titanium dioxide pigment. Materials Sciences and Applications.

Gogate, P. R. and Pandit, A. B. 2004. A review of imperative technologies for wastewater treatment I: oxidation technologies at ambient conditions. Advances in Environmental Research, 8 (3–4): 501-551.

Hanaor, D. H. and Sorrell, C. 2011. Review of the anatase to rutile phase transformation. Journal of Materials Science, 46 (4): 855-874.

Haney, D. C. 1997. Water. Available: http://www.uky.edu/KGS/home.htm (Accessed March 2016).

Herrmann, J.-M. 1999. Heterogeneous photocatalysis: fundamentals and applications to the removal of various types of aqueous pollutants. Catalysis Today, 53 (1): 115-129.

Herrmann, J. M. 2005. Heterogeneous photocatalysis: state of the art and present applications In honor of Pr. R.L. Burwell Jr. (1912–2003), Former Head of Ipatieff Laboratories, Northwestern University, Evanston (Ill). Topics in Catalysis, 34 (1-4): 49-65.

Hoffmann, M. R., Martin, S. T., Choi, W. and Bahnemann, D. W. 1995. Environmental applications of semiconductor photocatalysis. Chemical reviews, 95 (1): 69-96.

Jain, N., Gupta, R., Rai, R. K., Ray, S. S. and Sharma, V. 2012. Anti-Microbial activity of TiO2 micro-particles in suspension on E.coli strains under UV irradiation. Pharmacy and biological Sciences, 1 (1): 21-30.

Johnson, D. L., Ambrose, S. H., Bassett, T. J., Bowen, M. L., Crummey, D. E., Isaacson, J. S., Johnson, D. N., Lamb, P., Saul, M. and Winter-Nelson, A. E. 1997. Meanings of Environmental Terms. J. Environ. Qual., 26 (3): 581-589.

Kabra, K., Chaudhary, R. and Sawhney, R. L. 2004. Treatment of Hazardous Organic and Inorganic Compounds through Aqueous-Phase Photocatalysis: A Review. Industrial & Engineering Chemistry Research, 43 (24): 7683-7696.

Khuri, A. I. and Mukhopadhyay, S. 2010. Response surface methodology. Wiley Interdisciplinary Reviews: Computational Statistics, 2 (2): 128-149.

Korus, R. A., Hoffman, D. S., Bam, N., Peterson, C. L. and Drown, D. C. 1993. Transesterification process to manufacture ethyl ester of rape oil. In: Proceedings of The Proceedings of the First Biomass Conference of the Americas: Energy, Environment, Agriculture, and Industry. 815-826.

Ku, Y., Leu, R. and Lee, K. 1996. Decomposition of 2-chlorophenol in aqueous solution by UV irradiation with the presence of titanium dioxide. Wat. Res, 30 (11): 2569-2578.

Kuznesof, P. M. and Rao, M.W. 2006. Titanuim dioxide-Chemical and Technical Assessment. JECFA, Rome, Italy: 1-8.

Leckie, J., Sun, D. and Robertson, A. P. 2004. Membrane-Coagulation reactor for water treatment. Available: http://web.stanford.edu/group/sspprogram/SSP_PhDTopics/9WaterTreatment.htm http://web.stanford.edu/group/sspprogram/SSP_PhDTopics/SSP_PhD_Topics_Mar_2004_p9.pdf (Accessed October 2014).

Legrini, O., Oliveros, E. and Braun, A. 1993. Photochemical Processes for Water Treatment. ChemInform, 24 (28)

LennTech. 1998-2014a. Water Treatment Solution: River Water Quality and Pollution. Available: www.lenntech.com/rivers-pollution-quality.htm (Accessed June 2014).

LennTech. 1998-2014b. Water Treatment Solution:Water Health. Available: www.lenntech.com/water-health-faq.htm (Accessed May 2014).

Macwan, D. P., Dave, P. N. and Chaturvedi, S. 2011. A review of nano-TiO_2 sol-gel type syntheses and its applications. Journal of Materials Science, 46: 3669-3686.

Malato, S., Fernandez-Ibanez, P., Maldonado, M. I., Blanco, J. and Gernjak, W. 2009. Decontamination and disinfection of water by solar photocatalysis: Recent overview and trends. Catalysis Today, 147 (1): 1-59.

Mallevialle, J., Odendaal, P. E., Foundation, A. R., Wiesner, M. R., eaux-Dumez, L. d. and Commission, S. A. W. R. 1996. Water Treatment Membrane Processes. McGraw-Hill.

McCullagh, C., Robertson, J. C., Bahnemann, D. and Robertson, P. J. 2007. The application of TiO2 photocatalysis for disinfection of water contaminated with pathogenic micro-organisms: a review. Research on Chemical Intermediates, 33 (3-5): 359-375.

McNulty, G. 2007. Production of titanium dioxide. In: Proceedings of Proceedings of NORM V International Conference, Seville, Spain. Citeseer, 169-189.

Milani, A. S., Wang, H., Frey, D. D. and Abeyaratne, R. C. 2008. Evaluating Three DOE Methodologies: Optimization of a Composite Laminate under Fabrication Error. Quality Engineering, 21 (1): 96-110.

Mirhosseini, H., Tan, C. P., Hamid, N. S. A. and Yusof, S. 2008. Effect of Arabic gum, xanthan gum and orange oil on flavor release from diluted orange beverage emulsion. Food Chemistry, 107 (3): 1161-1172.

Moellmann, J., Ehrlich, S., Tonner, R. and Grimme, S. 2012. A DFT-D Study of structural and enegertic properties of TiO2 modification. Journal of Physics: Condensed Matter, 24

Montgomery, D. C. 2009. Design and Analysis of Experiments. John Wiley & Sons, Inc.

Montgomery, D. C., Peck, E. A. and Vining, G. G. 2012. Introduction to Linear Regression Analysis. Fifth ed.

MoreSteam.com. 2015. Design of Experiments (DOE). Available: www.moresteam.com/index.cfm (Accessed August 2015)

Mozia, S. 2010. Photocatalytic membrane reactors (PMRs) in water and wastewater treatment. A review. Separation and Purification Technology, 73 (2): 71-91.

Mulder, M. 1996. Basic Princeples of Membrane Technology. Kluwer Academic: The Netherlands.

Mulder, M. 1998. Basic principles of membrane technology. Second ed. The Netherlands: Kluwer Academic.

Ní Mhurchú, J. 2008. Dead-end and crossflow microfiltration of yeast and bentonite suspensions: Experimental and modelling studies incorporating the use of artificial neural network. Dublin City University.

NIST/SEMATECH. 2012. e-Handbook of statistical Methods by reviewed in, Available: http://www.itl.nist.gov/div898/handbook/ (Accessed August 2015).

Pearce, G. 2007. Introduction to membranes: filtration for water and wastewater treatment. Filtration & separation, 44 (2): 24-27.

PennState. 2015. Design of Experiments. Available: https://onlinecourse.science.psu.edu/stat503/node/5 (Accessed August 2015)

Persahd, P. B. 2003. Development and Evaluation of an Activated Precoated Microfiltration systems. Masters of Technlogy: Chemical Engineering, Durban University of Technology.

Peter-Varbanets, M., Zurbrügg, C., Swartz, C. and Pronk, W. 2009. Decentralized systems for potable water and the potential of membrane technology. Water Research, 43 (2): 245-265.

Peterson, H. 2001. Rural Drinking Water and Waterborne Illness. Safe Drinking Water Foundation, Saskatoon. SK: 162-191.

Phillips, N. 2010. Ground Water & Surface Water: Understanding the Interaction. Conservation Technology Information Center., (Accessed May 2014)

Phys Org, P. August 2014. Water scarcity and climate change through 2095. Available: www.phys.org/news/2014-08-scarcity-climate.html (Accessed August 2014).

Pikwa, K., Dlamini, T. and Pillay, V. L. 2009. A gravity-fed microfilter for point-of-use potable water production in rural areas. Available: http://www.ewisa.co.za/literature/files/254_203%20Pikwa.pdf (Accessed October 2014)

Pillay, V. L. and Jacobs, E. P. 2005. The Development and Evaluation of a Reverse Flow Microfilter. WRC Report No. 1232/1/05

Pillay, V. L., Jacobs, E. P. and Commission, S. A. W. R. 2007. Development of a Combined Activated Carbon/microfiltration Process for the Treatment of Industrial Effluents. Water Research Commission.

Pillay, V. L. and Commission, S. A. W. R. 2009. The Development of an Immersed Membrane Microfiltration System for the Treatment of Rural Waters and Industrial Waters: Report to the Water Research Commission. Water Research Commission.

Porter, J., Li, Y.-G. and Chan, C. 1999. The effect of calcination on the microstructural characteristics and photoreactivity of Degussa P-25 TiO2. Journal of Materials Science, 34 (7): 1523-1531.

Pravettoni, R. 2011. Water Scarcity in Africa. Available: www.grida.no/graphicslib/detail/water-scarcity-in-africa_9d72 (Accessed August 2014).

Pritchard, M., Mkandawire, T., Edmondson, A., O'neill, J. and Kululanga, G. 2009. Potential of using plant extracts for purification of shallow well water in Malawi. Physics and Chemistry of the Earth, Parts A/B/C, 34 (13): 799-805.

Rand Water. 2014. Water Pollution. Available: http://www.randwater.co.za/corporateResponsibility/WWE/Pages/WaterPollution.aspx (Accessed March 2014).

Ritter, L., Keith, S., Paul, S., Ken, H., Patricia, K., Gevan, M. and Beth, L. 2002. Sources, Pathways, and Relative Risks of Contaminants in Surface Water and Groundwater: A Perspective Prepared for the Walderton Inquiry. Journal of Toxicology and Environmental Health, Part A, 65 (1): 1-142.

Robertson, P. K. J., Robertson, J. M. C. and Bahnemann, D. W. 2012. Removal of microorganisms and their chemical metabolites from water using semiconductor photocatalysis. Journal of Hazardous Materials, 211–212: 161-171.

Robinson, G. 2000. Practical Strategies for experiments. Chichester, UK: Wiley 265p.

Safe Drinking Water Foundation. 2014. Conventional Water Treatment: Coagulation and Filtration. Available: http://www.safewater.org/PDFS/knowthefacts/conventionalwaterfiltration.pdf (Accessed March 2014).

Schutte, C. and Focke, W. 2006. Handbook For The Operation Of Water Treatment Works. Water Research Commission, The Water Institute of Southern Africa.

Schwinge, J., Neal, P. R., Wiley, D. E., Fletcher, D. F. and Fane, A. G. 2004. Spiral wound modules and spacers - Review and analysis. Journal of Membrane Science, 242 (1-2): 129-153.

Shivaraju, H. P. 2011. Removal of Organic Pollutants in the Municipal Sewage Water by Tio2 based Heterogeneous Photocatalysis. International Journal of Environmental Sciences., 1 (5): 911-923.

Smyth, J. R. and Bish, D. L. 1988. Crystal Structure and Cation Sites of the Rock-Forming Mineral. Mineral Structure Data. Available: http://ruby.colorado.edu/~symth/min/minerals.html (Accessed August 2014).

Sophocleous, M. 2002. Interactions between groundwater and surface water: the state of the science. Hydrogeology Journal, 10 (1): 52-67.

South African National Standard, S. 2011. Microbiological, physical, aesthetic and chemical determinands. Pretoria: SABS Standard Division.October 2014).

Staff, A. 2011. Microfiltration and Ultrafiltration Membranes for Drinking Water (M53). American Water Works Association.

Third World Academy of Sciences, T. 2002. Safe Drinking Water: The need, the problem, solutions and an action plan. Available: http://www.twas.org/sites/default/files/safedrinkingwater.pdf (Accessed June 2014).

Thiruvekatachari, R., Vigneswaran, S. and Moon, S. 2008. A review on UV/TiO2 photocatalytic oxidation process. Korean Journal of Chemical Engineering, 25 (1): 64-72.

Thuy, T. N. 2010. Development of a water treatment system for emergency situations. Master degree, Asian Institute of Technology.

Unit-3. 2013. Environmental Pollution and Global Issues. In. Available: http://mptbc.nic.in (Accessed September 2014).

United States Environmental Protection Engency, U. 2014. Conventional Treatment: Drinking Water Treatability Database. Available: http://iaspub.epa.gov/tdb/pages/treatment/treatmentOverview.do (Accessed June 2014).

Vasiliev, P. O. 2008. Colloidal aspects relating to direct incoporation of TiO2 nanoparticle into mesoporous sphere by an aerosol assisted process. Colloid and Interface Science, 319: 144-151.

Wikipedia. 2014a. Water Pollution. Available: http://en.wikipedia.org/wiki/Water_pollution; https://en.wikipedia.org/w/index.php?title=Water_pollution&oldid=711260089 (Accessed March 2014).

Wikipedia. 2014b. Water Distribution of Earth. Available: http://en.wikipedia.org/w/index.php?title=Water_distribution_on_Earth&oldid=60961694 (Accessed May 2014).

Winston Ho, W. S. and Sirkar, K. K. 2001. Membrane Handbook. Massachusetts: Kluwer Academic Publishers.

World Health Organisation, W. 2011. Guidelines for drinking-water quality. Geneva: World Health Organisation. Available: http://www.who.int/water_sanitation_health/publications/2011/dwq_guidelines/en/ (Accessed October 2014).

World Resources Institute, W. 2009. Physical and economic water scarcity. Available: www.wri/resource/physical-and-economic-water-scarcity (Accessed August 2014)

Yu, J., Yu, J. C., Ho, W. and Jiang, Z. 2002. Effects of calcination temperature on the photocatalytic activity and photo-induced super-hydrophilicity of mesoporous TiO2 thin films. New Journal of Chemistry, 26 (5): 607-613.

Yu, J., Yu, J. C., Ho, W. and Jiang, Z. 2002. Effects of calcination temperature on the photocatalytic activity and photo-induced super-hydrophilicity of mesoporous TiO_2 thin films. New Journal of Chemistry, 26 (5): 607-613.

Zhang, J. H., Chen, S. X., Yang, R. and Yan, Y. Y. 2010. Biodiesel production from vegetable oil using heterogenous acid and alkali catalyst. Fuel, 89 (10): 2939-2944.

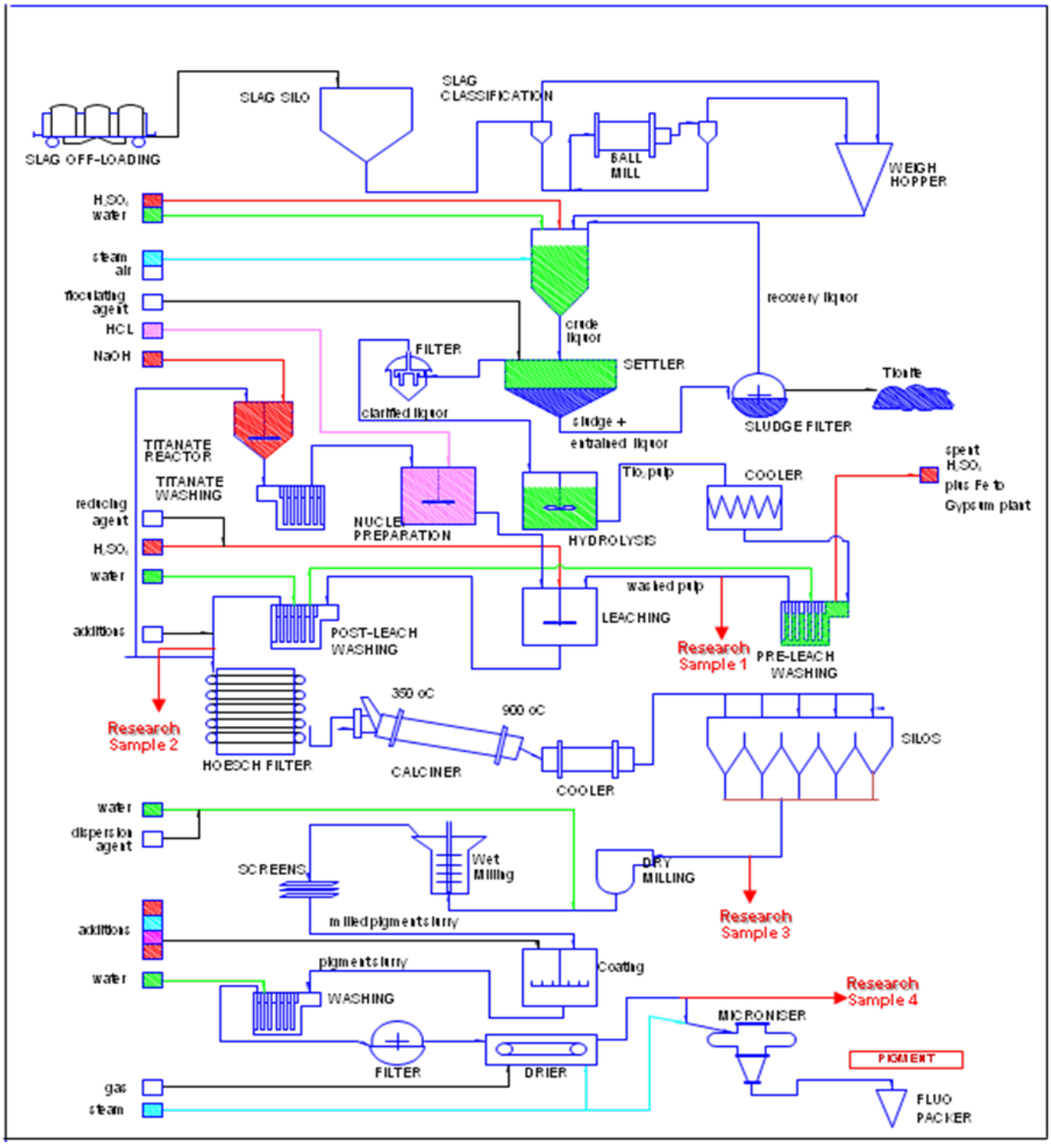

Figure 7.1: Schematic diagram of the Tioxide Sulphate Process for the sampling of the grades of $mTiO_2$.

APPENDIX A:

EVALUATE THE PHOTOCATALYTIC ACTIVITY MTIO$_2$ ON DEGRADATION OF ORGANIC COMPOUNDS IN RIVER WATER.

Table A-7.1: Calibration data curve for the TiO$_2$ Concentration

mTiO$_2$ Concentration (g/l)	Turbidity (NTU)			
	Run 1	Run 2	Run 3	Average
0	0.11	0.13	0.09	0.11
0.0872	125	123	121	123
0.146	175	185	180	180
0.193	252	255	249	252
0.262	348	353	355	352
0.383	456	450	462	456
0.532	630	680	640	650
0.619	780	830	790	800
0.743	1000	1000	1000	1000

Table A-7.2: Effect of Irradiation time on Organic degradation

Time	COD (mg/l)				Degradation Eff.
hr	Run 1	Run 2	Run 3	Run Ave.	Ave. (%)
0	68	68	68	68	0
1	50	60	55	55	19
2	38	35	37	37	46
3	10	8	15	11	84
4	7	10	9	9	87
5	7	9	5	7	90
6	5	4	6	5	93

Table A-7.3: Effect $mTiO_2$ concentration on organic degradation using particle size range of 0.2-53 µm.

$mTiO_2$ Conc.	COD (mg/l)						Ave. Degradation
g/l	Run 1	Run 2	Run 3	Run 4	Run 5	Average Run	(%)
0	55	55	68	61	45	57	0
2.5	20	25	26	25	22	24	58
3.75	10	10	10	15	9	11	82
5	7	6	5	6	1	5	89
7.5	7	6	5	6	3	5	89

Table A-7.4: Effect $mTiO_2$ concentration on organic degradation using particle size range of 53-75 µm

$mTiO_2$ Conc.	COD (mg/l)						Ave. Degradation
g/l	Run 1	Run 2	Run 3	Run 4	Run 5	Average Run	(%)
0	55	55	68	61	45	57	0
2.5	39	43	42	39	36	40	30
3.75	23	25	29	29	20	25	55
5	12	15	16	14	7	13	73
7.5	13	15	15	14	7	13	73

Table A-7.5: Trial 1 on Percentage Recovery of TiO_2 using a new PWFMF.

TRAIL 1: NEW PWFMF (FEED TURBIDITY = 455 NTU, TiO_2 Conc = 354 mg/l)

Time	Run 1		Run 2		Run 3		Ave. Turbidity	TiO_2 Conc	TiO_2 Recovery (%)
Min	Permeate Vol (ml)	Turbidity (NTU)	Permeate Vol (ml)	Turbidity (NTU)	Permeate Vol (ml)	Turbidity (NTU)	NTU	mg/l	Trial 1
5	1150	4.39	1180	3.89	1210	4.65	4.31	7.15	97.98
10	2250	1.8	2330	1.6	2410	2	1.80	5.22	98.53
15	3250	1.16	3380	1.12	3510	1.18	1.15	4.72	98.67
20	4350	0.81	4505	0.8	4660	0.82	0.81	4.46	98.74
25	5395	0.58	5600	0.59	5805	0.57	0.58	4.28	98.79
30	6445	0.54	6670	0.6	6895	0.56	0.57	4.27	98.79
35	7495	0.44	7750	0.42	8005	0.46	0.44	4.18	98.82
40	8555	0.43	8860	0.43	9165	0.45	0.44	4.17	98.82
45	9605	0.4	9960	0.39	10315	0.41	0.40	4.14	98.83
50	10625	0.34	11030	0.34	11435	0.34	0.34	4.10	98.84
55	11645	0.33	12100	0.33	12555	0.35	0.34	4.10	98.84
60	12695	0.32	13200	0.32	13705	0.33	0.32	4.09	98.85
65	13755	0.29	14310	0.3	14865	0.28	0.29	4.06	98.85
70	14855	0.27	15460	0.29	16065	0.25	0.27	4.04	98.86
75	15865	0.3	16520	0.3	17165	0.33	0.31	4.08	98.85
80	16965	0.3	17640	0.29	18305	0.31	0.30	4.07	98.85
85	18115	0.28	18740	0.28	19355	0.29	0.28	4.05	98.85
90	19175	0.27	19750	0.27	20315	0.27	0.27	4.04	98.86
95	20225	0.27	20815	0.28	21395	0.26	0.27	4.04	98.86
100	21375	0.33	21915	0.33	22445	0.29	0.32	4.08	98.85
105	22495	0.29	22995	0.27	23485	0.32	0.29	4.06	98.85
110	23545	0.25	24065	0.23	24555	0.27	0.25	4.03	98.86
115	24645	0.25	25145	0.23	25635	0.27	0.25	4.03	98.86
120	25705	0.25	26195	0.23	26675	0.27	0.25	4.03	98.86

Table A-7.6: Trial 2 Percentage Recovery of TiO_2 using PWFMF (cleaned after trial 1)

TRIAL 2: CLEANED AFTER TRIAL 1 (FEED TURBIDITY = 465 NTU, TiO_2 Conc = 361 mg/l)

Time	Run 1		Run 2		Run 3		Ave. Turbidity	TiO_2 Conc	TiO_2 Recovery (%)
Min	Permeate Vol (ml)	Turbidity (NTU)	Permeate Vol (ml)	Turbidity (NTU)	Permeate Vol (ml)	Turbidity (NTU)	NTU	mg/l	Trial 2
5	1060	2.34	1110	1.98	1160	2.32	2.21	5.54	98.44
10	2020	1.50	2120	1.45	2220	1.80	1.58	5.05	98.57
15	2970	1.00	3120	0.90	3270	1.15	1.02	4.62	98.70
20	3915	0.50	4115	0.50	4315	0.86	0.62	4.31	98.78
25	4885	0.30	5135	0.50	5385	0.65	0.48	4.21	98.81
30	5835	0.19	6135	0.26	6435	0.36	0.27	4.04	98.86
35	6810	0.17	7160	0.17	7510	0.25	0.20	3.99	98.87
40	7710	0.16	8110	0.15	8510	0.22	0.18	3.97	98.88
45	8650	0.13	9100	0.13	9550	0.18	0.15	3.95	98.88
50	9550	0.15	10040	0.15	10540	0.19	0.16	3.96	98.88
55	10515	0.15	11055	0.19	11605	0.20	0.18	3.98	98.88
60	11415	0.11	11995	0.14	12595	0.15	0.13	3.94	98.89
65	12415	0.15	13045	0.14	13695	0.13	0.14	3.94	98.89
70	13455	0.18	14135	0.11	14835	0.18	0.16	3.96	98.88
75	14375	0.16	15105	0.20	15865	0.14	0.17	3.97	98.88
80	15345	0.12	16125	0.16	16935	0.17	0.15	3.95	98.88
85	16345	0.15	17175	0.11	18035	0.16	0.14	3.94	98.89
90	17315	0.13	18195	0.12	19105	0.15	0.13	3.94	98.89
95	18335	0.15	19265	0.10	20225	0.16	0.14	3.95	98.88
100	19265	0.17	20245	0.13	21255	0.16	0.15	3.95	98.88
105	20215	0.16	21245	0.13	22305	0.14	0.14	3.94	98.89
110	21155	0.14	22235	0.13	23345	0.17	0.15	3.95	98.88
115	22115	0.15	23245	0.15	24405	0.15	0.15	3.95	98.88
120	23055	0.14	24235	0.13	25445	0.11	0.08	3.90	98.90

Table A-7.7: Trial 3 Percentage Recovery of TiO_2 using PWFMF (cleaned after trial 2)

TRIAL 3: CLEANED PWFMF AFTER TRIAL 2 (FEED TURBIDITY = 490 NTU, TiO_2 Conc = 380 mg/l)

Time	Run 1		Run 2		Run 3		Ave. Turbidity	TiO_2 Conc	TiO_2 Recovery (%)
Min	Permeate Vol (ml)	Turbidity (NTU)	Permeate Vol (ml)	Turbidity (NTU)	Permeate Vol (ml)	Turbidity (NTU)	NTU	mg/l	Trial 3
5	1049	0.91	1060	0.95	1040	1.01	0.96	4.57	98.80
10	1969	0.24	1990	0.26	1955	0.28	0.26	4.04	98.94
15	2869	0.16	2890	0.17	2865	0.19	0.17	3.97	98.96
20	3744	0.13	3770	0.15	3730	0.17	0.15	3.95	98.96
25	4694	0.14	4745	0.13	4655	0.12	0.13	3.94	98.96
30	5574	0.17	5630	0.15	5530	0.13	0.15	3.95	98.96
35	6529	0.17	6580	0.19	6490	0.18	0.18	3.98	98.95
40	7399	0.13	7470	0.14	7340	0.15	0.14	3.94	98.96
45	8289	0.14	8370	0.14	8220	0.15	0.14	3.95	98.96
50	9139	0.13	9210	0.14	9080	0.14	0.14	3.94	98.96
55	10029	0.1	10110	0.11	9960	0.11	0.11	3.92	98.97
60	10954	0.18	11040	0.2	10880	0.19	0.19	3.98	98.95
65	11834	0.15	11920	0.16	11750	0.17	0.16	3.96	98.96
70	12779	0.1	12870	0.11	12690	0.12	0.11	3.92	98.97
75	13609	0.11	13710	0.11	13510	0.12	0.11	3.92	98.97
80	14509	0.1	14620	0.12	14400	0.12	0.11	3.92	98.97
85	15439	0.09	15460	0.1	15220	0.11	0.10	3.91	98.97
90	16269	0.08	16320	0.1	16030	0.12	0.10	3.91	98.97
95	17159	0.9	17215	0.13	16830	0.12	0.13	3.94	98.96
100	18069	0.14	18135	0.13	17730	0.11	0.13	3.93	98.96
105	18959	0.14	19045	0.12	18600	0.12	0.12	3.93	98.97
110	19809	0.13	19895	0.15	19460	0.17	0.15	3.95	98.96
115	20659	0.12	20755	0.13	20300	0.14	0.13	3.94	98.96
120	21544	0.12	21645	0.13	21180	0.14	0.09	3.91	98.97

APPENDIX B:

INVESTIGATION OF THE BEST PERFORMING GRADES OF $mTIO_2$ ON DEGRADATION OF BACTERIA IN RIVER WATER.

Table B-7.1: Effect of Grades of mTiO2 on *E. coli* and Total coliform bacteria for 2g/L

Time	E-coli (count/100ml) 2 g/l							
	GRADE 1		GRADE 2		GRADE 3		GRADE4	
hr	E-coli	Total Coliform	E-coli	Total Coliform	E-coli	Total Coliform	E-coli	Total Coliform
0	205.5	205.5	205.5	205.5	205.5	205.5	205.5	205.5
0.5	27.1	205.5	16.4	200.5	32.4	205.5	22.2	200.5
2	13.7	165.2	8.7	69.7	27.1	205.5	9.9	129.8
4	12.4	109.1	3.1	42.9	15	205.5	8.7	73.8

Table B-7.2: Effect of Grades of mTiO2 on *E. coli* and Total coliform bacteria for 5g/L

Time	E-coli (count/100ml) 5 g/l							
	GRADE 1		GRADE 2		GRADE 3		GRADE4	
hr	E-coli	Total Coliform	E-coli	Total Coliform	E-coli	Total Coliform	E-coli	Total Coliform
0	205.5	205.5	205.5	205.5	205.5	205.5	205.5	205.5
0.5	5.3	144.5	2	16.4	7.5	205.5	3.1	88.5
2	4.2	118.4	0	6.3	5.3	205.5	2	12.4
4	3.1	78.2	0	1	4.2	205.5	1	9.9

Table B-7.3: Effect of Grades of mTiO2 on *E. coli* and Total coliform bacteria for 7g/L

Time	E-coli (count/100ml) 7 g/l							
	GRADE 1		GRADE 2		GRADE 3		GRADE4	
hr	E-coli	Total Coliform	E-coli	Total Coliform	E-coli	Total Coliform	E-coli	Total Coliform
0	205.5	205.5	205.5	205.5	205.5	205.5	205.5	205.5
0.5	3.1	50.4	0	8.7	4.2	205.5	2	9.9
2	2	32.4	0	4.2	3.1	205.5	1	6.3
4	1	23.8	0	0	2	205.5	0	4.2

APPENDIX C:

THE RAW DATA FOR THE DESIGN OF EXPERIMENTS.

Table C-7.1: The raw data for run 16 CCD and run 13 BBD

Table C-7.1 CCD: Run 16 with $mTiO_2$ of 5 g/l and Aeration of 14 L/min

Time hr	Turbidity NTU	Flux LMH	Temperature ^oC	pH	COD mg/l	E-coli mL
0	1000		30.0	8.00	1	378.4
0.5	7.57		31.5	7.78	9	200.0
2	2.72		30.6	7.02	3	110.0
4	2.74		30.0	7.07	11	99.1

Table C-7.1 BB: Run 13 with $mTiO_2$ of 3.5 g/l and Aeration of 10 L/min

Time hr	Turbidity NTU	Flux LMH	Temperature ^oC	pH	COD mg/l	E-coli count/100 mL
0	313		20.0	6.00	7	378.4
0.5	6.66		20.0	6.08	14	50.0
2	5.66		17.8	4.27	21	16.8
4	1.75		21.2	4.16	11	3.8

Table C-7.2: The raw data for run 19 CCD and run 6 BBD

Table C-7.2 CCD: Run 19 with $mTiO_2$ of 3.5 g/ land Aeration of 10 L/min

Time hr	Turbidity NTU	Flux LMH	Temperature ^oC	pH	COD mg/l	E-coli count/100 mL
0	865		15.0	7	7	378.4
0.5	27.5		14.9	7	6	100.0
2	10.44		15.1	6.96	3	50.0
4	13.9		14.3	6.76	1	18.9

Table C-7.2 BB: Run 6 with $mTiO_2$ of 3.5 g/l and Aeration of 6 L/min

Time hr	Turbidity NTU	Flux LMH	Temperature ^oC	pH	COD mg/l	E-coli count/100 mL
0	1000	12.7	25.3	8.30	7	1986.3
0.5	1.22	10.4	24.5	8.36	7	1651
2	51.95	10.4	24.2	8.05	124	1403
4	36.95	9.0	25.4	8.23	12	993.2

Table C-7.3: The raw data for run 27 CCD and run 25 BBD

Table C-7.3 CCD: Run 27 with $mTiO_2$ of 3.5 g/l & 10 L/min (A new PWFMF)

Time hr	Turbidity NTU	Flux LMH	Temperature ^oC	pH	COD mg/l	E-coli count/100 mL
0	1000	23.9	25.0	7.00	7	378.4
0.5	1.91	20.9	25.0	7.00	6	60.0
2	0.85	14.9	25.3	6.96	3	20.0
4	1.00	11.9	25.0	6.76	1	5.7

Table C-7.3 BB: Run 25 with $mTiO_2$ of 3.5 g/l and Aeration of 10 L/min

Time hr	Turbidity NTU	Flux LMH	Temperature ^oC	pH	COD mg/l	E-coli count/100 mL
0	1000	23.9	25	7	7	378.4
0.5	1.91	20.9	25	7	6	60.0
2	0.85	14.9	25.3	6.96	3	20.0
4	1	11.9	25	6.76	1	5.7

Table C-7.4: The raw data for run 11 CCD and run 21 BBD

Table C-7.4 CCD: Run 11 with $mTiO_2$ of 2 g/l and Aeration of 14 L/min

Time hr	Turbidity NTU	Flux LMH	Temperature ^oC	pH	COD mg/l	E-coli count/100 mL
0	833	1.7	30.4	6.11	7	1986.3
0.5	0.95	1.5	31.1	6.30	6	800.0
2	0.64	3.6	31.0	5.99	11	500.0
4	1.21	4.1	29.9	5.90	10	211.0

Table C-7.4 BB: Run 21 with $mTiO_2$ of 3.5 g/l and Aeration of 6 L/min

Time hr	Turbidity NTU	Flux LMH	Temperature OC	pH	COD mg/l	E-coli count/100 mL
0	1000	4.5	20.5	7.04	5	2419.6
0.5	2.18	4.0	20.4	7.40	3	1037
2	1.07	3.5	20.2	7.76	0	728.0
4	0.95	3.6	20.2	7.85	0	411.3

Table C-7.5: The raw data for run 23 CCD and run 23 BBD

Table C-7.5 CCD: Run 23 with $mTiO_2$ of 3.5 g/l and Aeration of 2 L/min

Time hr	Turbidity NTU	Flux LMH	Temperature OC	pH	COD mg/l	E-coli count/100 mL
0	1000	9.0	24.7	6.90	8	1986.3
0.5	0.46	7.5	25.1	6.66	8	1005.0
2	0.25	5.7	24.5	7.76	0	1000.0
4	0.38	4.2	25.3	7.45	11	754.8

Table C-7.5 BB: Run 23 with $mTiO_2$ of 3.5 g/l and Aeration of 14 L/min

Time hr	Turbidity NTU	Flux LMH	Temperature ^oC	pH	COD mg/l	E-coli count/100 mL
0	833	8.4	21.0	7.06	5	2419.6
0.5	0.95	6.6	19.6	7.36	6	517.0
2	0.64	5.5	20.3	7.55	10	103.5
4	1.21	5.1	20.3	7.56	12	48.4

Table C-7.6: The raw data for run 8 CCD and run 4 BBD

Table C-7.6 CCD: Run 8 with $mTiO_2$ of 5 g/l and Aeration of 6 L/min

Time hr	Turbidity NTU	Flux LMH	Temperature ^oC	pH	COD mg/l	E-coli count/100 mL
0	1000	5.7	30.1	8.16	5	2419.6
0.5	2.49	5.0	32.0	7.78	16	2018.0
2	0.78	4.3	31.5	7.82	14	1500.0
4	0.95	3.7	31.0	7.87	13	1088.8

Table C-7.6 BB: Run 4 with $mTiO_2$ of 5 g/l and Aeration of 10 L/min

Time hr	Turbidity NTU	Flux LMH	Temperature ^oC	pH	COD mg/l	E-coli count/100 mL
0	1755	10.4	29.0	7.07	5	2419.6
0.5	421.00	16.4	32.0	6.45	0	862.0
2	400.00	16.2	29.3	5.73	4	126.3
4	800.00	24.6	31.0	6.39	2	48.5

Table C-7.7: The raw data for run 2 CCD and run 18 BBD

Table C-7.7 CCD: Run 2 with $mTiO_2$ of 5 g/l and Aeration of 6 L/min

Time hr	Turbidity NTU	Flux LMH	Temperature ^oC	pH	COD mg/l	E-coli count/100 mL
0	1755	9.0	21.0	6.12	5	2419.6
0.5	0.45	5.8	21.6	6.19	15	1033.0
2	0.27	8.4	19.8	6.06	6	650.0
4	4.46	9.3	20.3	5.94	14	242.0

Table C-7.7 BB: Run 18 with $mTiO_2$ of 5 g/l and Aeration of 6 L/min

Time hr	Turbidity NTU	Flux LMH	Temperature ^oC	pH	COD mg/l	E-coli count/100 mL
0			25.1	7.14	5	2419.6
0.5			25.3	7.06	8	559.8
2			25.1	7.07	3	110.3
4			25.0	7.09	3	24.2

Table C-7.8: The raw data for run 30 CCD and run 29 BBD

Table C-7.8 CCD: Run 30 with $mTiO_2$ of 3.5 g/l and Aeration of 10 L/min

Time hr	Turbidity NTU	Flux LMH	Temperature ^oC	pH	COD mg/l	E-coli count/100 mL
0	1355	34.3	25.2	7.12	5	2419.6
0.5	3.32	40.8	25.0	7.00	0	1681.0
2	6.76	39.8	25.6	6.98	12	865.0
4	4.59	35.8	25.3	6.69	10	73.0

Table C-7.8 BB: Run 29 with $mTiO_2$ of 3.5 g/l and Aeration of 10 L/min

Time hr	Turbidity NTU	Flux LMH	Temperature ^oC	pH	COD mg/l	E-coli count/100 mL
0	1355	34.3	25.2	7.12	5	2419.6
0.5	3.32	40.8	25.0	7.00	0	1681.0
2	6.76	39.8	25.6	6.98	12	865.0
4	4.59	35.8	25.3	6.69	10	73.0

Table C-7.9: The raw data for run 1 CCD and run 14 BBD

Table C-7.9 CCD: Run 1 with $mTiO_2$ of 2 g/l and Aeration of 6 L/min

Time hr	Turbidity NTU	Flux LMH	Temperature ^oC	pH	COD mg/l	E-coli count/100 mL
0	834.5	49.8	21.3	6.14	12	2419.6
0.5	1.20	56.7	20.4	6.10	0	1989.0
2	0.81	56.7	19.5	5.83	11	1589.0
4	0.75	56.7	21.0	5.73	13	912.2

Table C-7.9 BB: Run 14 with $mTiO_2$ of 3.5 g/l and Aeration of 10 L/min

Time hr	Turbidity NTU	Flux LMH	Temperature ^oC	pH	COD mg/l	E-coli count/100 mL
0	1355	41.8	30.0	6.02	12	2419.6
0.5	0.55	39.8	31.6	5.65	11	892.3
2	0.52	49.8	29.9	5.50	6	300.1
4	0.26	37.3	28.6	5.48	3	48.3

Table C-7.10: The raw data for run 10 CCD and run 22 BBD

Table C-7.10 CCD: Run 10 with $mTiO_2$ of 5 g/l and Aeration of 14 L/min

Time hr	Turbidity NTU	Flux LMH	Temperature ^oC	pH	COD mg/l	E-coli count/100 mL
0	1755	56.7	21.3	6.10	12	2419.6
0.5	1.74	56.7	19.9	5.98	12	867.0
2	1.09	57.7	21.3	5.61	17	300.0
4	0.46	56.7	21.2	5.51	19	0.0

Table C-7.10 BB: Run 22 with $mTiO_2$ of 3.5 g/l and Aeration of 6 L/min

Time hr	Turbidity NTU	Flux LMH	Temperature ^oC	pH	COD mg/l	E-coli count/100 mL
0	2710	50.7	30.1	7.00	12	2419.6
0.5	0.83	47.8	30.7	7.05	10	1342.0
2	0.57	46.3	29.6	7.15	21	956.2
4	0.75	43.8	30.4	7.23	11	435.5

Table C-7.11: The raw data for run 4 CCD and run 7 BBD

Table C-7.11 CCD: Run 4 with $mTiO_2$ of 5 g/l and Aeration of 6 L/min

Time hr	Turbidity NTU	Flux LMH	Temperature ^oC	pH	COD mg/l	E-coli count/100 mL
0	1755	44.8	30.2	6.00	12	2419.6
0.5	0.28	37.8	31.0	6.30	4	1623.0
2	0.27	36.8	30.5	6.30	8	1081.0
4	1.02	35.8	29.5	6.40	9	604.5

Table C-7.11 BB: Run 7 with $mTiO_2$ of 3.5 g/l and Aeration of 14 L/min

Time hr	Turbidity NTU	Flux LMH	Temperature ^oC	pH	COD mg/l	E-coli count/100 mL
0	2710	40.3	25.9	6.07	12	2419.6
0.5	0.43	37.8	25.8	6.43	2	21.5
2	0.90	36.8	24.9	6.46	2	9.2
4	0.69	35.8	25.6	6.71	7	0.0

Table C-7.12: The raw data for run 21 CCD and run 12 BBD

Table C-7.12 CCD: Run 21 with $mTiO_2$ of 3.5 g/ land Aeration of 10 L/min

Time hr	Turbidity NTU	Flux LMH	Temperature ^oC	pH	COD mg/l	E-coli count/100 mL
0	1340	39.8	25.0	5	12	2419.6
0.5	0.21	42.0	24.4	4.34	14	1431.0
2	0.145	43.5	25.1	4.29	13	1102.0
4	0.08	41.5	25.3	4.31	7	846.9

Table C-7.12 BB: Run 12 with $mTiO_2$ of 5 g/l and Aeration of 14 L/min

Time hr	Turbidity NTU	Flux LMH	Temperature ^oC	pH	COD mg/l	E-coli count/100 mL
0	1920	42.0	25.2	7.05	12	2419.6
0.5	0.295	40.2	24.6	6.76	12	1109.0
2	0.14	36.0	24.6	6.28	3	525.1
4	0.085	36.0	25.7	5.42	10	72.5

Table C-7.13: The raw data for run 5 CCD and run 19 BBD

Table C-7.13 CCD: Run 5 with $mTiO_2$ of 2 g/l and (Aeration of 6L/min)

Time hr	Turbidity NTU	Flux LMH	Temperature ^oC	pH	COD mg/l	E-coli count/100 mL
0	855	27.4	20.3	8.00	12	2419.6
0.5	0.31	22.4	19.2	7.58	12	2356.0
2	0.27	18.0	20.5	7.38	12	1925.0
4	0.12	15.3	20.5	7.35	15	1246.0

Table C-7.13 BB: Run 19 with $mTiO_2$ of 2 g/l and Aeration of 10 L/min

Time hr	Turbidity NTU	Flux LMH	Temperature ^oC	pH	COD mg/l	E-coli count/100 mL
0	800	27.0	25.4	8	12	2419.6
0.5	0.545	23.3	23.5	7.81	13	2321.0
2	0.195	18.9	25.6	7.38	9	1998.0
4	0.145	17.1	25.1	7.36	18	1330.8

Table C-7.14: The raw data for run 25 CCD and run 28 BBD

Table C-7.14 CCD: Run 25 with $mTiO_2$ of 3,5 g/l and Aeration of 10 L/min

Time hr	Turbidity NTU	Flux LMH	Temperature ^oC	pH	COD mg/l	E-coli count/100 mL
0	1370	30.3	25.0	8.20	12	2419.6
0.5	0.69	26.6	25.0	7.86	9	1235.0
2	0.14	24.6	25.4	7.05	5	768.0
4	0.11	25.0	25.4	6.24	9	121.0

Table C-7.14 BB: Run 28 with $mTiO_2$ of 3.5 g/l and Aeration of 10 L/min

Time hr	Turbidity NTU	Flux LMH	Temperature OC	pH	COD mg/l	E-coli count/100 mL
0	1370	30.3	25.0	8.20	12	2419.6
0.5	0.69	26.6	25.0	7.86	9	1235.0
2	0.14	24.6	25.4	7.05	5	768.0
4	0.11	25.0	25.4	6.24	9	121.0

Table C-7.15: The raw data for run 6 CCD and run 20 BBD

Table C-7.15 CCD: Run 6 with $mTiO_2$ of 5 g/l and Aeration of 6 L/min

Time hr	Turbidity NTU	Flux LMH	Temperature ^oC	pH	COD mg/l	E-coli count/100 mL
0	1755	18.4	21.4	8.00	10	2419.6
0.5	0.23	16.3	20.2	7.45	0	1662.0
2	0.15	17.0	19.3	7.29	3	1076.0
4	0.17	16.5	20.7	7.26	8	822.7

Table C-7.15 BB: Run 20 with $mTiO_2$ of 5 g/l and Aeration of 10 L/min

Time hr	Turbidity NTU	Flux LMH	Temperature ^oC	pH	COD mg/l	E-coli count/100 mL
0	1755	23.4	25.2	8.20	10	2419.6
0.5	0.36	21.0	24.0	7.86	0	1906.0
2	0.12	19.5	21.0	7.05	0	1354.0
4	0.11	21.0	23.0	6.24	0	944.0

Table C-7.16: The raw data for run 20 CCD and run 2 BBD

Table C-7.16 CCD: Run 20 with $mTiO_2$ of 3.5 g/l and Aeration of 10 L/min

Time hr	Turbidity NTU	Flux LMH	Temperature ^oC	pH	COD mg/l	E-coli count/100 mL
0	814	18.0	35.3	7.07	10	2419.6
0.5	0.46	15.8	34.9	7.34	9	1415.0
2	0.24	13.1	35.6	6.40	10	668.0
4	0.22	12.3	34.9	6.17	20	121.0

Table C-7.16 BB: Run 2 with $mTiO_2$ of 5 g/l and Aeration of 10 L/min

Time hr	Turbidity NTU	Flux LMH	Temperature ^oC	pH	COD mg/l	E-coli count/100 mL
0	1920		222.0	7.10	10	2419.6
0.5			20.4	7.10	1	1403.0
2			21.0	6.36	15	869.0
4			21.1	6.04	0	242.0

Table C-7.17: The raw data for run 17 CCD and run 11 BBD

Table C-7.17 CCD: Run 17 with $mTiO_2$ of 0.5 g/l and Aeration of 10 L/min

Time hr	Turbidity NTU	Flux LMH	Temperature ^oC	pH	COD mg/l	E-coli count/100 mL
0	508	21.7	26.0	7.03	10	2419.6
0.5	0.36	15.7	25.6	7.13	30	2000.0
2	0.21	11.7	25.6	7.25	9	1852.0
4	0.35	11.0	25.6	7.34	9	1209.8

Table C-7.17 BB: Run 11 with $mTiO_2$ of 2 g/l and Aeration of 14 L/min

Time hr	Turbidity NTU	Flux LMH	Temperature ^oC	pH	COD mg/l	E-coli count/100 mL
0	820	18.0	24.8	7.09	10	2419.6
0.5	0.46	15.8	25.2	7.32	24	1915.0
2	0.24	13.1	25.9	7.50	2	1009.0
4	0.22	12.3	25.0	7.53	21	532.3

Table C-7.18: The raw data for run 7 CCD and run 9 BBD

Table C-7.18 CCD: Run 7 with $mTiO_2$ of 2 g/l and Aeration of 6 L/min

Time hr	Turbidity NTU	Flux LMH	Temperature ^oC	pH	COD mg/l	E-coli count/100 mL
0	826	13.5	32.7	8.02	9	2419.6
0.5	0.62	11.1	29.6	7.77	7	2103.0
2	0.41	10.2	29.1	7.86	-2	1878.0
4	0.36	9.3	30.4	7.83	8	1234.0

Table C-7.18 BB: Run 9 with $mTiO_2$ of 2 g/l and Aeration of 6 L/min

Time hr	Turbidity NTU	Flux LMH	Temperature ^oC	pH	COD mg/l	E-coli count/100 mL
0	827.5	9.0	25.4	7.01	9	2419.6
0.5	0.37	8.8	25.0	6.35	-7	2012.0
2	0.12	8.7	25.4	5.91	10	1208.0
4	0.23	9.0	24.6	5.62	10	605.0

Table C-7.19: The raw data for run 29 CCD and run 26 BBD

Table C-7.19 CCD: Run 29 with $mTiO_2$ of 3.5 g/l and Aeration of 10 L/min

Time hr	Turbidity NTU	Flux LMH	Temperature ^oC	pH	COD mg/l	E-coli count/100 mL
0	1400	6.4	25.1	7.08	9	2419.6
0.5	0.53	6.2	25.5	7.13	13	1143.0
2	0.24	6.0	25.3	7.37	15	657.0
4	0.30	6.0	25.8	7.41	4	60.5

Table C-7.19 BB: Run 26 with $mTiO_2$ of 3.5 g/l and Aeration of 10 L/min

Time hr	Turbidity NTU	Flux LMH	Temperature ^oC	pH	COD mg/l	E-coli count/100 mL
0	1400	6.4	25.1	7.08	9	2419.6
0.5	0.53	6.2	25.5	7.13	13	1143.0
2	0.24	6.0	25.3	7.37	15	657.0
4	0.30	6.0	25.8	7.41	4	60.5

Table C-7.20: The raw data for run 12 CCD and run 16 BBD

Table C-7.20 CCD: Run 12 with $mTiO_2$ of 5 g/l and Aeration of 14 L/min

Time hr	Turbidity NTU	Flux LMH	Temperature ^oC	pH	COD mg/l	E-coli count/100 mL
0	2153.5	9.3	30.5	6.05	9	2419.6
0.5	0.34	8.3	29.6	6.84	4	876.0
2	0.18	7.8	30.7	7.02	7	434.0
4	0.23	7.5	29.0	7.07	19	24.2

Table C-7.20 BB: Run 16 with $mTiO_2$ of 3.5 g/l and Aeration of 10 L/min

Time hr	Turbidity NTU	Flux LMH	Temperature ^oC	pH	COD mg/l	E-coli count/100 mL
0	1390	9.7	31.1	8.17	9	2419.6
0.5	0.51	8.2	29.2	8.04	-3	2213.0
2	0.33	7.4	30.7	8.03	21	1806.0
4	0.34	6.3	29.0	8.10	10	944.0

Table C-7.21: The raw data for run 18 CCD and run 1 BBD

Table C-7.21 CCD: Run 18 with $mTiO_2$ of 6.5 g/l and Aeration of 10 L/min

Time hr	Turbidity NTU	Flux LMH	Temperature ^oC	pH	COD mg/l	E-coli count/100 mL
0	2930	5.4	25.3	7.06	9	2419.6
0.5	0.42	5.3	25.2	7.37	45	1372.0
2	0.23	5.8	25.0	7.24	-4	903.0
4	0.16	5.0	25.0	7.00	7	523.3

Table C-7.21 BB: Run 1 with $mTiO_2$ of 2 g/l and Aeration of 10 L/min

Time hr	Turbidity NTU	Flux LMH	Temperature ^oC	pH	COD mg/l	E-coli count/100 mL
0	845	8.8	20.4	7.10	9	2419.6
0.5	0.19	8.8	20.0	5.84	17	1325.0
2	0.07	9.6	19.7	5.08	8	792.0
4	0.20	9.7	18.0	5.02	13	436.0

Table C-7.22: The raw data for run 14 CCD and run 5 BBD

Table C-7.22 CCD: Run 14 with $mTiO_2$ of 5 g/l and Aeration of 14 L/min

Time hr	Turbidity NTU	Flux LMH	Temperature ^oC	pH	COD mg/l	E-coli count/100 mL
0	2303	2.6	20.2	8.00	9	2419.6
0.5	0.39	2.6	20.3	7.53	7	1763.0
2	0.22	2.6	19.7	7.43	4	1279.0
4	0.25	2.6	19.8	7.38		967.8

Table C-7.22 BB: Run 5 with $mTiO_2$ of 3.5 g/l and Aeration of 6 L/min

Time hr	Turbidity NTU	Flux LMH	Temperature ^oC	pH	COD mg/l	E-coli count/100 mL
0	1400	6.2	25.7	6.00	9	2419.6
0.5	0.16	5.6	25.5	6.61	11	2056.0
2	0.15	5.1	25.3	6.87	14	862.0
4	0.14	5.0	25.2	6.87	15	218.0

Table C-7.23: The raw data for run 15 CCD and run 17 BBD

Table C-7.23 CCD: Run 15 with $mTiO_2$ of 2 g/l and Aeration of 14 L/min

Time hr	Turbidity NTU	Flux LMH	Temperature ^oC	pH	COD mg/l	E-coli count/100 mL
0	975	3.4	30.9	8.12	9	2419.6
0.5	0.78	3.0	29.0	8.01	19	1402.0
2	0.58	2.7	30.0	7.96	12	890.0
4	0.66	2.5	28.0	7.98	16	532.0

Table C-7.23 BB: Run 17 with $mTiO_2$ of 2 g/l and Aeration of 10 L/min

Time hr	Turbidity NTU	Flux LMH	Temperature ^oC	pH	COD mg/l	E-coli count/100 mL
0	950	3.6	24.5	6.00	9	2419.6
0.5	0.33	3.7	24.5	5.17	34	1137.0
2	0.59	3.8	25.0	5.01	12	706.0
4	0.34	4.0	24.0	5.00	46	363.0

Table C-7.24: The raw data for run 28 CCD and run 27 BBD

Table C-7.24 CCD: Run 28 with $mTiO_2$ of 3.5 g/l and Aeration of 10 L/min						
Time hr	Turbidity NTU	Flux LMH	Temperature ^oC	pH	COD mg/l	E-coli count/100 mL
0	1400	34.7	26.0	7.00	9	2419.6
0.5	0.41	33.9	26.0	7.25	2	1014.0
2	0.17	30.7	25.0	7.19	14	656.0
4	0.16	28.2	24.0	7.11	19	96.8

Table C-7.24 BB: Run 27 with $mTiO_2$ of 3.5 g/l and Aeration of 10 L/min						
Time hr	Turbidity NTU	Flux LMH	Temperature ^oC	pH	COD mg/l	E-coli count/100 mL
0	1400	34.7	26.0	7.00	9	2419.6
0.5	0.41	33.9	26.0	7.25	2	1014.0
2	0.17	30.7	25.0	7.19	14	656.0
4	0.16	28.2	24.0	7.11	19	96.8

Table C-7.25: The raw data for run 9 CCD and run 3 BBD

Table C-7.25 CCD: Run 9 with $mTiO_2$ of 2 g/l and Aeration of 14 L/min						
Time hr	Turbidity NTU	Flux LMH	Temperature ^oC	pH	COD mg/l	E-coli count/100 mL
0	955	1.7	20.0	6.11	9	2419.6
0.5	0.46	1.8	21.0	6.74	13	986.0
2	0.25	1.8	18.0	7.08	3	801.0
4	0.30	1.7	20.0	7.08	5	509.0

Table C-7.25 BB: Run 3 with $mTiO_2$ of 2 g/l and Aeration of 10 L/min						
Time hr	Turbidity NTU	Flux LMH	Temperature ^oC	pH	COD mg/l	E-coli count/100 mL
0	940	20.5	30.8	7.07	9	2419.6
0.5	0.22	16.7	29.0	7.32	20	1806.0
2	0.24	12.8	29.8	7.29	27	1045.0
4	0.16	12.8	30.0	7.29	49	509.0

Table C-7.26: The raw data for run 24 CCD and run 8 BBD

Table C-7.26 CCD: Run 24 with $mTiO_2$ of 3.5 g/l and Aeration of 18 L/min						
Time hr	Turbidity NTU	Flux LMH	Temperature ^oC	pH	COD mg/l	E-coli count/100 mL
0	1400	18.4	30.8	7.07	9	2419.6
0.5	0.29	16.7	29.0	7.32	20	926.0
2	0.14	12.8	29.8	7.29	27	380.0
4	0.17	12.7	30.0	7.29	49	145.2

Table C-7.26 BB: Run 8 with $mTiO_2$ of 3.5 g/l and Aeration of 14 L/min						
Time hr	Turbidity NTU	Flux LMH	Temperature ^oC	pH	COD mg/l	E-coli count/100 mL
0	1375	17.2	25.3	8.02	6	2419.6
0.5	0.30	14.6	24.6	7.54	-1	2401.0
2	0.32	12.7	26.0	7.39	8	2001.0
4	0.17	11.6	24.0	7.32	10	1089.0

Table C-7.27: The raw data for run 3 CCD and run 15 BBD

Table C-7.27 CCD: Run 3 with $mTiO_2$ of 2 g/l and Aeration of 6 L/min						
Time hr	Turbidity NTU	Flux LMH	Temperature ^oC	pH	COD mg/l	E-coli count/100 mL
0	905	10.0	31.0	6.12	6	2419.6
0.5	0.43	10.5	30.3	5.44	15	2398.0
2	0.20	11.2	29.5	5.14	3	1309.0
4	0.16	10.5	28.6	5.02	0	967.5

Table C-7.27 BB: Run 15 with $mTiO_2$ of 3.5 g/l and Aeration of 10 L/min						
Time hr	Turbidity NTU	Flux LMH	Temperature ^oC	pH	COD mg/l	E-coli count/100 mL
0	1382	23.3	20.0	8.13	6	2419.6
0.5	0.15	21.3	20.3	7.10	0	2298.0
2	0.13	19.1	20.4	6.86	18	1721.0
4	0.10	18.3	20.5	7.34	12	968.0

Table C-7.28: The raw data for run 22 CCD and run 10 BBD

Table C-7.28 CCD: Run 22 with $mTiO_2$ of 3.5 g/l and Aeration of 10 L/min

Time hr	Turbidity NTU	Flux LMH	Temperature ^oC	pH	COD mg/l	E-coli count/100 mL
0	1352.5	13.1	25.1	9.07	6	2419.6
0.5	14.55	8.3	26.0	8.63	14	2410.2
2	9.29	7.5	25.4	8.08	-7	2013.0
4	3.30	6.7	24.8	7.91	-5	1815.0

Table C-7.28 BB: Run 10 with $mTiO_2$ of 5 g/l and Aeration of 6 L/min

Time hr	Turbidity NTU	Flux LMH	Temperature ^oC	pH	COD mg/l	E-coli count/100 mL
0	2218.5	8.7	25.6	7.09	6	2419.6
0.5	0.51	8.1	25.1	6.36	-8	1203.0
2	0.17	8.3	25.3	5.25	5	687.0
4	0.10	7.8	25.0	5.24	2	484.0

Table C-7.29: The raw data for run 13 CCD and run 24 BBD

Table C-7.29 CCD: Run 13 with $mTiO_2$ of 2 g/l and Aeration of 14 L/min

Time hr	Turbidity NTU	Flux LMH	Temperature ^oC	pH	COD mg/l	E-coli count/100 mL
0	882.5	11.5	21.7	8.02	6	2419.6
0.5	0.53	11.5	20.2	7.55	6	2018.0
2	0.19	9.4	19.2	7.54	89	1795.0
4	0.16	8.3	20.2	7.50	50	1210.0

Table C-7.29 BB: Run 24 with $mTiO_2$ of 3.5 g/l and Aeration of 14 L/min

Time hr	Turbidity NTU	Flux LMH	Temperature ^oC	pH	COD mg/l	E-coli count/100 mL
0	1351.5	10.1	30.5	7.04	6	2419.6
0.5	0.12	10.1	30.1	6.46	9	956.0
2	0.11	8.2	29.8	6.11	21	630.0
4	0.17	9.7	29.0	6.00	12	121.0

Table C-7.30: The raw data for run 26 CCD and run 30 BBD

Table C-7.30 CCD: Run 26 with $mTiO_2$ of 3.5 g/l and Aeration of 10 L/min

Time hr	Turbidity NTU	Flux LMH	Temperature ^oC	pH	COD mg/l	E-coli count/100 mL
0	1338.5	7.5	25.4	7.04	6	2419.6
0.5	0.26	7.1	25.3	6.97	-4	612.0
2	0.14	6.3	25.4	7.11	2	231.0
4	0.20	5.7	24.9	7.10	8	24.2

Table C-7.30 BB: Run 30 with $mTiO_2$ of 3.5 g/l and Aeration of 10 L/min

Time hr	Turbidity NTU	Flux LMH	Temperature ^oC	pH	COD mg/l	E-coli count/100 mL
0	1338.5	7.5	25.4	7.04	6	2419.6
0.5	0.26	7.1	25.3	6.97	-4	612.0
2	0.14	6.3	25.4	7.11	2	231.0
4	0.20	5.7	24.9	7.10	8	24.2

APPENDIX D:

BOX-BEHNKEN'S COMPUTER OUTPUT FROM DESIGN EXPERT 9 FOR FITTING A MODEL.

***** WARNING: The Cubic Model and higher are Aliased! *****

Response : Degradation Efficiency Transform: None

Table D-7.1: Sequential Model Sum of Squares [Type I] on the Box-Behnken Design

Source	Sum of Squares	df	Mean Square	F Value	p-value Prob > F	
Mean vs Total	2.12E+05	1	2.12E+05			
Linear vs Mean	5667.17	4	1416.79	14.93	< 0.0001	
2FI vs Linear	86.25	6	14.38	0.12	0.9927	
Quadratic vs 2FI	2221.13	4	555.28	127.33	< 0.0001	Suggested
Cubic vs Quadratic	53.33	8	6.67	3.86	0.0458	Aliased
Residual	12.08	7	1.73			
Total	2.20E+05	30	7346.42			

Table D-7.2: Lack-of-fit Test on the Box-Behnken Design

Source	Sum of Squares	df	Mean Square	F Value	p-value Prob > F	
Linear	2361.47	20	118.07	52.09	0.0002	
2FI	2275.22	14	162.52	71.7	< 0.0001	
Quadratic	54.08	10	5.41	2.39	0.1747	Suggested
Cubic	0.75	2	0.38	0.17	0.852	Aliased
Pure Error	11.33	5	2.27			

Table D-7.3: Model Summary Statistic on the Box-Behnken Design

Source	Std. Dev.	R-Squared	Adjusted R-Squared	Predicted R-Squared	PRESS	
Linear	9.74	0.7049	0.6577	0.602	3200.12	
2FI	10.97	0.7156	0.5659	0.3464	5254.94	
Quadratic	2.09	0.9919	0.9843	0.9592	327.84	Suggested
Cubic	1.31	0.9985	0.9938	0.9845	124.32	Aliased

Table D-7.4: ANOVA for Response Surface Quadratic model on the Box-Behnken Design

Analysis of variance table [Partial sum of squares - Type III]						
Source	**Sum of Squares**	**df**	**Mean Square**	**F Value**	**p-value Prob > F**	
Model	7974.55	14	569.61	130.61	< 0.0001	significant
A-TiO_2 Concentration	*546.75*	*1*	*546.75*	*125.37*	*< 0.0001*	
B-Temperature	*0.083*	*1*	*0.083*	*0.019*	*0.8919*	
C-Starting pH	*4800*	*1*	*4800*	*1100.64*	*< 0.0001*	
D-Aeration	*320.33*	*1*	*320.33*	*73.45*	*< 0.0001*	
AB	*30.25*	*1*	*30.25*	*6.94*	*0.0188*	
AC	*1*	*1*	*1*	*0.23*	*0.6389*	
AD	*49*	*1*	*49*	*11.24*	*0.0044*	
BC	*1*	*1*	*1*	*0.23*	*0.6389*	
BD	*1*	*1*	*1*	*0.23*	*0.6389*	
CD	*4*	*1*	*4*	*0.92*	*0.3534*	
A^2	*476.19*	*1*	*476.19*	*109.19*	*< 0.0001*	
B^2	*12.19*	*1*	*12.19*	*2.8*	*0.1153*	
C^2	*1857.44*	*1*	*1857.44*	*425.91*	*< 0.0001*	
D^2	*286.01*	*1*	*286.01*	*65.58*	*< 0.0001*	
Residual	65.42	15	4.36			
Lack of Fit	*54.08*	*10*	*5.41*	*2.39*	*0.1747*	*not significant*
Pure Error	*11.33*	*5*	*2.27*			
Cor Total	8039.97	29				

Factor	**Coefficient Estimate**	**df**	**Standard Error**	**95% CI Low**	**95% CI High**	**VIF**
Intercept	97.17	1	0.85	95.35	98.98	
A-TiO_2 Concentration	6.75	1	0.6	5.47	8.03	1
B-Temperature	0.083	1	0.6	-1.2	1.37	1
C-Starting pH	-20	1	0.6	-21.28	-18.72	1
D-Aeration	5.17	1	0.6	3.88	6.45	1
AB	2.75	1	1.04	0.52	4.98	1
AC	0.5	1	1.04	-1.73	2.73	1
AD	3.5	1	1.04	1.27	5.73	1
BC	0.5	1	1.04	-1.73	2.73	1
BD	-0.5	1	1.04	-2.73	1.73	1
CD	-1	1	1.04	-3.23	1.23	1
A^2	-8.33	1	0.8	-10.03	-6.63	1.05
B^2	-1.33	1	0.8	-3.03	0.37	1.05
C^2	-16.46	1	0.8	-18.16	-14.76	1.05
D^2	-6.46	1	0.8	-8.16	-4.76	1.05

Final Equation in Terms of Coded Factors:

Degradation Efficiency	=
97.17	
6.75	* A
0.08	* B
-20.00	* C
5.17	* D
2.75	* AB
0.50	* AC
3.50	* AD
0.50	* BC
-0.50	* BD
-1.00	* CD
-8.33	* A^2
-1.33	* B^2
-16.46	* C^2
-6.46	* D^2

Final Equation in Terms of Actual Factors:

Degradation Efficiency	=
-77.72	
9.97	* TiO_2 Concentration
0.18	* Temperature
39.32	* Starting pH
8.57	* Aeration
0.11	* TiO_2 Concentration * Temperature
0.10	* TiO_2 Concentration * Starting pH
0.35	* TiO_2 Concentration * Aeration
0.03	* Temperature * Starting pH
-0.01	* Temperature * Aeration
-0.13	* Starting pH * Aeration
-1.33	* TiO_2 Concentration^2
-0.01	* Temperature^2
-4.11	* Starting pH^2
-0.40	* Aeration^2

Table D-7.5: Diagnostics Case Statistics on the Box-Behnken Design

Run Order	Actual Value	Predicted Value	Residual	Leverage	Internally Studentized Residual	Externally Studentized Residual	Cook's Distance	Influence on Fitted Value DFFITS	Standard Order
1	91	88.08	2.92	0.583	2.164	2.52	0.437	2.982 *	5
2	99	98.63	0.37	0.583	0.278	0.269	0.007	0.319	18
3	55	58.42	-3.42	0.583	-2.535	-3.238	0.6	-3.832 *	8
4	98	94.96	3.04	0.583	2.256	2.682	0.475	3.174 *	23
5	98	97.08	0.92	0.583	0.68	0.667	0.043	0.79	4
6	82	84.79	-2.79	0.583	-2.071	-2.368	0.4	-2.801 *	22
7	75	73.96	1.04	0.583	0.773	0.762	0.056	0.901	9
8	60	58.79	1.21	0.583	0.896	0.89	0.075	1.053	15
9	61	59.96	1.04	0.583	0.773	0.762	0.056	0.901	16
10	50	50.08	-0.083	0.583	-0.062	-0.06	0	-0.071	6
11	95	94.13	0.87	0.583	0.649	0.636	0.039	0.753	24
12	97	97.17	-0.17	0.167	-0.087	-0.084	0	-0.038	30
13	100	100.42	-0.42	0.583	-0.309	-0.3	0.009	-0.354	7
14	80	80.46	-0.46	0.583	-0.34	-0.33	0.011	-0.39	10
15	97.5	97.17	0.33	0.167	0.175	0.169	0	0.076	29
16	98	98.96	-0.96	0.583	-0.711	-0.699	0.047	-0.827	14
17	97	97.79	-0.79	0.583	-0.587	-0.574	0.032	-0.679	12
18	79	78.08	0.92	0.583	0.68	0.667	0.043	0.79	3
19	85	86.13	-1.13	0.583	-0.835	-0.826	0.065	-0.977	17
20	90	91.42	-1.42	0.583	-1.051	-1.055	0.103	-1.248	2
21	61	59.63	1.37	0.583	1.02	1.021	0.097	1.209	20
22	82	83.42	-1.42	0.583	-1.051	-1.055	0.103	-1.248	1
23	96	97.17	-1.17	0.167	-0.612	-0.599	0.005	-0.268	28
24	99	97.17	1.83	0.167	0.962	0.959	0.012	0.429	26
25	78	77.29	0.71	0.583	0.525	0.512	0.026	0.606	11
26	45	45.13	-0.13	0.583	-0.093	-0.09	0.001	-0.106	19
27	83	83.63	-0.63	0.583	-0.464	-0.451	0.02	-0.534	21
28	98.5	97.17	1.33	0.167	0.699	0.687	0.007	0.307	27
29	99	99.79	-0.79	0.583	-0.587	-0.574	0.032	-0.679	13
30	95	97.17	-2.17	0.167	-1.137	-1.149	0.017	-0.514	25

Box-Cox Power Transformation				
Constant k	95% CI Low	95% CI High	Best Lambda	Rec. Transform
0	0.32	2.16	1.09	None

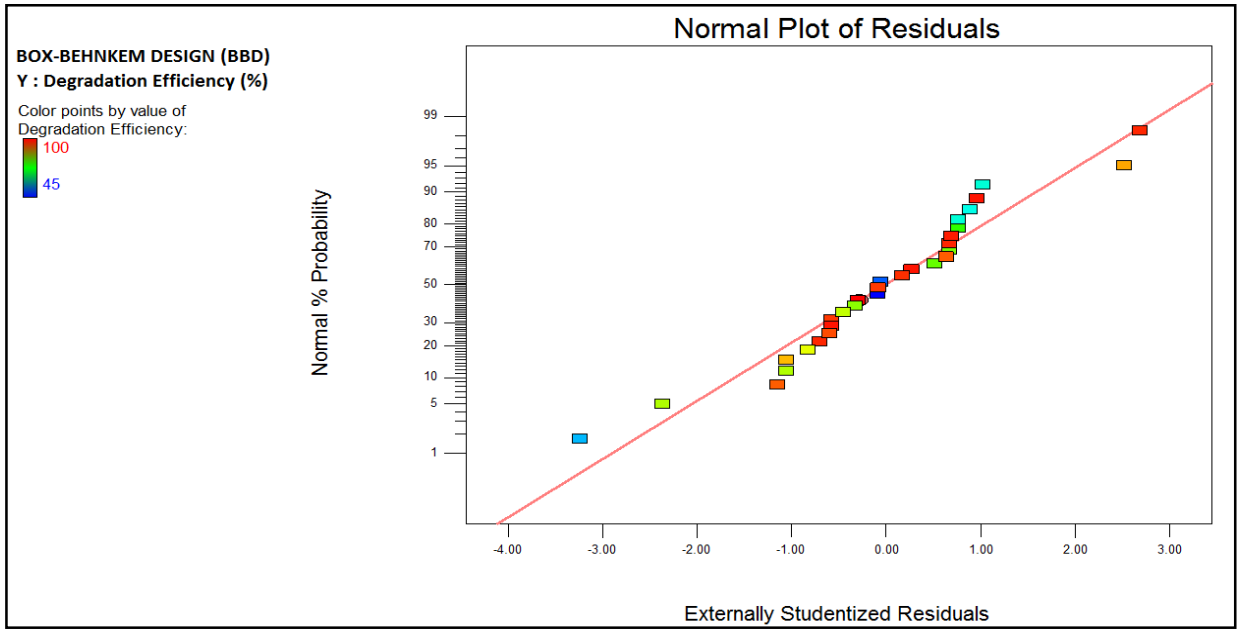

Figure D -7.1: Normal Probability plot of the Studentized Residuals of the $mTiO_2$ water treatment.

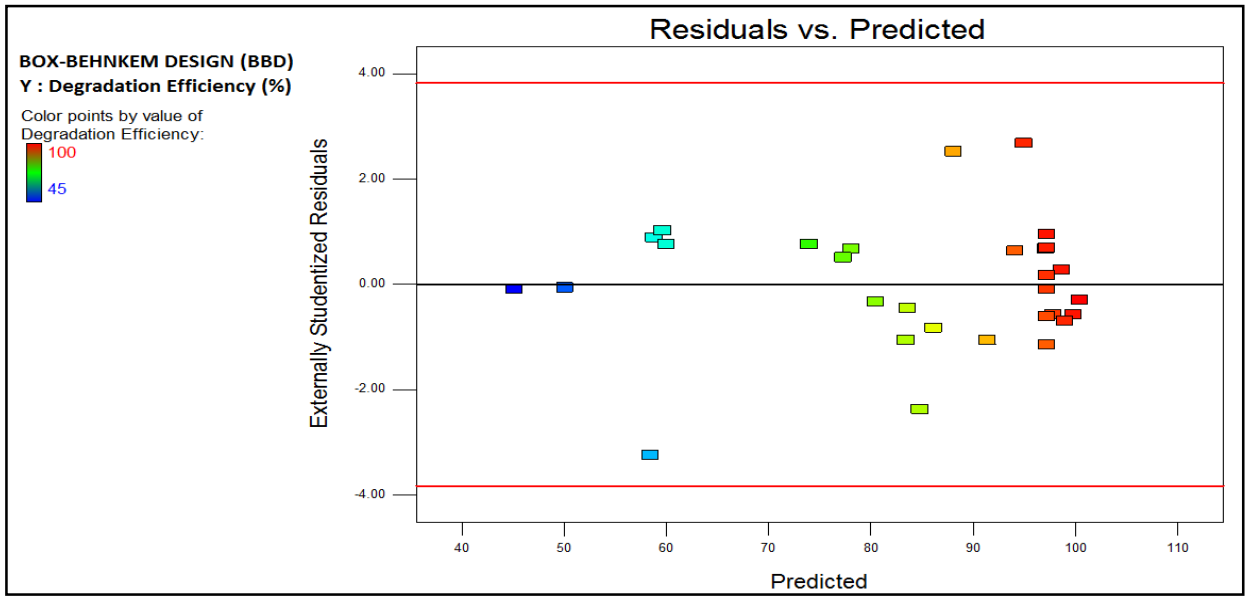

Figure D -7.2: Residuals vs the Fitted values the $mTiO_2$ water treatment.

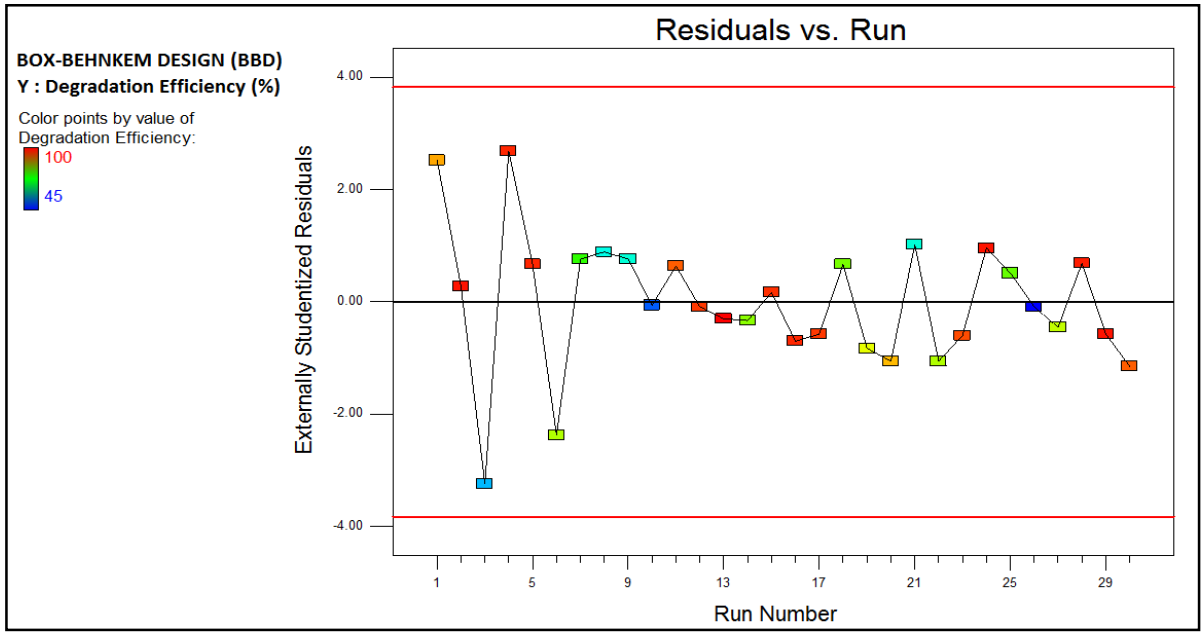

Figure D -7.3: Residuals vs Run Order of the $mTiO_2$ water treatment.

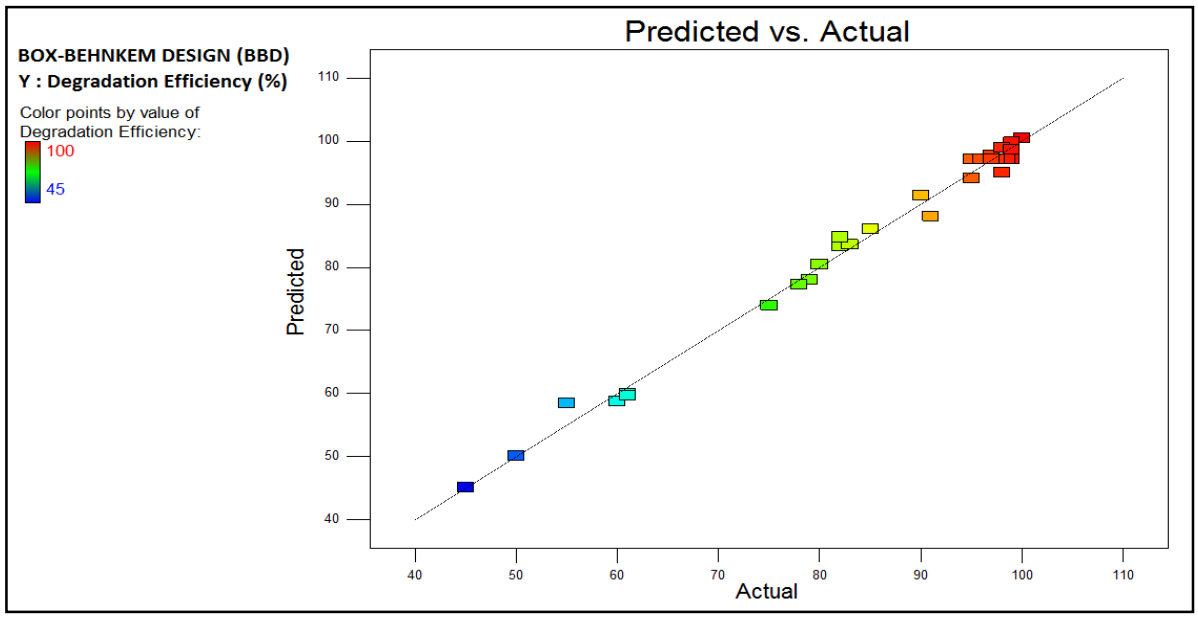

Figure D -7.4: Plot of Predicted values vs Actual values.

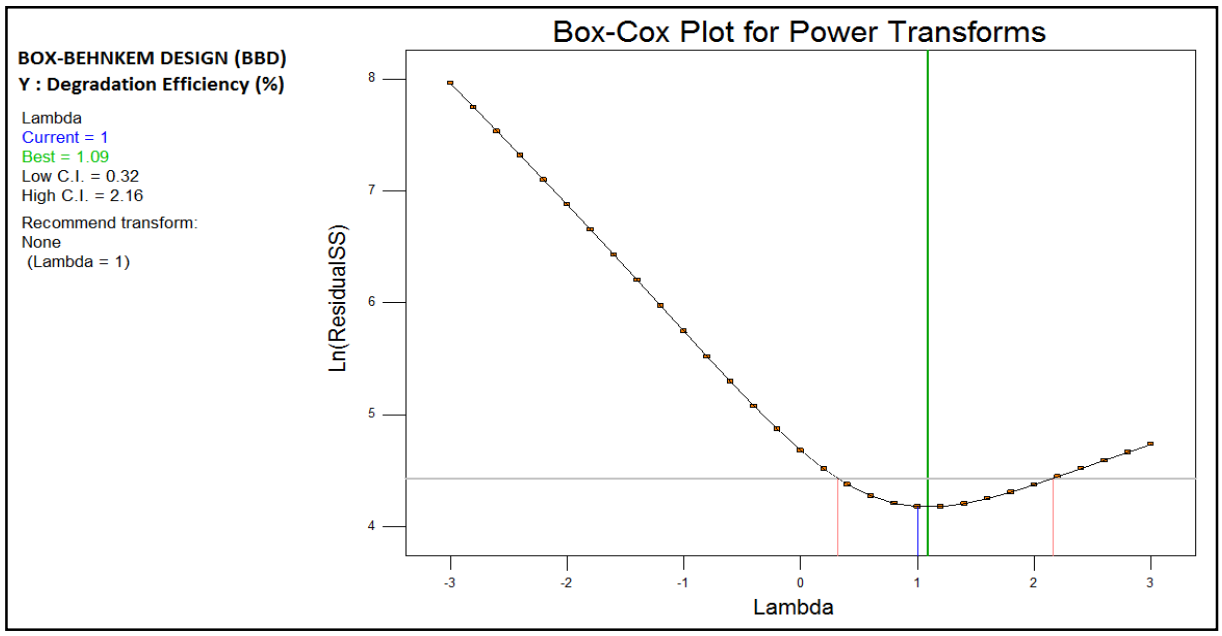

Figure D -7.5: Box-Cox Plot Power Transforms.

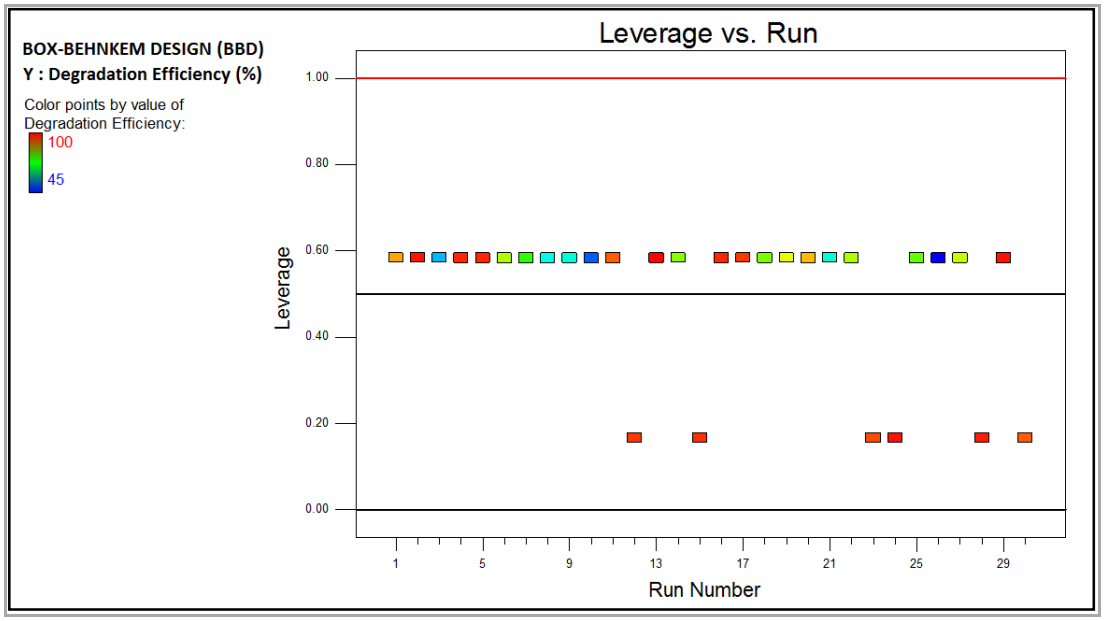

Figure D -7.6: Plot of Leverage vs Run Order.

Table D-7.6: Optimization Report of Constrains and Solutions on the Box-Behnken Design

Constraints						
Name	**Goal**	**Lower Limit**	**Upper Limit**	**Lower Weight**	**Upper Weight**	**Importance**
A:TiO_2 Concentration	is in range	3	8	1	1	3
B:Temperature	is in range	20	30	1	1	3
C:Starting pH	is in range	6	8	1	1	3
D:Aeration	is in range	6	14	1	1	3
Degradation Efficiency	is in range	98	100	1	1	3

Solutions							
Number	**TiO_2 Concentration**	**Temperature**	**Initial pH**	**Aeration**	**Degradation Efficiency**	**Desirability**	
1	5.84	29.63	6.01	10.55	98.43	1	
2	6.00	29.86	6.08	11.05	98.42	1	
3	6.35	27.66	6.14	12.11	98.29	1	
4	5.70	29.79	6.04	11.02	98.23	1	
5	7.65	29.66	6.02	13.45	98.82	1	
6	5.97	28.79	6.02	13.40	98.19	1	
7	6.54	22.01	6.02	12.03	98.39	1	
8	6.63	25.19	6.11	12.17	98.32	1	
9	6.27	28.00	6.06	11.29	98.94	1	
10	6.28	21.26	6.02	12.49	98.13	1	
11	6.64	22.01	6.02	12.57	98.30	1	
12	6.22	20.36	6.00	12.18	98.04	1	
13	5.52	27.75	6.02	11.66	98.07	1	
14	6.45	26.22	6.01	11.63	99.46	1	
15	6.06	24.41	6.04	11.90	98.53	1	
16	6.41	22.06	6.00	10.96	98.05	1	
17	5.60	29.66	6.02	10.94	98.13	1	
18	6.45	28.28	6.02	12.21	99.80	1	Selected
19	6.21	27.52	6.01	13.23	98.92	1	
20	6.20	29.32	6.12	12.48	98.44	1	
21	6.53	20.81	6.01	11.82	98.07	1	
22	6.32	28.16	6.14	11.23	98.12	1	
23	6.90	27.59	6.07	11.60	99.01	1	
24	7.20	25.10	6.00	12.73	98.90	1	
25	6.32	28.98	6.10	11.38	98.76	1	
26	6.34	20.93	6.01	12.79	98.01	1	
27	7.34	28.53	6.09	12.32	98.70	1	

Solutions						
Number	TiO_2 Concentration	Temperature	Initial pH	Aeration	Degradation Efficiency	Desirability
28	6.02	29.92	6.03	13.52	98.07	1
29	7.48	25.94	6.04	11.97	98.16	1
30	6.78	28.84	6.13	11.57	98.62	1
31	6.69	21.61	6.00	12.73	98.30	1
32	6.86	28.87	6.09	11.44	99.03	1
33	7.92	27.84	6.00	12.63	98.14	1
34	6.20	29.15	6.13	11.47	98.31	1
35	7.32	29.23	6.04	12.37	99.45	1
36	6.81	23.08	6.02	12.66	98.54	1
37	5.77	29.96	6.02	10.38	98.04	1
38	5.87	23.82	6.00	11.35	98.45	1
39	6.61	27.15	6.15	12.53	98.18	1
40	6.75	27.89	6.09	12.55	98.99	1
41	6.37	20.18	6.00	12.16	98.01	1
42	7.00	29.15	6.09	10.77	98.29	1
43	6.28	20.23	6.00	11.99	98.00	1
44	7.56	28.46	6.06	12.97	98.54	1
45	6.12	29.50	6.03	11.71	99.41	1
46	6.09	25.19	6.06	12.12	98.54	1
47	6.45	29.62	6.03	10.39	98.78	1
48	7.17	24.70	6.01	13.02	98.68	1
49	6.48	21.70	6.04	12.12	98.06	1
50	6.48	29.62	6.11	12.26	98.98	1
51	6.79	26.55	6.09	11.31	98.46	1
52	6.77	28.90	6.06	10.25	98.10	1
53	6.08	21.91	6.01	11.57	98.21	1
54	6.55	26.48	6.08	13.29	98.35	1
55	6.62	20.91	6.01	12.76	98.04	1
56	6.32	20.83	6.00	11.62	98.14	1
57	6.53	24.17	6.09	12.25	98.28	1
58	6.03	28.68	6.06	11.24	98.69	1
59	6.18	28.94	6.05	12.29	99.16	1
60	6.86	23.84	6.01	11.15	98.43	1
61	6.01	29.71	6.05	11.73	98.96	1
62	5.70	29.43	6.01	11.73	98.68	1
63	6.28	27.86	6.02	10.71	98.96	1

APPENDIX E:

CENTRAL COMPOSITE DESIGN'S COMPUTER OUTPUT FROM DESIGN EXPERT 9 FOR FITTING A MODEL.

***** WARNING: The Cubic Model and higher are Aliased! *****

Response : Degradation Efficiency Transform: None

Table E-7.1: Sequential Model Sum of Squares [Type I] on the Central Composite Design.

Source	Sum of Squares	df	Mean Square	F Value	p-value Prob > F	
Mean vs Total	1.74E+05	1	1.74E+05			
Linear vs Mean	5230.82	4	1307.7	4.66	0.006	
2FI vs Linear	902.25	6	150.37	0.47	0.8238	
Quadratic vs 2FI	6037.07	4	1509.27	303.61	< 0.0001	Suggested
Cubic vs Quadratic	61.21	8	7.65	4.01	0.0417	Aliased
Residual	13.35	7	1.91			
Total	1.86E+05	30	6194.29			

Table E-7.2: Lack-of-fit Test on the Central Composite Design.

Source	Sum of Squares	df	Mean Square	F Value	p-value Prob > F	
Linear	7002.55	20	350.13	154.47	< 0.0001	
2FI	6100.31	14	435.74	192.24	< 0.0001	
Quadratic	63.23	10	6.32	2.79	0.1345	Suggested
Cubic	2.02	2	1.01	0.45	0.6635	Aliased
Pure Error	11.33	5	2.27			

Table E-7.3: Model Summary Statistic on the Central Composite Design.

Source	Std. Dev.	R-Squared	Adjusted R-Squared	Predicted R-Squared	PRESS	
Linear	16.75	0.4272	0.3355	0.2128	9638.44	
2FI	17.94	0.5009	0.2382	0.1751	10100.9	
Quadratic	2.23	0.9939	0.9882	0.9689	380.54	Suggested
Cubic	1.38	0.9989	0.9955	0.9749	307.32	Aliased

Table E-7.4: ANOVA for Response Surface Quadratic model on the Central Composite Design

Analysis of variance table [Partial sum of squares - Type III]						
Source	Sum of Squares	df	Mean Square	F Value	p-value Prob > F	
Model	12170.14	14	869.3	174.87	< 0.0001	significant
A-TiO_2	*1048.08*	*1*	*1048.08*	*210.84*	*< 0.0001*	
B-	*22.81*	*1*	*22.81*	*4.59*	*0.049*	
C-Starting	*2696.64*	*1*	*2696.64*	*542.47*	*< 0.0001*	
D-Aeration	*1463.28*	*1*	*1463.28*	*294.36*	*< 0.0001*	
AB	*155*	*1*	*155*	*31.18*	*< 0.0001*	
AC	*121*	*1*	*121*	*24.34*	*0.0002*	
AD	*55.5*	*1*	*55.5*	*11.17*	*0.0045*	
BC	*96.04*	*1*	*96.04*	*19.32*	*0.0005*	
BD	*390.06*	*1*	*390.06*	*78.47*	*< 0.0001*	
CD	*84.64*	*1*	*84.64*	*17.03*	*0.0009*	
A^2	*1852.74*	*1*	*1852.74*	*372.71*	*< 0.0001*	
B^2	*6.03*	*1*	*6.03*	*1.21*	*0.2882*	
C^2	*4613.17*	*1*	*4613.17*	*928.01*	*< 0.0001*	
D^2	*610.74*	*1*	*610.74*	*122.86*	*< 0.0001*	
Residual	74.57	15	4.97			
Lack of Fit	*63.23*	*10*	*6.32*	*2.79*	*0.1345*	*not significant*
Pure Error	*11.33*	*5*	*2.27*			
Cor Total	12244.71	29				

Factor	Coefficient Estimate	df	Standard Error	95% CI Low	95% CI High	VIF
Intercept	97.17	1	0.91	95.23	99.11	
A-TiO_2 Concentration	6.61	1	0.46	5.64	7.58	1
B-Temperature	0.97	1	0.46	4.95E-03	1.95	1
C-Starting pH	-10.6	1	0.46	-11.57	-9.63	1
D-Aeration	7.81	1	0.46	6.84	8.78	1
AB	-3.11	1	0.56	-4.3	-1.92	1
AC	-2.75	1	0.56	-3.94	-1.56	1
AD	-1.86	1	0.56	-3.05	-0.67	1
BC	2.45	1	0.56	1.26	3.64	1
BD	4.94	1	0.56	3.75	6.13	1
CD	-2.3	1	0.56	-3.49	-1.11	1
A^2	-8.22	1	0.43	-9.13	-7.31	1.05
B^2	-0.47	1	0.43	-1.38	0.44	1.05
C^2	-12.97	1	0.43	-13.88	-12.06	1.05
D^2	-4.72	1	0.43	-5.63	-3.81	1.05

Final Equation in Terms of Coded	
Degradation Efficiency	=
97.17	
6.61	* A
0.97	* B
-10.6	* C
7.81	* D
-3.11	* AB
-2.75	* AC
-1.86	* AD
2.45	* BC
4.94	* BD
-2.3	* CD
-8.22	* A^2
-0.47	* B^2
-12.97	* C^2
-4.72	* D^2

Final Equation in Terms of Actual Factors:	
Degradation Efficiency	=
-105.33094	
26.00583	* TiO_2
-0.90588	* Temperature
35.83125	* Starting pH
6.89677	* Aeration
-0.1245	* TiO_2 Concentration * Temperature
-0.55	* TiO_2 Concentration * Starting pH
-0.18625	* TiO_2 Concentration * Aeration
0.1225	* Temperature * Starting pH
0.12344	* Temperature * Aeration
-0.2875	* Starting pH * Aeration
-1.315	* TiO_2 Concentration^2
-4.69E-03	* Temperature^2
-3.24219	* Starting pH^2
-0.29492	* Aeration^2

Table E-7.5: Diagnostics Case Statistics on the Central Composite Design

Run Order	Actual Value	Predicted Value	Residual	Leverage	Internally Studentized Residual	Externally Studentized Residual	Cook's Distance	Influence on Fitted Value DFFITS	Standard Order
1	73.8	72.95	0.85	0.583	0.594	0.58	0.033	0.687	16
2	89.4	90.58	-1.18	0.583	-0.819	-0.81	0.063	-0.958	11
3	99	99.35	-0.35	0.583	-0.24	-0.233	0.005	-0.275	12
4	95	97.17	-2.17	0.167	-1.065	-1.07	0.015	-0.478	25
5	94	93.91	0.092	0.583	0.064	0.062	0	0.073	24
6	25	24.09	0.91	0.583	0.631	0.618	0.037	0.731	22
7	95	93.34	1.66	0.583	1.152	1.166	0.124	1.38	19
8	62.3	63.36	-1.06	0.583	-0.738	-0.727	0.051	-0.86	1
9	48.5	47.36	1.14	0.583	0.79	0.78	0.058	0.923	5
10	66	65.03	0.97	0.583	0.675	0.662	0.042	0.783	6
11	97.5	97.17	0.33	0.167	0.164	0.158	0	0.071	29
12	49	50.56	-1.56	0.583	-1.086	-1.093	0.11	-1.293	7
13	79	77.43	1.57	0.583	1.091	1.099	0.111	1.3	9
14	60	62.45	-2.45	0.583	-1.699	-1.827	0.27	-2.162 *	14
15	65	66.49	-1.49	0.583	-1.036	-1.039	0.1	-1.23	21
16	99	97.17	1.83	0.167	0.901	0.895	0.011	0.4	26
17	98.5	97.17	1.33	0.167	0.655	0.642	0.006	0.287	27
18	50	52.23	-2.23	0.583	-1.549	-1.633	0.224	-1.932 *	13
19	100	98.65	1.35	0.583	0.941	0.937	0.083	1.109	10
20	75	72.98	2.02	0.583	1.404	1.456	0.184	1.722 *	4
21	95	97.24	-2.24	0.583	-1.558	-1.644	0.226	-1.945 *	20
22	50	51.08	-1.08	0.583	-0.747	-0.735	0.052	-0.87	17
23	78	77.51	0.49	0.583	0.342	0.331	0.011	0.392	18
24	96	97.17	-1.17	0.167	-0.573	-0.56	0.004	-0.25	28
25	55	55.78	-0.78	0.583	-0.541	-0.528	0.027	-0.625	8
26	90	92.03	-2.03	0.583	-1.41	-1.462	0.186	-1.730 *	2
27	60	56.76	3.24	0.583	2.25	2.67	0.472	3.159 *	3
28	97	97.17	-0.17	0.167	-0.082	-0.079	0	-0.035	30
29	78	75.18	2.82	0.583	1.96	2.195	0.359	2.598 *	15
30	62	62.68	-0.68	0.583	-0.469	-0.456	0.021	-0.54	23

Box-Cox Power Transformation				
Constant k	95% CI Low	95% CI High	Best Lambda	Rec. Transform
0	0.67	1.36	0.99	None

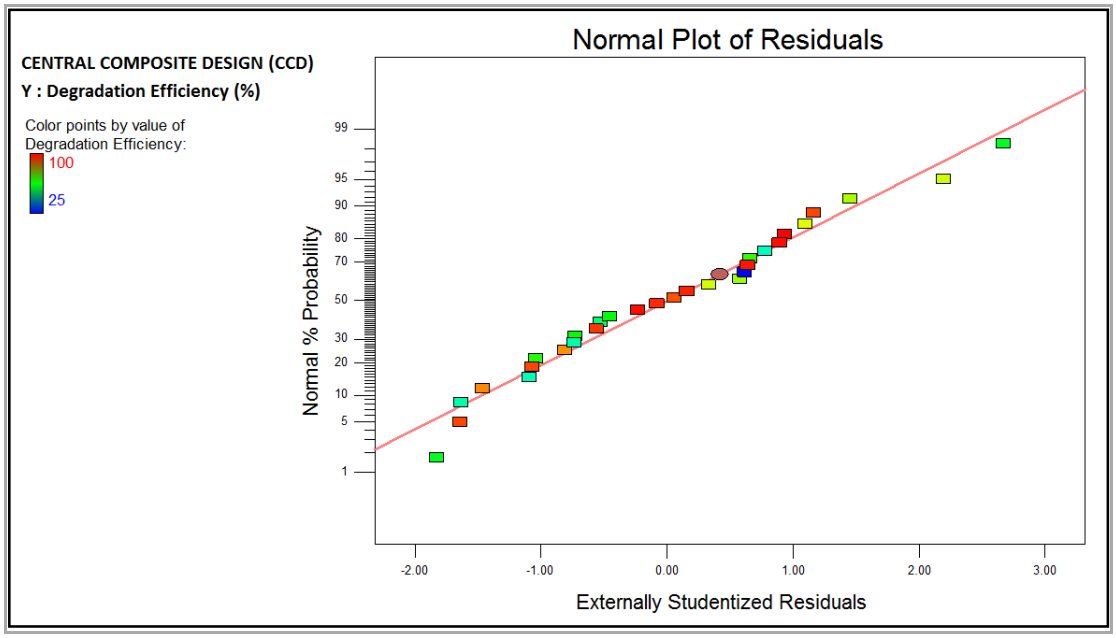

Figure E -7.1: Normal Probability plot of the Studentized Residuals of the $mTiO_2$ water treatment.

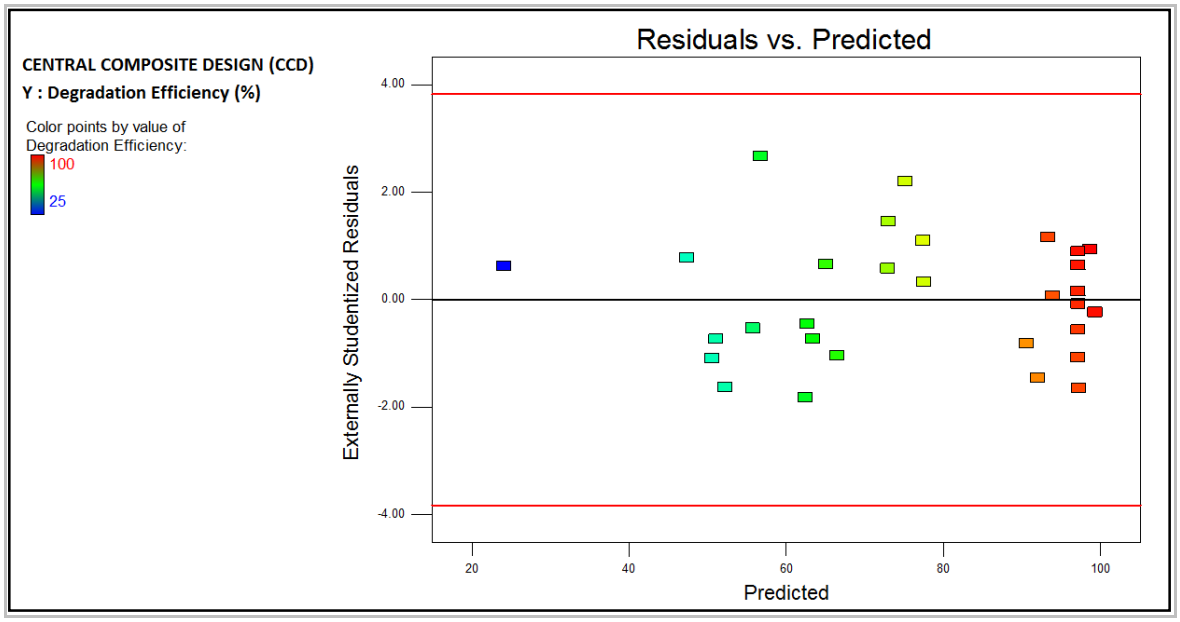

Figure E -7.2: Residuals vs the Fitted values the $mTiO_2$ water treatment.

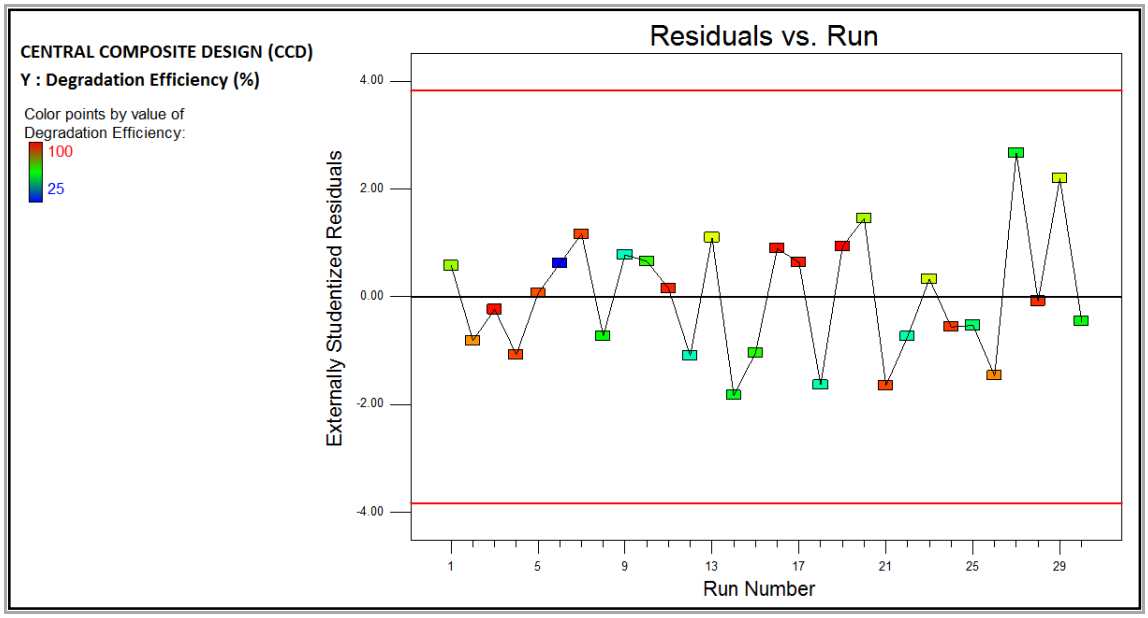

Figure E -7.3: Residuals vs Run Order of the $mTiO_2$ water treatment.

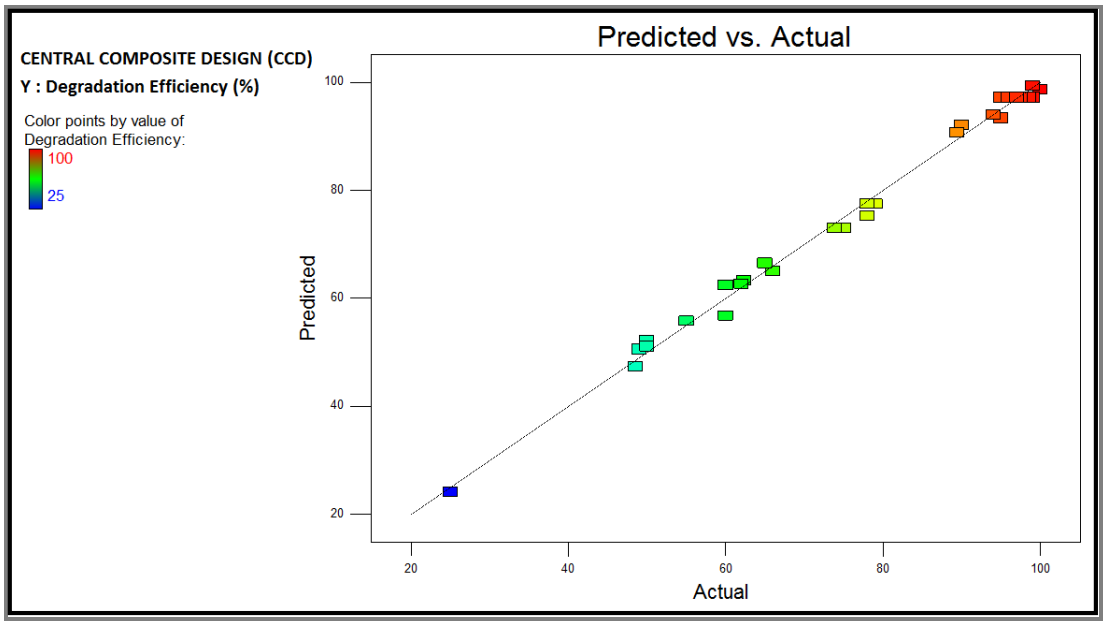

Figure E -7.4: Plot of Predicted values vs Actual values.

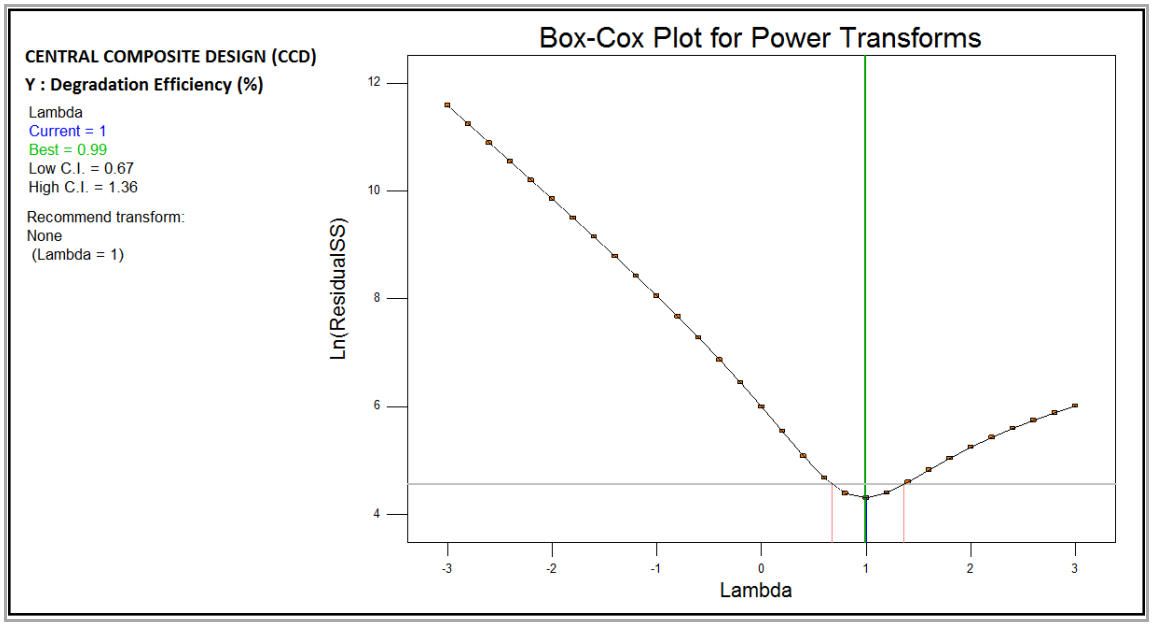

Figure E -7.5: Box-Cox Plot Power Transforms.

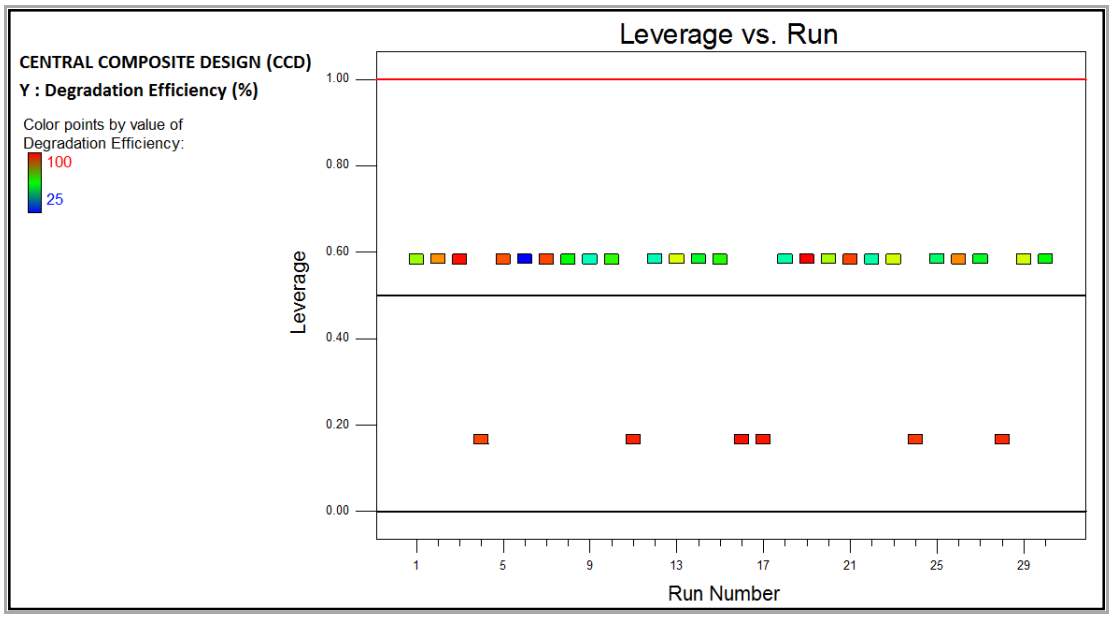

Figure E -7.6: Plot of Leverage vs Run Order.

APPENDIX F:

VERIFICATION OF THE OPTIMUM VALUES OF THE FACTORS.

CENTRAL COMPOSITE DESIGN (CCD)

Table F-7.1 CCD: Run 1 with $mTiO_2$ of 6.94 g/l and Aeration of 13.5 L/min

Time hr	Turbidity NTU	Temperature ^{O}C	pH	E-coli count/100 mL	Degradation Efficiency (%)
0	3462	28.8	6.00	2419.6	0.0
4	0.38	28.8	5.03	7.9	99.7

Table F-7.2 CCD: Run 2 with $mTiO_2$ of 6.94 g/l and Aeration of 13.5 L/min

Time hr	Turbidity NTU	Temperature ^{O}C	pH	E-coli count/100 mL	Degradation Efficiency (%)
0	3398	28.8	6.03	2419.6	0.0
4	0.38	28.8	5.51	13.1	99.5

Table F-7.3 CCD: Run 3 with $mTiO_2$ of 6.94 g/l and Aeration of 13.5 L/min

Time hr	Turbidity NTU	Temperature ^{O}C	pH	E-coli count/100 mL	Degradation Efficiency (%)
0	3627	28.8	6.00	2419.6	0.0
4	0.405	28.8	4.55	2.6	99.9

BOX-BENHKEN DESIGN (BB)

Table F-7.1 BB: Run 1 with $mTiO_2$ of 6.45 g/l and Aeration of 12 L/min

Time hr	Turbidity NTU	Temperature ^{O}C	pH	E-coli count/100 mL	Degradation Efficiency (%)
0	3218	28.3	6.00	2419.6	0.0
4	0.355	28.3	4.89	28.0	98.8

Table F-7.2 BB: Run 2 with $mTiO_2$ of 6.45 g/l and Aeration of 12 L/min

Time hr	Turbidity NTU	Temperature ^{O}C	pH	E-coli count/100 mL	Degradation Efficiency (%)
0	2964	28.3	6.00	2419.6	0.0
4	0.335	28.3	5.47	10.4	99.6

Table F-7.3 BB: Run 3 with $mTiO_2$ of 6.45 g/l and Aeration of 12 L/min

Time hr	Turbidity NTU	Temperature ^{O}C	pH	E-coli count/100 mL	Degradation Efficiency (%)
0	3309	28.3	6.00	2419.6	0.0
4	0.25	28.3	5.62	15.0	99.4